

2012-09-28

Cadmium (II) Complex Formation with N-Acetylcysteine, Selenourea and Thiourea in Solution

Amini, Zahra

Amini, Z. (2012). Cadmium (II) Complex Formation with N-Acetylcysteine, Selenourea and Thiourea in Solution (Master's thesis, University of Calgary, Calgary, Canada). Retrieved from <https://prism.ucalgary.ca>. doi:10.11575/PRISM/25190

<http://hdl.handle.net/11023/240>

Downloaded from PRISM Repository, University of Calgary

UNIVERSITY OF CALGARY

Cadmium (II) Complex Formation with N-Acetylcysteine, Selenourea and Thiourea in
Solution

by

Zahra Amini

A THESIS

SUBMITTED TO THE FACULTY OF GRADUATE STUDIES
IN PARTIAL FULFILMENT OF THE REQUIREMENTS FOR THE
DEGREE OF MASTER OF SCIENCE

DEPARTMENT OF CHEMISTRY

CALGARY, ALBERTA

SEPTEMBER, 2012

© Zahra Amini 2012

Abstract

Cd(II) complexes with *N*-acetylcysteine (H₂NAC), selenourea (SeU), and thiourea (TU) in solution were investigated using ¹¹³Cd NMR and XAS spectroscopic techniques.

From the Cd K-edge EXAFS spectrum of a Cd(II)-SeU methanol solution at 200 K containing C_{Cd(II)}=0.1 M and C_{SeU}≥0.4 M, the local structure of a Cd(SeU)₄ tetrahedral species with Cd-Se bond distance of 2.64±0.02 Å was determined. ¹¹³Cd NMR measurement of this solution shows a single sharp peak at 578 ppm, which is in agreement with the reported CdSe₄ speciation. For Cd(II)-SeU solutions with a lower concentration of selenourea, a mixture of species was observed.

¹¹³Cd NMR spectra of Cd(II)-TU solutions revealed a mixture of species at low TU/Cd(II) mole ratios. The structures of these complexes were determined using Cd K-edge EXAFS spectroscopy, L_{III}-edge XANES, and ¹¹³Cd NMR.

Cd(II)-*N*-acetylcysteine solutions with C_{Cd(II)} = 0.1 M and NAC/Cd(II) mole ratios of 2.0–20.0 at pH = 7.5 and 11.0 have been investigated. They show a mixture of CdS₃O₃, CdS₃O, and CdS₄ species at low NAC concentration and CdS₄ species at high NAC concentration.

Preface

Since the industrial revolution, human exposure to heavy metals such as cadmium has drastically increased and hence the interference of these heavy metals with different biological processes becomes a global concern. Many studies have been conducted to investigate the complex formation of these toxic metals with different ligands, especially those of biological importance. The focus of this thesis is the characterization of cadmium complex formation, as one of the above mentioned heavy metals, with selenourea, thiourea and N-acetylcysteine.

In the first chapter, the structure and coordination chemistry of cadmium, selenourea, thiourea and N-acetylcysteine are surveyed. The experimental techniques that were used for the purpose of this study are also addressed.

In the second chapter, the chemistry and complex formation of cadmium with thiourea and selenourea using different spectroscopic methods such as X-ray absorption spectroscopy (i.e. EXAFS and XANES), and multinuclear NMR spectroscopy are described.

In the third chapter, cadmium complex formation with the thiol-containing N-acetylcysteine in solution was studied using a multi-spectroscopic approach including ^{113}Cd NMR, EXAFS and XANES.

Acknowledgment

I would like to express my deepest gratitude to my supervisory committee for their help and support. I sincerely acknowledge technical staffs of NMR facilities and department of chemistry staffs for their continuous assistance. Special thanks to Dr. Parvez for solving the crystal structure presented in this thesis.

“Portions of this research were carried out at the Stanford Synchrotron Radiation Lightsource (proposal numbers 2848 and 3391), a Directorate of SLAC National Accelerator Laboratory and an Office of Science User Facility operated for the U.S. Department of Energy Office of Science by Stanford University. The SSRL Structural Molecular Biology Program is supported by the DOE Office of Biological and Environmental Research, and by the National Institutes of Health, National Institute of General Medical Sciences (including P41GM103393) and the National Center for Research Resources (P41RR001209). The contents of this publication are solely the responsibility of the authors and do not necessarily represent the official views of NIGMS, NCRR or NIH.”

I also acknowledge the Natural Sciences and Engineering Research Council (NSERC) of Canada for providing financial support of this project.

I would also like to thank my family for their everyday support and encouragement and my friends for making this experience a memorable one.

Dedication

This thesis is dedicated to my constant foundation of encouragement and support,
My Parents

Table of Contents

Abstract	ii
Preface.....	iii
Acknowledgment	iv
Dedication	v
Table of Contents	vi
List of Tables	viii
List of Figures and Illustrations	x
List of Publications	xvii
 CHAPTER ONE: INTRODUCTION.....	1
1.1 Cadmium Coordination Chemistry	1
1.1.1 The Chemistry of the Hydrated Cd(II) Ion	2
1.2 N-Acetylcysteine	3
1.2.1.1 N-Acetylcysteine as a Pharmaceutical Drug	3
1.2.2 N-Acetylcysteine's Biological Roles	6
1.2.3 N-Acetylcysteine Solution Chemistry	6
1.2.4 N-Acetylcysteine Coordination Chemistry	9
1.3 Selenourea and Thiourea Chemistry	10
1.3.1 Selenourea and Thiourea Cd(II) Coordination Chemistry	10
1.3.2 Role of Selenium in Biological System and as Drug	13
1.4 Spectroscopic Methods	16
1.4.1 X-ray Absorption Spectroscopy (XAS).....	16
1.4.1.1 Synchrotron Radiation Sources	16
1.4.1.2 Optic Hutch and Experimental Hutch.....	19
1.4.1.3 Theory and Principles of X-ray Absorption Spectroscopy	20
1.4.1.4 Extended X-ray Absorption Fine Structure (EXAFS) Spectroscopy	24
1.4.1.5 EXAFS Equation	26
1.4.1.6 X-ray Absorption Spectroscopy Data Analysis	27
1.4.1.7 Advantages and Limitations of X-ray Absorption Spectroscopy	28
1.4.2 Nuclear Magnetic Resonance (NMR) Spectroscopy.....	29
1.4.2.1 Theory	29
1.4.2.2 Pulsed NMR.....	35
1.4.2.3 ¹¹³ Cd NMR Spectroscopy	36
1.4.2.4 Advantages and Limitations of NMR Spectroscopy	41
 CHAPTER TWO: COMPARATIVE STUDY OF CADMIUM COMPLEX FORMATION WITH SELENOUREA AND ITS ANALOGUE THIOUREA.....	42
2.1 Introduction.....	42
2.2 Experimental Methods	44
2.2.1 Sample Preparation.....	44
2.2.2 Synthesis of Cd(CF ₃ SO ₃) ₂	44
2.2.3 Synthesis of Cd(II)-selenourea 100 mM solutions in methanol	45
2.2.4 Synthesis of Cd(II)-thiourea 100 mM solutions in methanol	45
2.2.5 Synthesis and Crystal Structure of cis-[Cd(TU) ₂ (OH ₂) ₄] ²⁺ and fac- [Cd(TU) ₃ (OH ₂) ₃] ²⁺ disulfate	46

2.2.6 ^{113}Cd NMR Spectroscopy	49
2.2.7 Cd K- and L _{III} -edge X-ray absorption spectroscopy data collection	50
2.2.8 X-ray absorption spectroscopy data analysis	52
2.3 Result	53
2.3.1 Speciation of Cd(II)-selenourea complexes in methanol solution	53
2.3.2 Speciation of Cd(II)-thiourea complexes in methanol solution at low temperature	60
2.3.3 Speciation of Cd(II)-thiourea complexes in methanol solution at room temperature	73
2.3.4 X-ray Absorption Near Edge Structure of Cd(II)-thiourea Solutions at room temperature	77
2.4 Conclusion and Future Work	79
CHAPTER THREE: STRUCTURE OF CADMIUM (II) N-ACETYL CYSTEINE COMPLEX	
3.1 Introduction	82
3.2 Experimental Methods	85
3.2.1 Sample Preparation	85
3.2.2 Synthesis of Cd(II)-N-Acetylcysteine 100 mM Solutions in Water	85
3.2.3 ^{113}Cd NMR Spectroscopy	86
3.2.4 X-ray Absorption Spectroscopy Data Collection	87
3.2.5 X-ray Absorption Spectroscopy Data Analysis	87
3.3 Result and Discussion	89
3.3.1 ^{113}Cd NMR Spectroscopy of Cd(II)-N-Acetylcysteine Solutions at pH = 11.0	89
3.3.2 Extended X-ray Absorption Fine Structure of Cd(II) N-Acetylcysteine Solutions at pH = 11.0	93
3.3.3 X-ray Absorption Near Edge Structure of Cd(II) N-Acetylcysteine Solutions at pH = 11.0	95
3.3.4 ^{113}Cd NMR Spectroscopy of Cd(II)-N-Acetylcysteine Solutions at pH = 7.5	98
3.3.5 Extended X-ray Absorption Fine Structure of Cd(II) N-Acetylcysteine Solutions at pH = 7.5	101
3.4 Conclusion and Future Work	104
APPENDIX A-1 SURVEY OF CD(II) COMPLEXES WITH THIONE (CDS_4 , CDS_3O , CDSO_6 , CDS_2O_4 , CDS_3O_3 , AND CDS_6) LIGANDS IN CSD VERSION 5.30 (NOVEMBER 2008).	
APPENDIX B- EXAFS FEFF MODEL	117
APPENDIX C MEDUSA INPUT FILE	120
APPENDIX D- Total number of scans collected during the ^{113}Cd NMR measurements	121
REFERENCES	123

List of Tables

Table 1-1 Some of metal ion complexes with thiourea.	13
Table 1-2 Electron binding and X-ray fluorescence energies for Cd.	26
Table 1-3 NMR related properties of some of the nuclei.	29
Table 1-4 ^{113}Cd Chemical shifts of different coordination environments.	38
Table 1-5 ^{113}Cd Chemical shifts of different selenium coordination number.	39
Table 1-6 ^{113}Cd coupling constants.....	40
Table 1-7 The effect of solvent on the ^{113}Cd chemical shift of 1.0 M $\text{Cd}(\text{CH}_3)_2$	40
Table 1-8 The effect of concentration on the ^{113}Cd chemical shift of $\text{Cd}(\text{ClO}_4)_2$ in water.....	41
Table 2-1 Composition of SeU / Cd(II) solutions in MeOH.	45
Table 2-2 Composition of TU / Cd(II) solutions in MeOH.	46
Table 2-3 Crystal data and structure refinement for <i>cis</i> - $[\text{Cd}(\text{TU})_2(\text{OH}_2)_4]^{2+}$ and <i>fac</i> - $[\text{Cd}(\text{TU})_3(\text{OH}_2)_3]^{2+}$ disulfateComplex.....	48
Table 2-4 EXAFS curve fitting results for Cd(II)-SeU solution A ₁ , B ₁ , and E ₁ at : 200 K and fixed $S_0^2 = 1.0$	55
Table 2-5 EXAFS curve fitting results for Cd(II)-TU solution A ₂ -G ₂ at 200 – 205 K.....	66
Table 2-6 EXAFS curve fitting results for Cd(II)-TU solution A ₂ -G ₂ at room temperature. S_0^2 value was fixed at 1.0.....	74
Table 3-1 Stability constants for Cd^{2+} complexes with N-acetylcysteine (NAC).	84
Table 3-2 Composition of Cd(II)-N-acetylcysteine solutions.	86
Table 3-3 ^{113}Cd chemical shifts for various thiolate coordination environments..	90
Table 3-4 EXAFS curve-fitting results for Cd(II)-NAC solutions A ₁ – G ₁ at pH = 11.0.....	94
Table 3-5 A survey of Cd(II)-S bond distance available in CSD for thiolate complexes.	94

Table 3-6 EXAFS curve-fitting results for Cd(II)-NAC solutions $A_2 - G_2$ (pH = 7.5). 101

List of Figures and Illustrations

Figure 1-1 Speciation diagrams for Cd(II) in aqueous solution over the pH 1-12 range, at $[Cd^{2+}] = 100$ mM. Solid Cd(II) hydroxide forms above pH = 7.0. (cr = crystal).....	3
Figure 1-2 Structure of cysteine (1), homocysteine (2), methionine (3), reduced lipoic acid (4), glutathione (5), N-acetylcysteine (6), and cystine (7).	5
Figure 1-3 Possible mercapturic acid pathway.	6
Figure 1-4 Protonation of N-acetyl cysteine functional groups.	7
Figure 1-5 Fraction diagram of N-acetyl cysteine as a function of pH in 0.1 M N-acetyl cysteine, based on the reported formation constants.	8
Figure 1-6 Selected structures of N-acetylcysteine metal complexes with different coordination modes for N-acetylcysteine.	9
Figure 1-7 Crystal structures of selenourea metal complexes.	12
Figure 1-8 Se-containing ligands.	14
Figure 1-9 Schematics of a typical synchrotron facility with its main components.	17
Figure 1-10 Bending magnet and insertion device.	19
Figure 1-11 A typical beam line in a synchrotron facility.	20
Figure 1-12 An X-ray absorption spectrum, showing the absorption edge, XANES and EXAFS regions for Cd K-edge.	22
Figure 1-13 (A) A schematic experimental set up with ion chambers in transmission mode (used for Cd K-edge measurement) and (B) fluorescence mode (used for Cd L _{III} -edge measurement).	23
Figure 1-14 The photoelectric effect (left) and X-ray fluorescence (right).	24
Figure 1-15 XAS spectrum of Cd K-edge of Cd(II)-selenourea solution. The inset shows the k^3 -weighted EXAFS oscillation.	25
Figure 1-16 The effect of a static magnetic field (B_0) on nuclear spins (modified from [94]).	30
Figure 1-17 Precession of nuclear dipoles with $I = 1/2$ and spin configurations according to applied magnetic field.	31

Figure 1-18 The energy difference between two states (α and β) for nuclei with $I = \frac{1}{2}$ as a function of a magnetic field B_0	32
Figure 1-19 A single pulsed NMR experiment (D_1 = delay time, τ_p = pulse duration, D_E = dead time, AQ = acquisition time).....	35
Figure 2-1 a) The molecular structure of cis -[Cd(TU) ₂ (OH ₂) ₄] ²⁺ and fac -[Cd(TU) ₃ (OH ₂) ₃] ²⁺ disulfate with Cd-O and Cd-S bond distances in the ranges of 2.323(8) - 2.421(9) Å and 2.580(4) - 2.599(4) Å respectively for Cd1 and Cd2 atoms in bis(thiourea) complex, cis -[Cd(TU) ₂ (OH ₂) ₄] ²⁺ , and 2.303(7) - 2.480(10) Å and 2.559(4) - 2.706(3) Å for Cd3 and Cd4 atoms in the tris(thiourea) complex, fac -[Cd(TU) ₃ (OH ₂) ₃] ²⁺ respectively. and b) corresponding unit cell of cis -[Cd(TU) ₂ (OH ₂) ₄] ²⁺ and fac -[Cd(TU) ₃ (OH ₂) ₃] ²⁺ disulfate.	47
Figure 2-2 ¹¹³ Cd NMR sensitivity to solvent and temperature: 0.1 M Cd(ClO ₄) ₂ in - (a) D ₂ O at 298 K; (b) MeOH+ 30% MeOD at 298K; (c) MeOH+ 30% MeOD at 203 K.....	50
Figure 2-3 ¹¹³ Cd NMR spectra for Cd(II)-selenourea MeOH solutions A ₁ – E ₁ containing C _{Cd(II)} ~ 100 mM with varying SeU / Cd(II) molar ratios, measured at 203K.....	54
Figure 2-4 (Left) Cd K-edge EXAFS spectra and (Right) corresponding Fourier transforms for Cd(II)-SeU solution A ₁ , B ₁ , and E ₁ SeU / Cd(II) molar ratios 1.0, 2.0, and 5.0, C _{Cd(II)} ~ 100 mM.....	55
Figure 2-5 ¹¹³ Cd NMR spectra for Cd(CF ₃ SO ₃) ₂ in MeOH solutions at 203 K.	58
Figure 2-6 ¹¹³ Cd NMR spectra of Cd(II)-thiourea solutions A ₂ – G ₂ C _{Cd(II)} ~ 100 mM. All spectra were measured in a mixture of : 70% methanol and : 30% methanol - d ₄ at 203 K.....	61
Figure 2-7 Solid state ¹¹³ Cd NMR spectra of Cd(SCN ₂ H ₄) ₄ (NO ₃) ₂ at different spin rate at room temperature (CdS ₄ , δ_{iso} = 577 ppm, with δ_{11} = 651 ppm, δ_{22} = 576 ppm, and δ_{33} = 501 ppm).	62
Figure 2-8 Solid state ¹¹³ Cd NMR spectra of Cd(SCHN(CH ₃) ₂) ₄ (O ₃ SCF ₃) ₂ at different spin rate at room temperature (CdS ₄ O ₂ , δ_{iso} = 263 ppm, with δ_{11} = 562 ppm, δ_{22} = 263 ppm, and δ_{33} = -35 ppm).	63
Figure 2-9 Solid state ¹¹³ Cd NMR spectra of Cd(SCHN(CH ₃) ₂) ₆ (ClO ₄) ₂ at different spin rate at room temperature (CdS ₆ , δ_{iso} = 403 ppm, with δ_{11} = 553 ppm, δ_{22} = 403 ppm, and δ_{33} = 250 ppm).	64

Figure 2-10 Solid state ^{113}Cd NMR spectra of $\text{cis}[\text{Cd}(\text{TU})_2(\text{OH}_2)_4]^{2+}$ and $[\text{Cd}(\text{TU})_3(\text{SO}_4)]$ at 8000 Hz spin rate at room temperature (CdS_2O_4 and CdS_3O , $\delta = 148$ and 346 ppm respectively).....	65
Figure 2-11 (Left) Cd K-edge EXAFS spectra and (Right) corresponding Fourier transforms for Cd(II)-TU solutions $\text{A}_2\text{-G}_2$ with TU / Cd(II) molar ratios 1.0 to 10.0, $C_{\text{Cd(II)}} \sim 100$ mM at 200-205 K.	65
Figure 2-12 Comparison between k^3 -weighted EXAFS spectra of solutions D_2 and F_2 . .	71
Figure 2-13 Comparison between k^3 -weighted EXAFS spectra of solutions G_2 at 160 K and 200 K.	72
Figure 2-14 ^{113}Cd NMR spectra of Cd(II)-thiourea solutions $\text{D}_2 - \text{G}_2$ $C_{\text{Cd(II)}} \sim 100$ mM in : 70 % methanol and : 30 % methanol - d_4 at 298 K.	73
Figure 2-15 (Left) Cd K-edge EXAFS spectra and (Right) corresponding Fourier transforms for Cd(II)-TU solutions $\text{A}_2\text{-G}_2$ with TU / Cd(II) molar ratios 1.0 to 10.0, $C_{\text{Cd(II)}} \sim 100$ mM at room temperature.	74
Figure 2-16 (A) Cadmium L_{III} -edge XAS of cadmium(II) perchlorate hydrate $\text{Cd}(\text{ClO}_4)_2 \cdot 6\text{H}_2\text{O}$ (CdO_6 model), tetrakis(<i>N,N</i> -dimethylthioformamide) bis(trifluoromethanesulfonato) cadmium(II) $[\text{Cd}(\text{SCHN}(\text{CH}_3)_2)_4(\text{O}_3\text{SCF}_3)_2]$ (CdS_4O_2 model), hexakis(<i>N,N</i> -dimethylthioformamide) cadmium(II) perchlorate $[\text{Cd}(\text{SCHN}(\text{CH}_3)_2)_6](\text{ClO}_4)_2$ (CdS_6 model), imidazolium tris(thiosaccharinato)aqua cadmate(II) ($\text{HIm}[\text{Cd}(\text{tsac})_3(\text{H}_2\text{O})]$ (CdS_3O model), cadmium adamantane cage $(\text{Et}_3\text{NH})_4\text{-}[\text{S}_4\text{Cd}_{10}(\text{SPh})_{16}]$ (CdS_4 model) and Cd(II)-thiourea solutions $\text{A}_2 - \text{G}_2$ at room temperature, and (B) corresponding smoothed second derivatives; dotted lines correspond to 3539.2 eV and 3541.3 eV.	78
Figure 3-1 Fraction diagram of Cd(II)-N-acetylcysteine complexes in aqueous solution as a function of pH at $[\text{Cd}^{2+}] = 0.1$ M and $[\text{NAC}^{2-}] = 0.2$ M.”	83
Figure 3-2 Structure of $\text{Cd}((\text{tsac})_3(\text{H}_2\text{O}))$ (tsac = anion of thiosaccharine) used as a FEFF model to simulate EXAFS spectra.	88
Figure 3-3 ^{113}Cd NMR spectra of 0.1 M Cd(II)-NAC solutions $\text{B}_1 - \text{G}_1$ at pH = 11.0 and 298 K.	91
Figure 3-4 ^{113}Cd NMR spectra for Cd(II)-NAC solutions A_1 and I_1 at pH = 11.0	92
Figure 3-5 (Left)Cd K-edge EXAFS least-squares curve fitting of 0.1M Cd(II)-NAC solutions $\text{A}_1 - \text{G}_1$ at pH = 11.0 and (Right) their corresponding Fourier-transforms.	93

Figure 3-6 (Left) Cadmium L _{III} -edge XANES and (Right) corresponding second derivatives of (CdO ₆), Cd(ClO ₄) ₂ ·6H ₂ O; (CdS ₃ O ₃), [Ph ₄ P][Cd(SCO(CH ₃)) ₃]; [CdS ₂ O ₄ (II)], [Cd(tu) ₂ (NO ₃) ₂]; [CdS ₂ O ₄ (I)], [Cd(tmtu) ₂ (NO ₃) ₂] tmtu = tetramethyl thiourea; (CdS ₆), [Cd(SCHN(CH ₃) ₂) ₆](ClO ₄) ₂ ; (CdS ₃ N ₂), [Cd(SCH ₂ CH ₂ NH ₂) ₂]; (CdS ₂ N ₂), [Cd(tsac) ₂ (Im) ₂] Im = imidazole; (CdS ₃ O), (HIm)[Cd(tsac) ₃ (H ₂ O)] tsac = thiosaccharinato; and (CdS ₄), (Et ₃ NH) ₄ [S ₄ Cd ₁₀ (SPh) ₁₆]. Dotted lines are at 3539.1 and 3541.3 eV.	96
Figure 3-7 (Left) Cadmium L _{III} -edge XANES spectra Cd(II)-NAC solutions A ₁ – G ₁ and (Right) corresponding smoothed second derivatives.	97
Figure 3-8 ¹¹³ Cd NMR spectra of 0.1M Cd(II) - NAC solutions D ₂ – G ₂ at 298 K (L / M mole ratio = 5.0 – 20.0 at pH = 7.5).	99
Figure 3-9 (Left) EXAFS fitting of 0.1M solution of Cd(II)-NAC solutions A ₂ – G ₂ at pH = 7.5 and (Right) their corresponding Fourier-transforms.	101
Figure 3-10 ¹ H NMR spectra of 10 mM CdNAC solution A' ₁ - D' ₁ (pH 11.0) and A' ₂ - D' ₂ (pH 7.5) with NAC / Cd(II) = 2.0 – 5.0, comparing with free N-acetylcysteine.	103

List of Symbols, Abbreviations and Nomenclature

Symbol	Definition
α	phase shift
C.N.	coordination number
χ	EXAFS
R	bond distance
σ	Debye-Waller parameter
V	voltage
AQ	acquisition
β	stability constant
BBO	broad band 5 mm NMR probe
BL	beamline
$C_{\text{Cd(II)}}$	Cd(II) concentration
CSD	Cambridge Structural Database
E	energy
EA	elemental analysis
<i>eff</i>	effective
ESI-MS	electrospray ionization mass spectrometry
EXAFS	extended X-ray absorption fine structure
f_{eff}	effective amplitude function
FT	Fourier transform

γ	gyromagnetic ratio
h	Planck's constant
HT	high temperature
I	nuclear spin quantum number
k	photoelectron wavenumber
L	ligand
L / M	Ligand to metal
LT	low temperature
Λ	photoelectron mean free path
linac	linear accelerator
μ	linear absorption coefficient
m	mass
mol	moles
MS	multiple scattering
NAC	N-acetylcysteine
N_{α}	population in α state
N_{β}	population in β state
NEXAFS	near edge X-ray absorption fine structure
NMR	nuclear magnetic resonance
P1	pulse
φ_{ij}	phase shift
RF	radiofrequency
RT	room temperature

S_0^2	amplitude reduction factor
SeU	selenourea
SSRL	Stanford Synchrotron Radiation Laboratory
T	Temperature
T	Tesla
TGA	thermal gravimetric analysis
TU	thiourea
XANES	X-ray absorption near edge structure
XAS	X-ray absorption spectroscopy
z	charge

List of Publications

- i) F. Jalilehvand, Z. Amini, K. Parmar, EY. Kang, "Cadmium(II) *N*-acetyl Cysteine Complex Formation in Aqueous Solution" *Dalton Trans.* (2011) **40** 12771 – 12778.
- ii) M. Parvez, F. Jalilehvand, Z. Amini, "Tetraaquabis(thiourea-S)cadmium(II) triaquatris(thiourea-S)cadmium(II) disulfate" *Acta Cryst.* (2012) **E68** m949 – m950.
- iii) F. Jalilehvand, Z. Amini, K. Parmar, "Cadmium(II) Complex Formation with Selenourea and Thiourea in Solution: An XAS and ^{113}Cd NMR Study", *Inorg. Chem.* (2012) (DOI: 10.1021/ic300852t).

The contributions of the candidate in the Publications 1 and 3 are the materials presented in this thesis. The candidate prepared the crystalline compound for Publication 2.

Chapter One: Introduction

1.1 Cadmium Coordination Chemistry

The group 12 elements are of special interest: while zinc is an essential trace element for living organisms, mercury and cadmium are extremely toxic elements. These heavy metals can contaminate the food chain and water such that every living organism is exposed to them through their dietary habits or drinking water. Tobacco smoke has high cadmium content. Cadmium, calcium and zinc have some similarities: they all form stable 2+ ions; the ionic radii of Zn (II), Cd(II) and Ca (II) are 0.74 Å, 0.97 Å, and 0.99 Å respectively.¹ The other interesting part in studying the group 12 elements is that these +2 cations have a d^{10} closed valence shell with no crystal field stabilization energy, so their structural preference depends entirely on their environment, the complexing ability of the ligand, and the type of donor atoms. This is the reason for their ability to form complexes with different metal coordination numbers, such as 4-coordinated (planar² and tetrahedral³), 5-coordinated,⁴ or 6-coordinated.⁵ Similarities among group 12 elements can cause problems when cadmium interferes in the zinc or calcium functionalities.⁶ Cadmium is considered as one of the enzyme poisons since it has a high affinity for reacting with sulfhydryl groups; it can replace zinc in enzymes and block their activities. Most cadmium complexes are highly soluble in water, which is one of the reasons that

cadmium is an environmental concern. Cadmium (II) forms stable complexes with O, N, and S donor ligands. It can also form polymeric structures, with these ligands forming bridging bonds. Cadmium usage in batteries, metallic alloys, dyes and pigments, silver and pot polishes, shoe whiteners, and as plastic stabilizer, raises many health issues such as Itai-itai disease (combination of bone and renal damages), proteinuria and glucosuria.⁷ In fact Itai-itai disease in Japan was one of the first diseases that were directly attributed to cadmium poisoning and brought worldwide attention to the toxicity of cadmium. Because of its high carcinogenicity and toxicity, the industrial usage of cadmium is mainly limited to nickel-cadmium batteries. Cadmium can also be found as an impurity in zinc (0.2-0.4 %). Cadmium at low concentrations can be captured by some cysteine-rich proteins such as metallothioneins.⁸ Some thiol-containing ligands such as glutathione⁹ and N-acetylcysteine^{10,11} are considered as deactivating agents for cadmium toxicity.

1.1.1 The Chemistry of the Hydrated Cd(II) Ion

Cadmium (II) is a highly labile ion with a d^{10} closed shell and because of its d^{10} electronic configuration, cadmium has no preference in coordination number and can form 4-coordinate, 5-coordinate, 6-coordinate or 7-coordinate complexes (distorted pentagonal bipyramidal structures such as $\text{Cd}(\text{BrO}_3)_2 \cdot 2\text{H}_2\text{O}$ ¹² and

$\text{Cd}(\text{O}_3\text{SCH}_2\text{SO}_3)_2 \cdot 3\text{H}_2\text{O}$.¹³ Because of its electronic configuration, cadmium (II) is diamagnetic, making NMR studies possible.

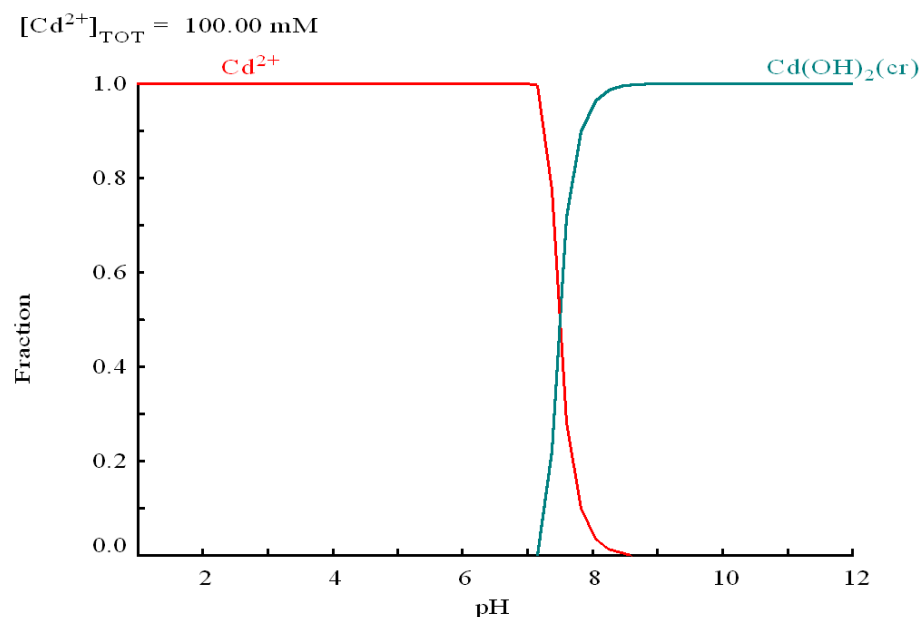


Figure 1-1 Speciation diagrams for Cd(II) in aqueous solution over the pH 1-12 range, at $[\text{Cd}^{2+}] = 100 \text{ mM}$.¹⁴ Solid Cd(II) hydroxide forms above pH = 7.0. (cr = crystal)

1.2 N-Acetylcysteine

Different pharmaceutical and biological uses have been found for N-acetylcysteine and the number of N-acetylcysteine applications in biological systems is growing every year.^{15,16}

1.2.1.1 N-Acetylcysteine as a Pharmaceutical Drug

Recently, several thiol-containing compounds have been used as drugs for different purposes, such as the removal of heavy metals (i.e., cadmium and mercury)

from physiological systems. N-acetylcysteine is one of these compounds. In the case of removing heavy metals, N-acetylcysteine chelates heavy metals through its sulfur and/or oxygen coordination sites. These kinds of coordination can involve two or more N-acetylcysteine groups resulting in a safe, nonreactive, transportable complex that can be easily removed from biological systems.

Cysteine itself is another important biomolecule. A comparison of cysteine and N-acetylcysteine shows some resemblance between these two ligands but they remain different in many respects. The difference between the size of -NH_2 (-NH_3^+) versus -N-COCH_3 and also the ability to form hydrogen bonds NH_2 (-NH_3^+) versus -N-COCH_3 are some of the reasons for the differences between cysteine and N-acetylcysteine. The acetyl group attached to nitrogen in N-acetylcysteine facilitates the absorption of N-acetylcysteine, allowing it to be much more readily absorbed than cysteine, following ingestion.¹⁷ It has been reported that N-acetylcysteine has the ability to coordinate heavy metal ions such as cadmium and lead, extracting them from biological systems.¹⁸

Since 1810, many thiol groups were discovered in both protein and non-protein structures. Following these discoveries, many studies have been conducted to characterize and identify different thiol-containing structures and their mechanism in

living organisms. Figure 1-2 shows some of the examples of biologically important sulfur-containing compounds.

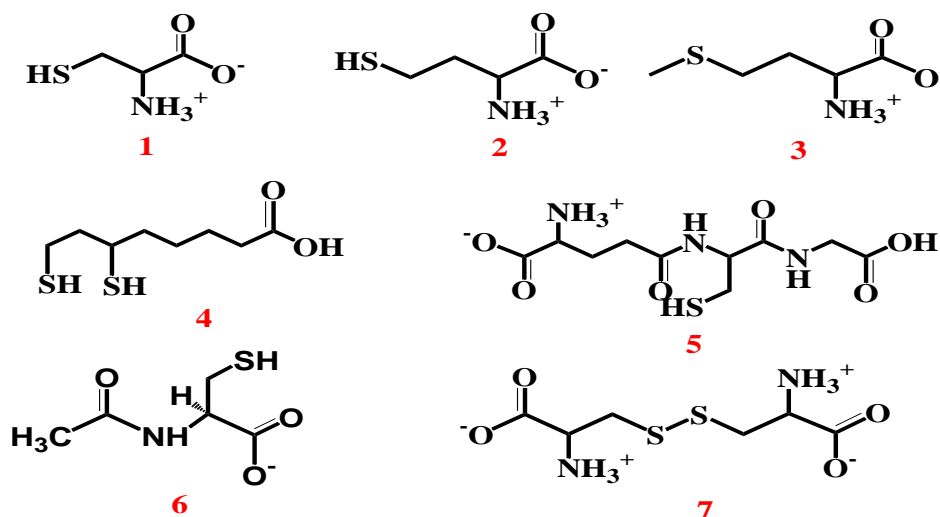


Figure 1-2 Structure of cysteine (1), homocysteine (2), methionine (3), reduced lipoic acid (4), glutathione (5), N-acetylcysteine (6), and cystine (7).

In most cases of metal poisoning, chelating agents are used in the treatment procedure. These agents should be able to form stable, water soluble and non-toxic compounds with the heavy metal that can be excreted from the body.¹⁹ In 1963 N-acetylcysteine (NAC, Figure 1-2(6)) was introduced as a mucolytic agent by Sheffner²⁰ and it has been used ever since. N-acetylcysteine can bind to disulfides in mucoprotein, breaking S-S bond and therefore break the mucoproteins into smaller units that are less viscous.²¹ Currently N-acetylcysteine is used as an antidote for acetaminophen overdose.^{22,23}

1.2.2 *N-Acetylcysteine's Biological Roles*

N-acetylcysteine is also considered as one of the precursors in glutathione biosynthesis^{24,25} that is a well-known antioxidant,²⁶ main defence agent²⁷ and a radical scavenger,²⁸ which prevents oxidative damage in oxidative stress. N-acetylcysteine can protect DNA from damage that can be caused by reactive oxygen species.²⁹ N-acetylcysteine S-conjugate (mercapturic acid) is also the product of the mercapturic acid pathway³⁰ that is the major pathway for degradation of the glutathione adducts. In Figure 1-3 a possible pathway of glutathione production is illustrated. According to some studies,³¹ the presence of N-acetylcysteine can increase the glutathione content.

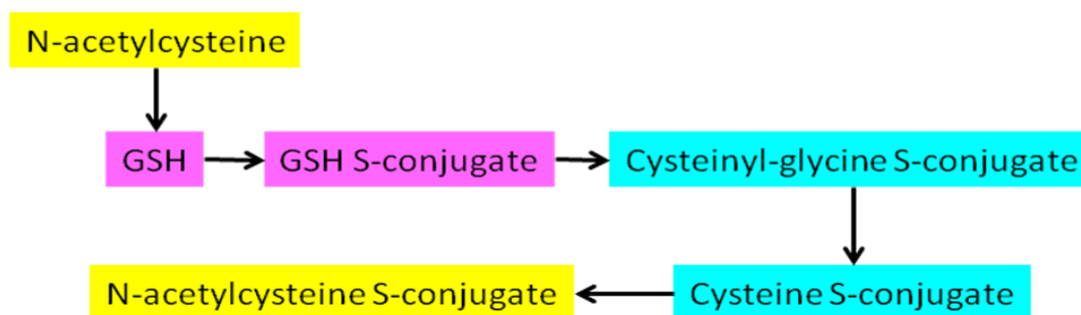


Figure 1-3 Possible mercapturic acid pathway.³²

1.2.3 *N-Acetylcysteine Solution Chemistry*

N-Acetylcysteine has two functional groups (i.e. thiol and carboxylate). The protonation state of the two functional groups of N-acetylcysteine in aqueous solution

depends on the pH of the solution. Figure 1-4 shows the equilibrium between N-acetylcysteine and its ionic forms.

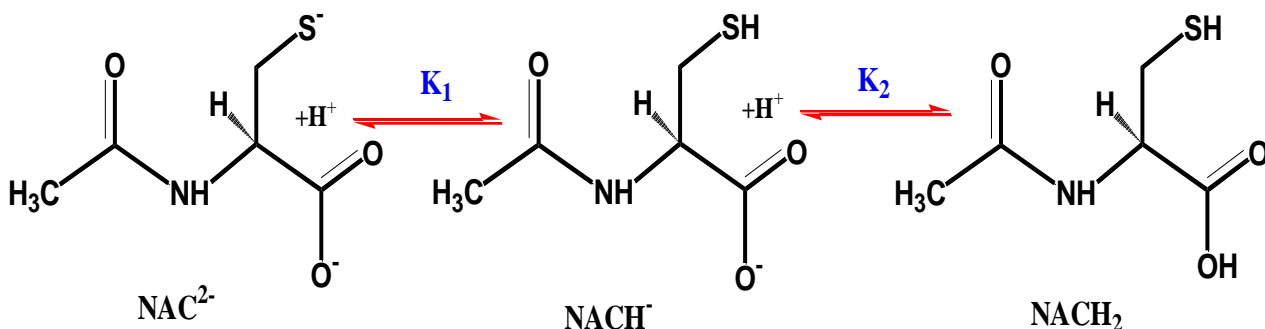


Figure 1-4 Protonation of N-acetyl cysteine functional groups.²¹

$$\text{NAC}^{2-} + \text{H}^+ \rightleftharpoons \text{NACH}^-, K_1 = \frac{[\text{NACH}^-]}{[\text{NAC}^{2-}][\text{H}^+]}, \log K_1 = 9.51 \quad (1-1)$$

$$\text{NACH}^- + \text{H}^+ \rightleftharpoons \text{NACH}_2, K_2 = \frac{[\text{NACH}_2]}{[\text{NACH}^-][\text{H}^+]}, \log K_2 = 3.03 \quad (1-2)$$

$$\text{NAC}^{2-} + 2\text{H}^+ \rightleftharpoons \text{NACH}_2, \beta_2 = \frac{[\text{NACH}_2]}{[\text{NAC}^{2-}][\text{H}^+]^2}, \log \beta_2 = \log K_1 + \log K_2 = 12.54 \quad (1-3)$$

(*I*=0.2M KNO₃, 25°C)²¹

Potentiometric techniques are used in the characterization of different complex formation processes in aqueous solution. By providing the stability constants of different possible complexes using computer based programs such as MEDUSA,¹⁴ these studies can predict the possible speciation in aqueous solution. The distribution of different N-acetylcysteine species is shown in Figure 1-5, where fractions of N-acetylcysteine are

illustrated as a function of pH. Below pH 2, N-acetylcysteine exists as the completely protonated form (NACH_2) (Figure 1-5). Above pH 2, the carboxylic acid begins to deprotonate forming carboxylate (NACH^-) and at $\text{pH} \geq 9$, it becomes completely deprotonated, forming thiolate (NAC^{2-}) (Figure 1-5). The thiolate site basicity is much higher than that of the carboxylate one, which is the reason for having distinct protonation steps at these two pH values (Figure 1-5).¹⁴

T. 0.1

$$[\text{NAC}^{2-}]_{\text{TOT}} = 100.00 \text{ mM}$$

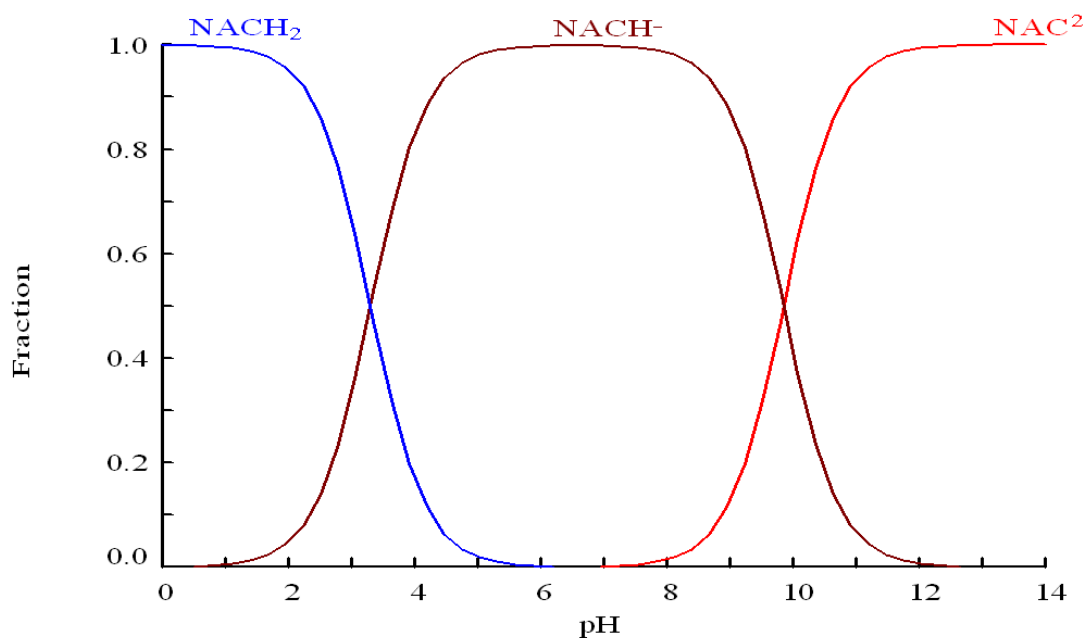


Figure 1-5 Fraction diagram of N-acetyl cysteine as a function of pH in 0.1 M N-acetyl cysteine, based on the reported formation constants.¹⁴

1.2.4 N-Acetylcysteine Coordination Chemistry

The -SH group in N-acetylcysteine is considered to be a more active functional group than the -COOH group to coordinate the late transition metals. Its soft nature according to the hard and soft (Lewis) acids and bases (HSAB) rule makes it a perfect chelator for soft heavy metals such as mercury, cadmium and lead. N-Acetylcysteine also can coordinate through the oxygens of the carboxylate group.³³ According to the existing structures of N-acetylcysteine metal complexes in the crystallography database, there is no evidence of nitrogen coordination in N-acetylcysteine.³³ A survey of metal- N-acetylcysteine complexes with known crystal structures shows that Re(III),³⁴ Os(VI)³⁵ are coordinated through both oxygen and sulfur, while Pt(II),³⁶ Co(III),³⁷ and Ru(II)³⁸ coordinate through sulfur (Figure 1-6).

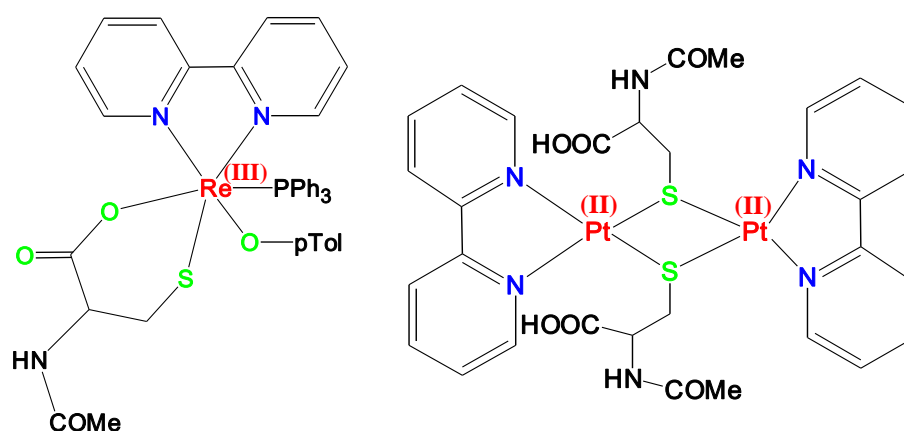


Figure 1-6 Selected structures of N-acetylcysteine metal complexes with different coordination modes for N-acetylcysteine.

1.3 Selenourea and Thiourea Chemistry

Selenourea and thiourea are both among the simplest known diamide structures and they both are of interest especially in the field of inorganic chemistry due to their in complex formation with various metals, especially transition metals

1.3.1 Selenourea and Thiourea Cd(II) Coordination Chemistry

Several studies have been done on the effect of selenium coordination to mercury and cadmium. Since selenium is a soft Lewis base,³⁹ selenium-containing ligands are good candidates for the interaction with soft d^{10} metal ions such as Zn^{2+} , Cd^{2+} , and Hg^{2+} . It has been shown that selenium can protect the body from mercury by preventing mercury's attachment to the thiol groups of proteins.^{40,41} Selenium is considered to be a softer Lewis base than sulfur; therefore, it forms stronger bonds with class b metal ions than sulfur.

The cadmium complexes of thiourea and selenourea recently received a great deal of attention due to their ability to produce semiconducting materials⁴² based on their decomposition.⁴³ Cadmium selenourea and thiourea complexes are possible precursors of semiconductor nanocrystals such as CdSe and CdS.⁴⁴ These complexes also have biological properties as antioxidant⁴⁵ and superoxide radical scavengers. There are some examples of substituted selenourea and thioureas which can be effective superoxidase scavengers as a consequence of their susceptibilities to oxidation.^{46,47}

Selenourea is one of the selenium-containing ligands that have been studied since the 1970s. Although selenourea complexes with metals have been known for some time, to the best of our knowledge there are only a few examples of known crystal structures comparing selenourea complexes to the analogous urea and thiourea complexes. The number of studies of selenourea complexes is small due to the difficulties with the synthesis, stability and lifetime of the complexes. Metal complexes of selenourea, in the solid state, with silver(I),^{48,49} gold(I),⁵⁰ mercury(II),⁴³ cadmium(II),⁴³ zinc(II),⁴³ copper(II),⁵¹ cobalt(II),⁵² and nickel(II)⁵² have been reported. Selenourea metal complexes with known crystal structures are limited to 6 structures including one Ag(I), three Au(I), one Pt(II), and one methylmercury Hg(II).³³ Selenourea has two possible coordination sites (Se and N of the NH₂ group). So far all the crystal structures reported for metal selenourea complexes show that the coordination is through selenium, and that the NH₂ group is not involved in the coordination.

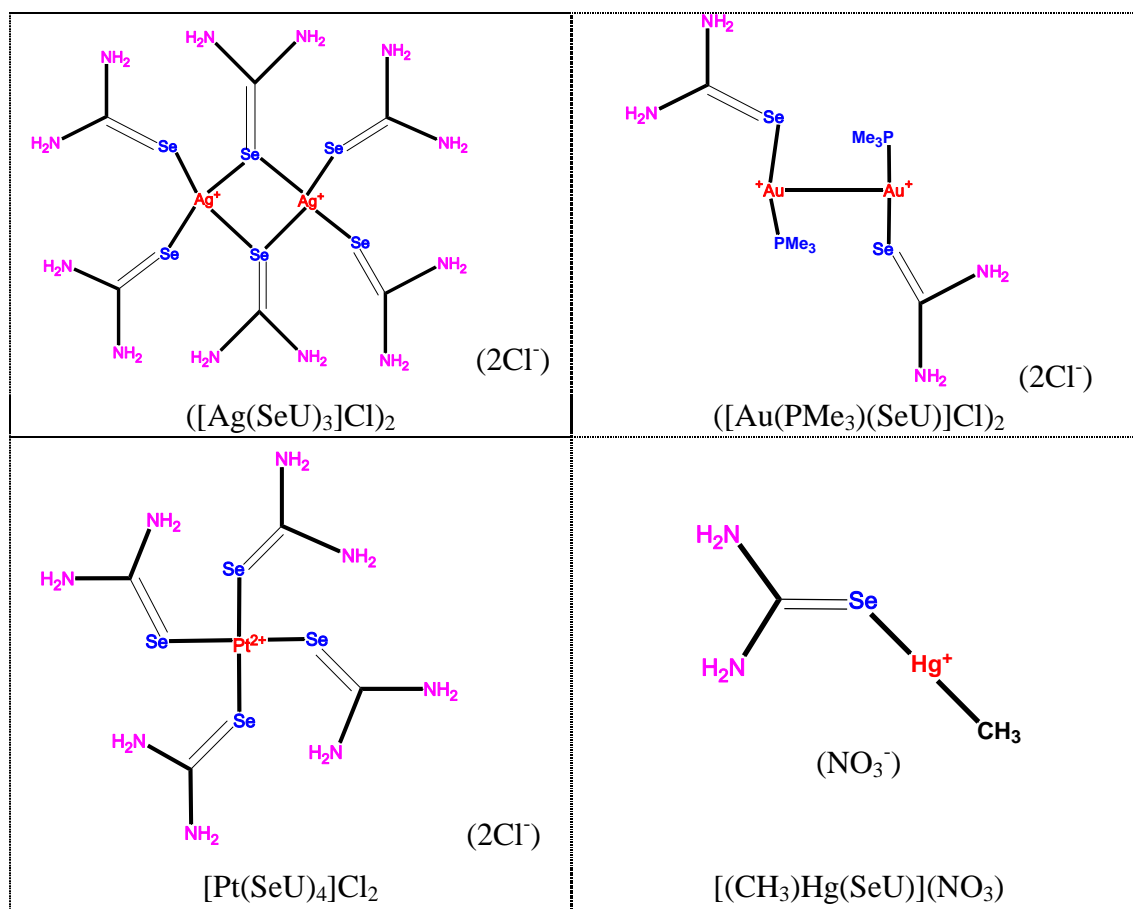
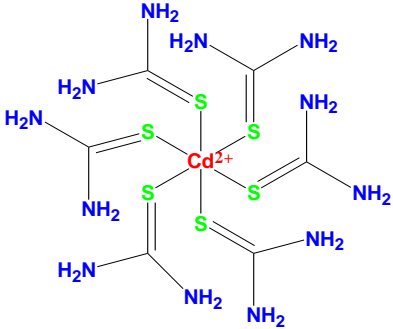
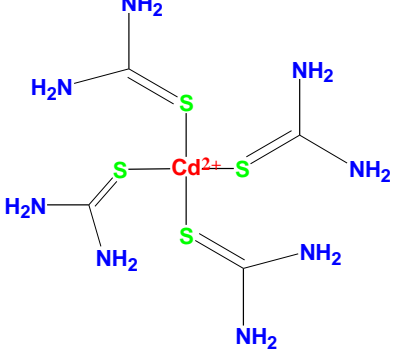
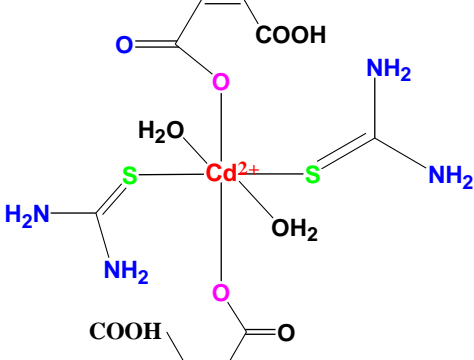


Figure 1-7 Crystal structures of selenourea metal complexes.³³

Thiourea has many applications in medicine (sulfathiazoles, thiouracils, tetramisole, and cephalosporins),⁵³ industry such as textile processing, resin production, silver polishing,⁵⁴ and analytical chemistry.⁵⁵ The final product of thermal decomposition of cadmium-thiourea complexes is CdS, which has been used in semiconductor films.⁵⁶ Thiourea complexes can form with a variety of coordination numbers with cadmium including 4-coordinated tetrahedral and 6-coordinated octahedral species (Table 1-1).⁵⁷ Considering thiourea's planar structure and its symmetry, many studies were dedicated to define metal thiourea crystal structures.⁵⁸

Table 1-1 Some of metal ion complexes with thiourea.³³

Metal Ion	Coordination Number/Site	Structure	Reference
Cd^{2+}	6S		59
Cd^{2+}	4S		60,61
Cd^{2+}	2S/4O		62

1.3.2 Role of Selenium in Biological System and as Drug

The discovery of selenium by Jöns Jacob Berzelius was in 1817; however, it is only recently that a growth in selenium studies has occurred. A few decades ago selenium

was considered to be a toxic element. In 1954 selenium was discovered to be a part of living microorganisms. In the 1970s, several studies^{63,64} led to the discovery of selenium-containing natural ligands such as selenocysteine, and selenomethionine (Figure 1-8). Selenium in large amounts is toxic, but selenium deficiency may also cause various problems such as Keshan disease,⁶⁵ thyroid disorders, psoriasis, cancer and human immunodeficiency virus infection / acquired immunodeficiency syndrome (HIV/AIDS).^{66,67,68,69} Moreover, selenium deficiency can change the balance of other elements and cause an overload of iron in the body.⁷⁰ Selenium is found in some anti-oxidants, and anti-aging products.⁷¹ Ebselen is one of the selenium-containing drugs with antioxidant properties.^{72,73}

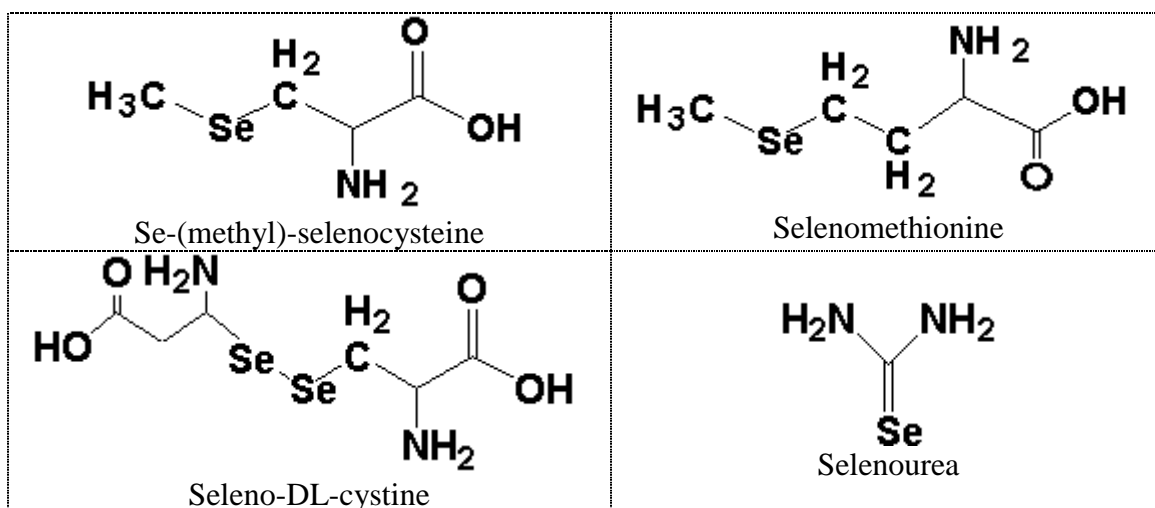


Figure 1-8 Se-containing ligands.

We now know that selenium is an essential trace element for our body and it is involved in some important protective processes such as in the active center of the

enzymes glutathione peroxidase and thioredoxin reductase. Currently about 35 selenoproteins have been discovered in mammals including humans.⁷⁴

Selenocysteine was discovered in the 1980s in *Escherichia coli*⁷⁵ and later was introduced as the 21st aminoacid;⁷⁶ it is considered the most dominant selenium containing species in mammals.⁴ Glutathione peroxidase, which is an enzyme that has antioxidative properties, and protects organs from such damage, is active in the presence of selenocysteine.⁷⁷ Also, several studies have been done on the ability of selenocysteine as a cancer-preventing agent.

Organoselenium compounds are similar to their sulfur analogues. However, selenium compounds are less stable because the carbon-selenium bond (243 kJmol^{-1}) is weaker than the carbon-sulfur bond (272 kJmol^{-1}),⁷⁸ making Se-compounds more difficult to work with. These compounds often decompose upon exposure to UV light,⁷⁹ heat and oxygen to give metallic selenium.

1.4 Spectroscopic Methods

In order to investigate the Cd(II) complex formation with selenourea, thiourea, and N-acetylcysteine, a combination of the following spectroscopic methods was used:

1.4.1 X-ray Absorption Spectroscopy (XAS)

1.4.1.1 Synchrotron Radiation Sources

In the 1950s, the first attempt to study the collision of subatomic particles was undertaken by creating the first particle accelerator in Bevatron (USA).⁸⁰ This led to a Nobel Prize in Physics for Emilio Segrè and Owen Chamberlain in 1959. Later bright radiation that was called synchrotron radiation was observed as a side product of the accelerator. Synchrotron radiation is the electromagnetic radiation that is emitted from charged particles that are travelling in a circular path. This radiation is a very bright and continuous beam that covers a wide range of the electromagnetic spectrum from infrared to hard X-ray. Since this discovery, many attempts have been made to improve the performance of synchrotron facilities in order to get more brilliant radiation, which has resulted in different generations of synchrotron radiation sources. The first generation of storage rings such as SURF II and CESR in the USA were mainly used for high-energy

physics research and a bending magnet was used to force the electrons to travel in a curved path.

The second generation (e.g., NSLS I and NSLS II in the USA) of storage rings were designed specifically as light sources and used MeV energy. The introduction of insertion devices (wiggler and undulator) resulted in the development of third generation storage rings (CLS in Canada, ALS in the USA), which work in the 3 GeV range.

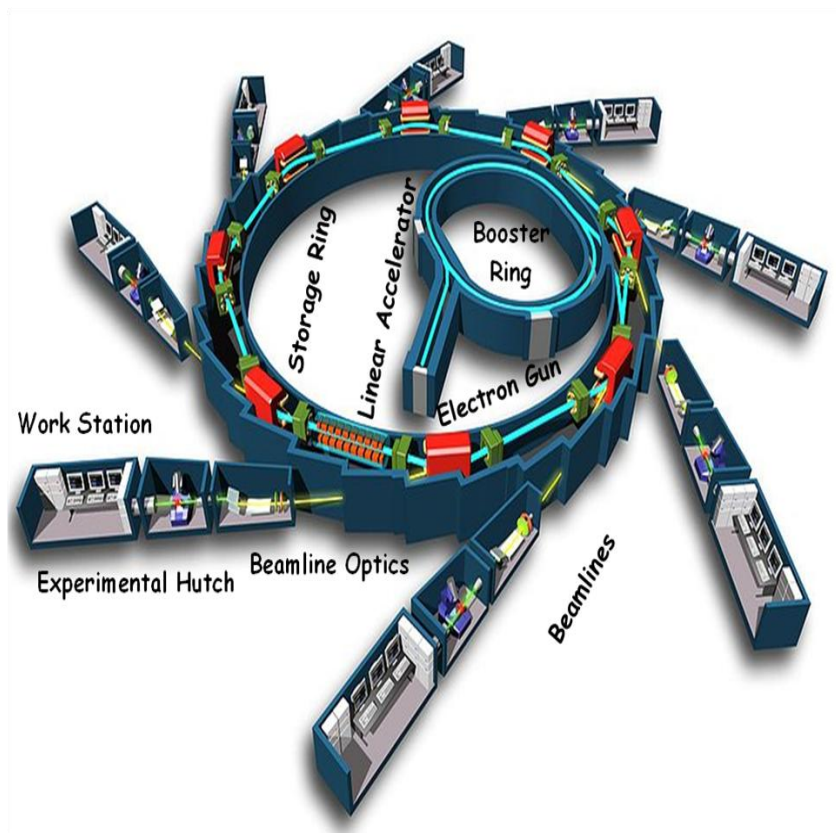


Figure 1-9 Schematics of a typical synchrotron facility with its main components.⁸¹

A storage ring is the synchrotron radiation source. Each storage ring has different components (Figure 1-9) that facilitate the circulation of electron (or positron) current at

the speed of light on a closed circle where the synchrotron radiation can be emitted tangentially to the curved section into channels (also known as beam lines). The storage ring is filled with electron (or positron) current that is produced by an electron gun. Before reaching the accelerator in the resonant cell, a radio frequency power source forces the electron current to travel as a bunch of electrons, which then is accelerated by a linear accelerator (also known as Linac) and/or cyclic accelerator (called booster) in an extremely high vacuum. These electrons gained energy by traveling at the speed of light, by the time that these electrons with high speed slow down when they bent, the radiation released which leaves the ring, and reaches the beam lines and experimental stations.⁸²

Each storage ring consists of curved and straight sections and contains two different types of magnet, namely: 1) a bending magnet (Figure 1-10) which is located in the curved part and forces electrons to travel in a curved trajectory, and 2) insertion devices, which are located in the straight parts of the storage ring. There are two different types of insertion devices, which are called undulators and wigglers. The insertion devices (Figure 1-10) are specially designed magnets that cause electrons to undulate, or wiggle, in order to produce an intense X-ray beam. The produced X-ray beam is 10^{11} times brighter than the X-ray beams produced by conventional methods, such as X-ray tubes.

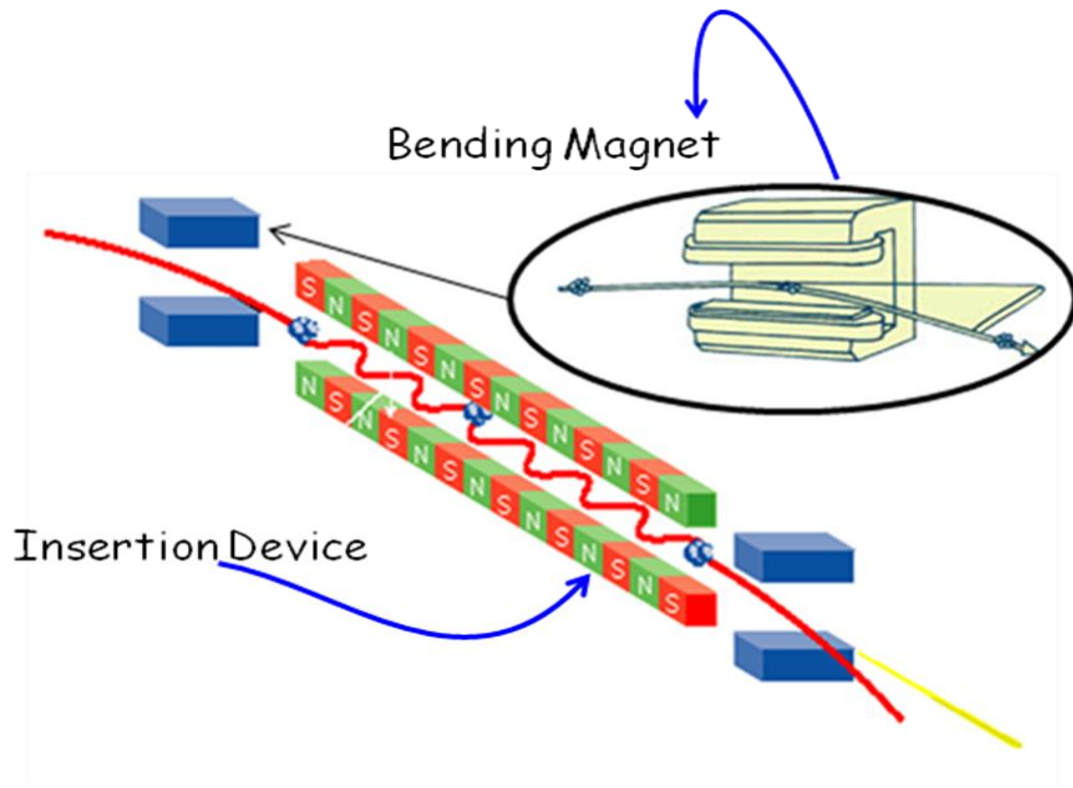


Figure 1-10 Bending magnet and insertion device.^{83,84}

There are also two other components to each storage ring 1) radio frequency (RF) cavities, which accelerate electrons in an electromagnetic field that has a radio frequency oscillation to replenish the energy loss due to its circulation, and 2) a vacuum pump that maintains the vacuum inside the ring.

1.4.1.2 Optic Hutch and Experimental Hutch

As the beam moves tangentially to the curved section, it slows down, generating radiation that reaches the beam lines. Each beam line (Figure 1-11) contains two main components: 1) optic hutch, and 2) experimental hutch, which is also called the end

station. Different optical devices such as mirrors, slits to focus, and monochromator crystals are placed in the optic hutch. Optical mirrors and slits help to focus the beam, and monochromator crystals are used to tune and separate the beam to provide the desired energy and experimental conditions.

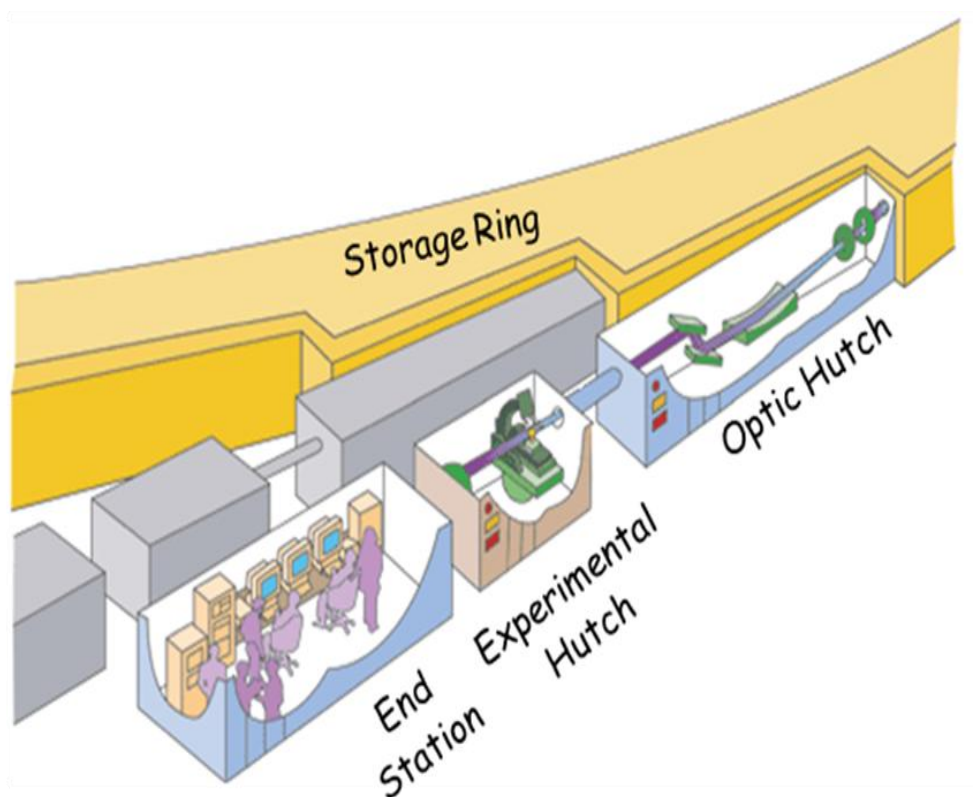


Figure 1-11 A typical beam line in a synchrotron facility.⁸⁵

1.4.1.3 Theory and Principles of X-ray Absorption Spectroscopy

X-ray absorption spectroscopy (XAS) is a modern technique for identifying the local structure around an absorbing atom. The X-ray source for measuring an XAS

spectrum is synchrotron radiation, which excites the core electrons to higher energy levels or to the continuum. Electron excitation from the 1s orbital is called the K-edge, and from 2s or 2p orbitals, is called the L-edge (2s orbital L_I -edge, 2p orbitals L_{II} and L_{III} -edges).⁸⁶ The XAS technique can be used on different physical states of a sample (crystalline or amorphous solid; liquid or gas). Each element has a unique absorption edge. An XAS spectrum consists of different parts (Figure 1-12): pre-edge, the near-edge and the extended region. The near-edge region is called the X-ray absorption near edge structure (XANES) and it is within ± 10 eV of the absorption edge. It contains information about the oxidation state of the absorbing atom and its geometry. The Extended X-ray Absorption Fine Structure (EXAFS) region is from 50 to 1000 eV after the absorption edge and contains information about the nature and number of nearest surrounding atoms (back scatterers) and their average distances from the central absorbing atom with accuracy of ± 0.02 Å, coordination number ($\pm 20\%$), and mean variation around the average bond distance. XAS includes both EXAFS and XANES.⁸⁶

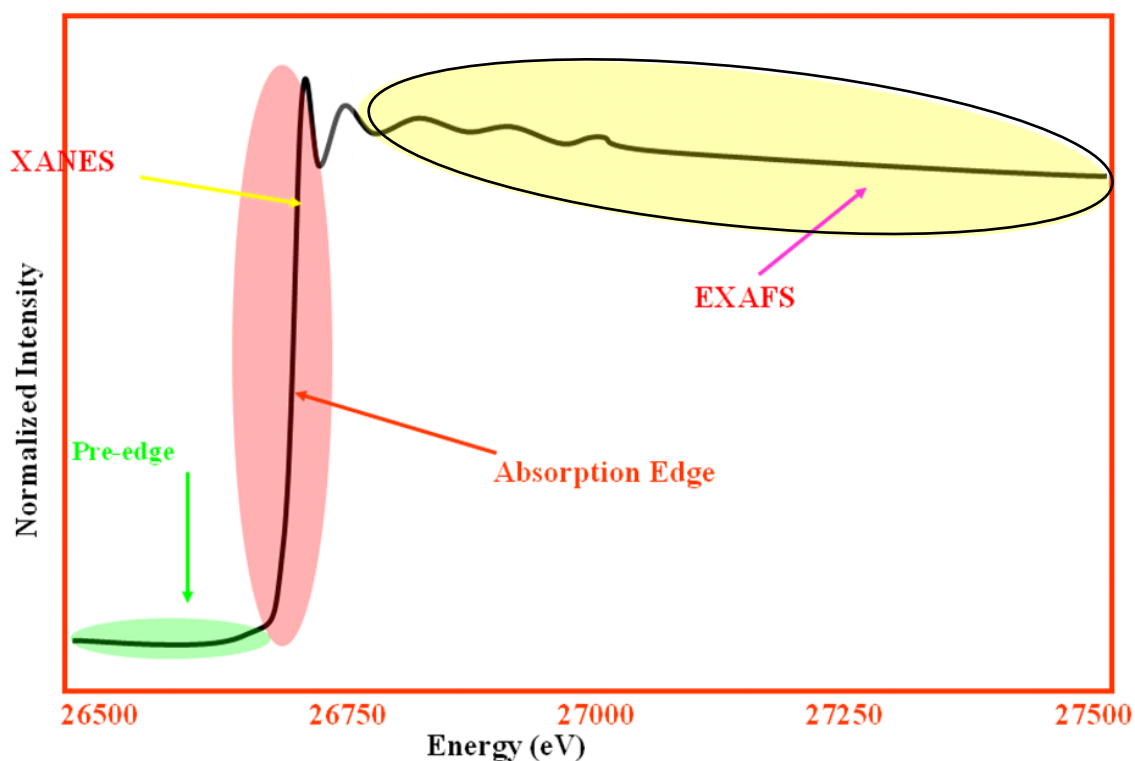


Figure 1-12 An X-ray absorption spectrum, showing the absorption edge, XANES and EXAFS regions for Cd K-edge.

The monochromatic beam with intensity of I_0 hits the sample of thickness x (cm); some part of the beam is absorbed or scattered by the sample and results in emitted radiation with intensity I_1 . Equation (1-4) shows the relationship between I_0 and I_1 , where μ is the linear absorption coefficient (cm^{-1}).

$$\log \frac{I_0}{I_1} = \mu x \quad (1-4)$$

Both I_0 and I_1 are monitored by gas ion chambers (Figure 1-14). Ion chambers can be filled with different gases (He, N_2 , Ar, and Kr) chosen based on the X-ray energy range

that is used. The gas molecules are ionized by the X-ray radiation that passes through the ion chamber and this produces an electric signal that is proportional to the intensity of I_0 or I_1 .

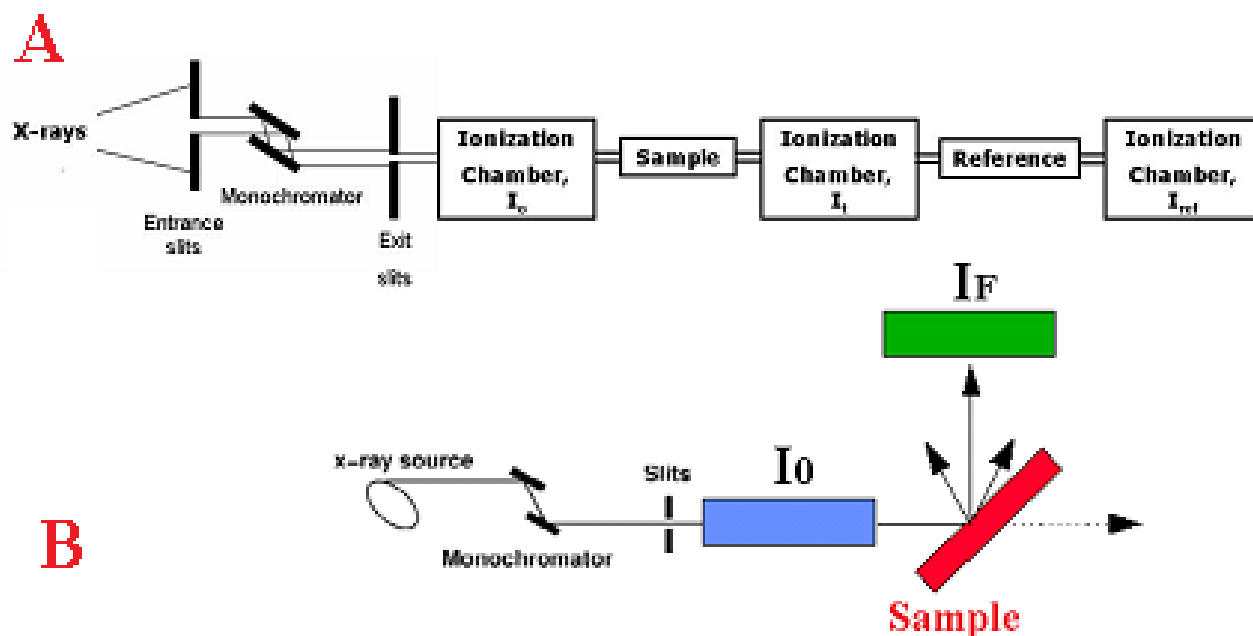


Figure 1-13 (A) A schematic experimental set up with ion chambers⁸⁷ in transmission mode (used for Cd K-edge measurement) and (B) fluorescence mode (used for Cd L_{III}-edge measurement).

The basis of XAS technique is the excitation of a core electron from the K, L or M shell into the continuum which produces a photoelectron. This phenomenon is called the photoelectric effect. The produced photoelectron becomes backscattered between neighboring atoms which can cause constructive and deconstructive interference. If the core hole is filled by an electron from a higher energy shell, relaxation occurs which releases fluorescence emission (Figure 1-14). As it was shown in Figure 1-13 (A), for calibration of energy a metal foil is placed between I_1 and I_2 chambers to allow internal

calibration of the X-ray energy. The x-ray absorption spectrum can be measured in transmission or fluorescence mode, plotting $\log(I_0/I)$ or I_f/I_0 as a function of energy (eV) is used for transmission and fluorescence modes respectively. In Cd K-edge measurements Ar gas was used in all chambers and for L_{III}-edge, He gas was used in I_0 and sample chamber.

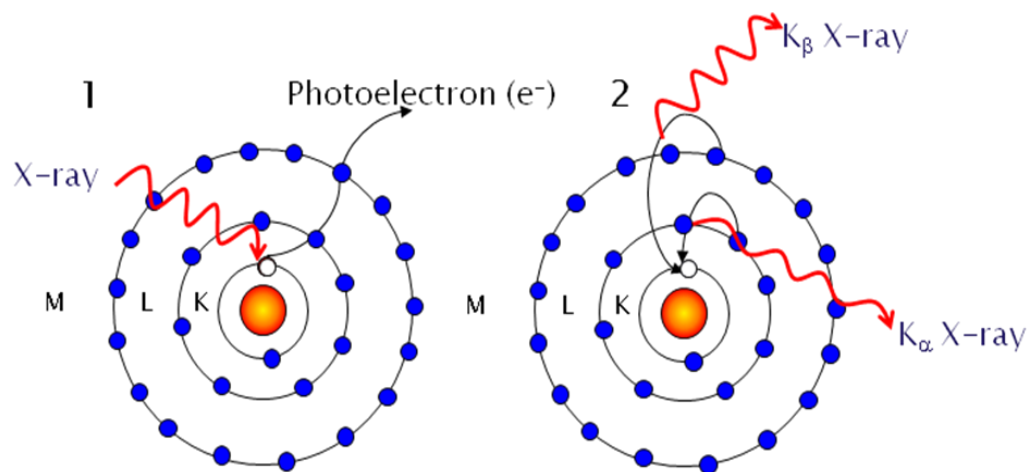


Figure 1-14 The photoelectric effect (left) and X-ray fluorescence (right).

1.4.1.4 Extended X-ray Absorption Fine Structure (EXAFS)⁸⁸ Spectroscopy

As the beam with an appropriate energy which is above the binding energy hits the absorber atom, a core electron is ejected as a photoelectron. It interacts with neighboring atoms and then scatters back to the absorbing atom, resulting in an XAS spectrum (Figure 1-15).

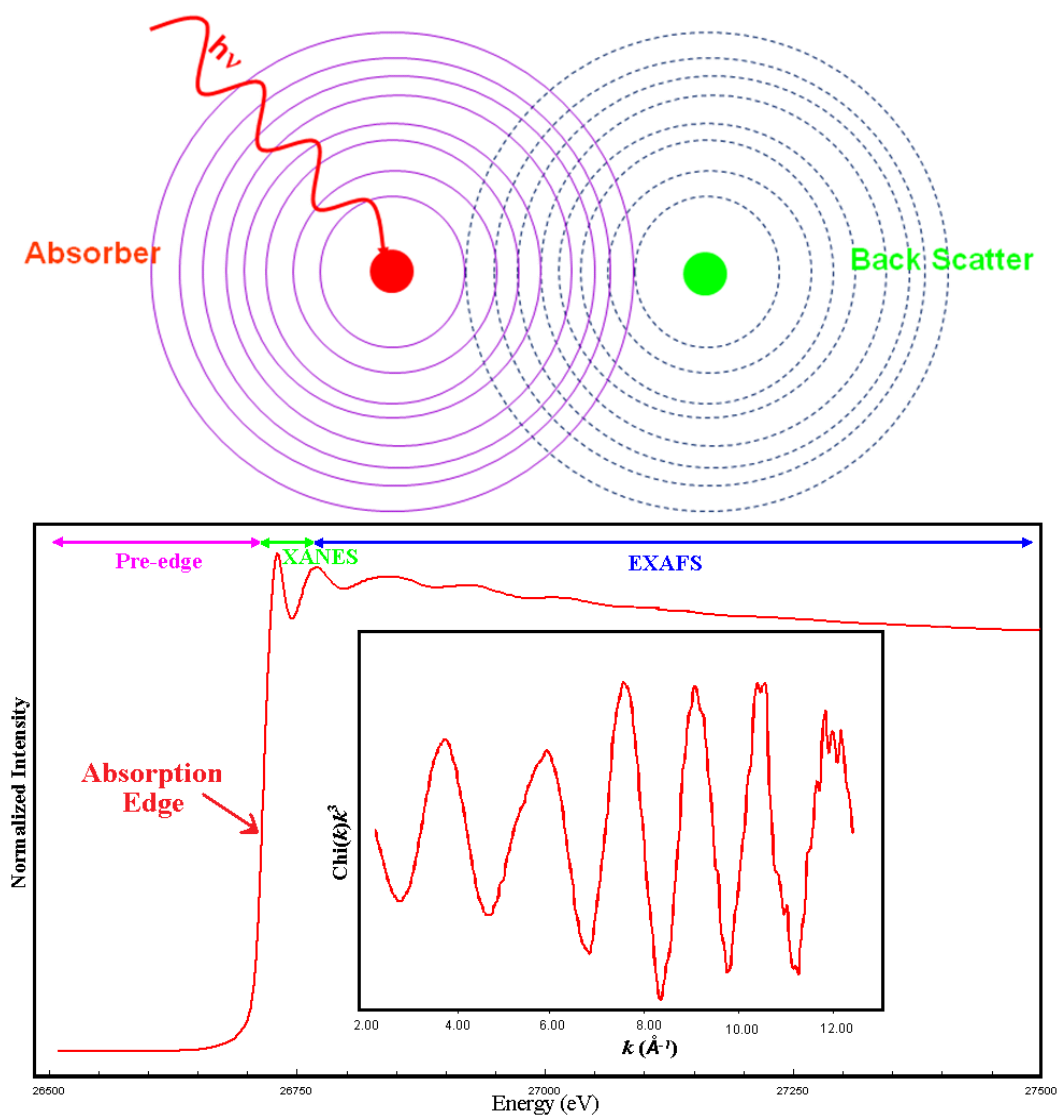


Figure 1-15 XAS spectrum of Cd K-edge of Cd(II)-selenourea solution. The inset shows the k^3 -weighted EXAFS oscillation.

Table 1-2 shows the electron binding energies and fluorescence lines for the K and L shells of Cd.

Table 1-2 Electron binding and X-ray fluorescence energies for Cd.

Binding energy (eV)			
K (1s)	L ₁ (2s)	L ₂ (2p _{1/2})	L ₃ (2p _{3/2})
26711	4018	3727	3538
Fluorescence energy (eV)			
Kα ₁	Kα ₂	Lα ₁	Lα ₂
23173.6	22984.1	3133.73	3126.91
Kα ₁ =L ₃ → K; Kα ₂ =L ₂ → K; Lα ₁ =M ₅ → L ₃ ; Lα ₂ =M ₄ → L ₃			
M ———			
L ₂ ,L ₃ =====			
L ₁ =====			
K ———			

1.4.1.5 EXAFS Equation

The EXAFS oscillation, $\chi(k)$, can be shown by Equations (1-5) and (1-6).⁸⁶

$$\chi_i(k) = \sum_j A_j(k) \sin[\Psi_{ij}(k)], \text{ where } \Psi_{ij}(k) = \sin[2kR_j + \phi_{ij}(k)] \quad (1-5)$$

Or in extended form:

$$\chi(k) = \underbrace{\sum_i \frac{N_i \cdot S_0^2(k)}{k \cdot R_i^2} |f_{\text{eff}}(k)|_i \cdot \exp(-2k^2 \sigma_i^2) \cdot \exp[-2R_i/\Lambda(k)]}_{\text{Amplitude}} \cdot \underbrace{\sin[2kR_i + \phi_{ij}(k)]}_{\text{Phase}} \quad (1-6)$$

where N_i is the number of backscattering atoms at the mean distance (R_i) from absorber

in the i^{th} shell; σ_i^2 is the Debye-Waller parameter, which is related to the mean-square

variation in a Gaussian distribution of distances around (R_i); k is the photoelectron wavevector; $|f_{\text{eff}}(k)|$ is the effective amplitude function; $\phi_{ij}(k)$ is the total phase-shift of the absorber scatterer pair; $\lambda(k)$ is the photoelectron mean free path, and S_0^2 is the amplitude reduction factor.⁸⁹

The EXAFS equation can be divided into two parts: amplitude and phase, based on the effect of each of the above parameters on the EXAFS oscillation. Parameters that affect the amplitude of oscillation are: N_i , R_i , σ_i^2 , k , $|f_{\text{eff}}(k)|$, S_0^2 , and $\Lambda(k)$ the photoelectron mean free path. Those parameters that affect the phase of oscillation are: R_i , k , and $\phi_{ij}(k)$.

1.4.1.6 X-ray Absorption Spectroscopy Data Analysis

Each X-ray absorption spectrum is averaged using the EXAFSPAK suite of programs.⁹⁰ The EXAFS oscillation is extracted using the WinXAS 3.1 program,⁹¹ using a first order polynomial over the pre-edge region to remove any absorption from other edges of the absorber or from other elements. This is followed by normalization of the edge step in order to remove any effects causing by variation in sample concentration or thickness (normalized to 1.0), then conversion of the energy into k -space. Any atomic contribution above the edge is removed by subtracting a 7-segment cubic spline.⁹²

In order to extract structural information from the EXAFS oscillation, a theoretical model $\chi(k)_{\text{theory}}$ should be fitted to the experimental model $\chi(k)_{\text{exp}}$ by curve fitting methods. The model $\chi(k)$ function was generated by means of *ab initio* calculations based on a similar model with the same absorber/backscattering atoms generating $|f_{\text{eff}}(k)|$, $\phi_{ij}(k)$, and $\lambda(k)$ using the FEFF 8.1⁹³ program. For most of EXAFS calculations, the amplitude reduction factor S_0^2 or coordination number N was fixed, allowing R , σ^2 , and ΔE_0 to float. S_0^2 values can be fixed in the range of 0.8 - 1.0.

1.4.1.7 Advantages and Limitations of X-ray Absorption Spectroscopy

Because of its use in the study of very dilute systems, EXAFS spectroscopy has become the technique that is used extensively to study metal ions in biological systems; however, there are some limitations in EXAFS spectroscopy such as accuracy of coordination number, obtaining an average oscillation for all species present in the system, atoms with similar atomic numbers such as C, O and N, or S and Cl cannot be differentiated, and difficulties in separating contribution of light scattering atoms (N/O) from heavier scattering atoms (S) in a molecule.

1.4.2 Nuclear Magnetic Resonance (NMR) Spectroscopy

1.4.2.1 Theory

Each atomic particle (electron, proton, or neutron) possesses intrinsic angular momentum. In nuclei, this property is called nuclear angular momentum (P). The nucleus can be described as a sphere that rotates about an axis. The nuclear angular momentum (P) can be quantized as in Equation (1-7).

$$P = \sqrt{I(I+1)}\hbar \quad (1-7)$$

where I is the angular momentum quantum number (also called nuclear spin) and \hbar is

$\hbar = h/2\pi$, where h is Planck's constant (6.6256×10^{-34} Js). Each nucleus can have

different nuclear angular momentum quantum number ($I = 0, 1/2, 1, 3/2, 2, 5/2, \dots, 6$).

Based on Equation (1-7) nuclei with I equal to zero have no magnetic moment and therefore will not be observed in NMR spectroscopy.

Table 1-3 NMR related properties of some of the nuclei.⁹⁴

Nuclide	Spin I	Natural abundance [%]	Magnetogyric ratio γ [$10^7 \text{ radT}^{-1} \text{ s}^{-1}$]	NMR Frequency [MHz] ($B_0 = 2.3488 \text{ T}$)	Relative receptivity*
^1H	1/2	99.985	26.7522	100.00	5.67×10^3
^{12}C	0	98.9	-	-	-
^{13}C	1/2	1.07	6.7283	25.1450	-
^{77}Se	1/2	7.58	5.1214	19.071523	3.02
^{111}Cd	1/2	12.75	-5.7046	21.201877	7.01
^{113}Cd	1/2	12.26	-5.9609	22.178946	7.69

*Receptivity relative to ^{13}C

Another important factor in NMR spectroscopy is called magnetogyric ratio γ , which is a constant specific for each isotope of an element (Table 1-3) and its value is related proportionally to both P and μ (the magnetic moment) as in Equation (1-8). In NMR experiments, the detection sensitivity of each nuclei depends on γ .

$$\mu = \gamma P \quad (1-8)$$

The larger the γ , the more sensitive the nucleus will be. By combining Equations (1-7) and (1-8), (1-9) is obtained, which shows the relationship of all of the above mentioned NMR parameters.

$$\mu = \gamma \sqrt{I(I+1)}\hbar \quad (1-9)$$

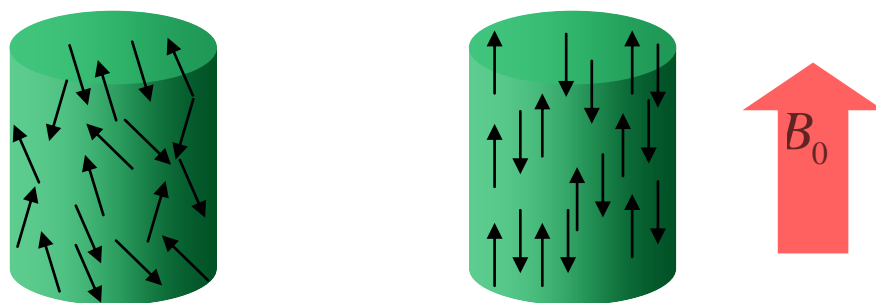


Figure 1-16 The effect of a static magnetic field (B_0) on nuclear spins (modified from [94]).

When a nucleus with a nuclear angular momentum P and magnetic moment μ is placed in a magnetic field (B_0), it will orient according to the magnetic field direction (Figure 1-16), which can be in the same or opposite direction of B_0 .

If the angular momentum component of this orientation along the z-axis is P_z , it is proportional to \hbar . This nuclear orientation in the magnetic field is called directional quantization (Equation (1-10)).

$$P_z = m\hbar \quad 1-10$$

where m can have integer or half-integer values: $m = I, I-1, \dots, -I$

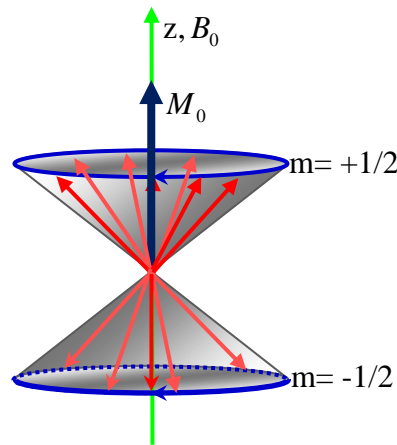


Figure 1-17 Precession of nuclear dipoles with $I = 1/2$ and spin configurations according to applied magnetic field.⁹⁵

For each nucleus, there are $2I+1$ possible orientations and therefore $2I+1$ energy states, as shown in Equation (1-11).

$$E = -m\gamma\hbar B_0 \quad (1-11)$$

For a nucleus such as a proton (1H) or a carbon atom (^{13}C) with $I = 1/2$, there are two possible energy states in the magnetic field, namely $m = +1/2$, which is called the “ α

state” and $m = -1/2$ that is called the “ β state”. The α state is parallel with the B_0 field direction (μ_z) and therefore has a lower energy. The β state has higher energy (Figure 1-18). The energy difference between these two states is shown in Equation (1-12):

$$\Delta E = \gamma \hbar B_0 \quad (1-12)$$

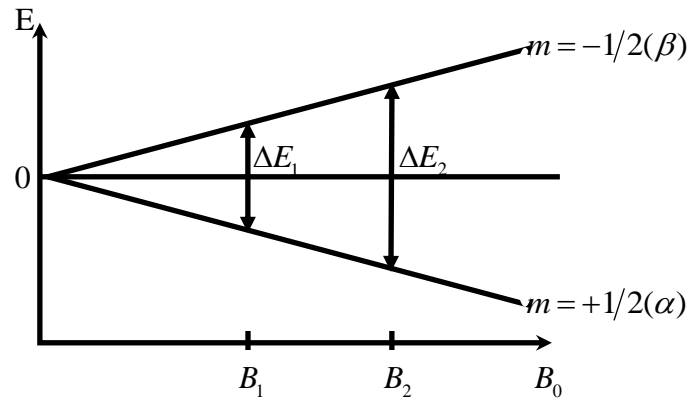


Figure 1-18 The energy difference between two states (α and β) for nuclei with $I = 1/2$ as a function of a magnetic field B_0 .⁹⁵

The distribution of the nuclei between these energy states follows Boltzmann distribution statistics. For a nucleus with $I = 1/2$, the distribution is given in Equation (1-13) :

$$\frac{N_\beta}{N_\alpha} = e^{-\Delta E/k_B T} \approx 1 - \frac{\Delta E}{k_B T} = 1 - \frac{\gamma \hbar B_0}{k_B T} \quad (1-13)$$

where N_α is the number of nuclei in the lower energy state, N_β is the population of nuclei in the higher energy state, k_B is the Boltzmann constant ($1.3805 \times 10^{-23} JK^{-1}$), and

T is the absolute temperature (in Kelvin). For all nuclei, the difference between energies is small and, therefore, the population of these states is almost equal.

In NMR experiments, the nucleus precesses around the z axis of the field in a double cone (Figure 1-17). Since the population in the α state is greater than that in the β state, by adding up all the z components of the nuclear moment in the sample, a macroscopic magnetization (M_0) will be obtained in the same direction as the magnetic field.

In NMR experiments, transitions in both directions between the two α and β states happens by absorbing ($\alpha \rightarrow \beta$) or releasing ($\beta \rightarrow \alpha$) energy in resonance with electromagnetic waves with an exact frequency, ν_1 . The magnetic component of the wave will interact with nuclear dipoles with a reversal of the spin orientation. Since there is a higher population in lower energy states (α), the absorption of the energy is slightly dominant. This absorption is observed as a signal proportional to $(N_\alpha - N_\beta)$ and, is therefore, related to the concentration in the sample. The transition is forbidden if it does not follow the transition rule of $\Delta m = \pm 1$. The condition called “saturation” will occur if radiation makes $N_\alpha = N_\beta$; in this case, they will cancel each other out and no signal will be observed.

In order to achieve resonance, the electromagnetic frequency (ν_1) of the radiation should match the so called Larmor frequency (ν_L) of a nucleus. The Larmor frequency depends on the structure of the sample, the solvent environment and magnetic environment (Equations (1-14) and (1-15)).

$$\Delta E = h\nu_1 \quad (1-14)$$

$$\nu_L = \nu_1 = \left| \frac{\gamma}{2\pi} \right| B_0 \quad (1-15)$$

In order to produce an NMR signal, there are two possible approaches:

- 1) Field Sweep Method, where the magnetic field (B_0) varies with a constant transmitter frequency (ν_1);
- 2) Frequency Sweep Method, in which the magnetic field (B_0) remains constant while the transmitter frequency (ν_1) will change.

Alternatively Pulsed Fourier Transform (PFT) NMR Spectroscopy can be employed and it becomes the basis for all modern NMR experiments. In this method, instead of sweeping the field or frequency, all the nuclei of the same species will be excited at the same time with a radio frequency range which depends on the type of nuclei being measured. A detailed discussion on Pulsed FT-NMR technique is provided in the following section.

1.4.2.2 Pulsed NMR

For a short period of time (on the order of μs), a radio frequency generator will produce a continuous range of frequencies (called a pulse) around the center frequency (ν_1).⁹⁶ Figure 1-19 shows a single NMR pulse. There are several important parameters when collecting each NMR pulse, including delay time between the two consecutive pulses (D_1), pulse duration (τ_p), dead time (D_E), and acquisition time (AQ). The delay time (D_1) allows the magnetic spins to reach equilibrium; this can be measured based on the spin lattice relaxation value (T_1). The delay time is usually $D_1 > 5 T_1$. During the pulse duration (τ_p), a pulse is applied to the sample to excite the nuclei from the α state to the β state. After a dead time (D_E) that allows for the electronics to stabilize, the free induction decay of the magnetization vector is recorded during the acquisition time (AQ) (Figure 1-19).

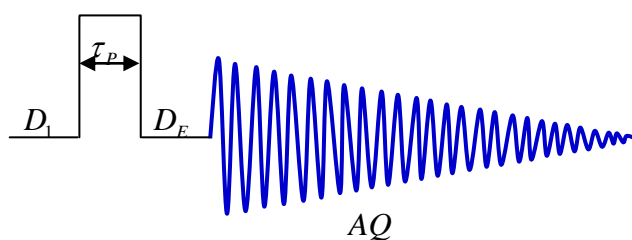


Figure 1-19 A single pulsed NMR experiment (D_1 = delay time, τ_p = pulse duration, D_E = dead time, AQ = acquisition time).⁹⁴

In order to induce an NMR transition, the radiofrequency pulse is applied in the x direction and the magnetic vector of this pulse interacts with nuclear dipoles and macroscopic magnetization (M_0) (Figure 1-17).

1.4.2.3 ^{113}Cd NMR Spectroscopy

Cadmium has two NMR active isotopes (^{111}Cd , and ^{113}Cd) with $I = 1/2$. The ^{113}Cd isotope has a higher relative receptivity (*Receptivity relative to ^{13}C) and therefore is the preferred isotope for NMR experiments. ^{113}Cd is an interesting NMR probe for various reasons: Cd^{2+} , Ca^{2+} , and Zn^{2+} have many similarities in their physical and chemical properties. Additionally, Ca^{2+} and Zn^{2+} are two of the most important biological cations and studying their chemistry is important to answer many questions that scientists have regarding their effect in biological systems. In the past few decades, NMR has become one of the most important tools in biological studies. The problem with these biologically important cations (Ca^{2+} and Zn^{2+}) is that these cations are NMR silent probes. Although zinc and calcium both have NMR active isotopes ^{67}Zn ($I = 5/2$, 4.11% abundance) and ^{43}Ca ($I = 7/2$, 0.145% abundance), their low abundance and the quadrupole effect observed for nuclei with $I > 1/2$, cause broad, weak signals, which makes their NMR measurement difficult and sometimes impossible. Therefore, use of cadmium instead of zinc or calcium has helped scientists to understand the structure of zinc or calcium-containing complexes, when crystallography was not an option. In the ^{113}Cd NMR experiment, using gated decoupling gives a better result.⁹⁷ The ^{113}Cd chemical shift covers around 900 ppm and is very sensitive to any change in coordination

environment and type of donor atom.⁹⁸ It has been reported that Cd(II) octahedral species coordinated to oxygen (CdO_6) gives a signal in the -100 to +150 ppm region, while Cd(II) N-coordinated (CdN_6) appears downfield around +200 to 380 ppm and the most deshielding donor atom, sulfur from +350 to +800 ppm. Selenium coordination will appear in the range between nitrogen and sulfur coordination, i.e. more deshielded than nitrogen and less than sulfur.⁹⁹ There is a general trend of increasing chemical shifts with decreasing coordination number (for the same type of coordination site). The ^{113}Cd chemical shift is also sensitive to the type of donor atom: $\text{S} > \text{Se} > \text{N} > \text{O}$. However there are some exceptions within these ranges, e.g., in the comparative solid state ^{113}Cd NMR study of $\text{Cd}(\text{SeU})_2\text{Cl}_2$ and $\text{Cd}(\text{TU})_2\text{Cl}_2$, the sulfur analogue is around 30 ppm more shielded than the selenium complex.⁴³ This observation was explained based on the fact that selenium has a better overlap with cadmium in the selenourea complex than sulfur in the thiourea complex. The geometry of the complex plays an important role in ^{113}Cd chemical shifts, i.e., the octahedral complexes appear at lower frequencies than tetrahedral complexes.¹⁰⁰ Studies of the effect of coordination environment on ^{113}Cd chemical shifts have been conducted by different groups in the past 30 years. Table 1-4 to Table 1-7 summarize the effect of the coordination environment on the ^{113}Cd chemical shifts.

Table 1-4 ^{113}Cd Chemical shifts of different coordination environments.

Coordination Environment	$\delta(^{113}\text{Cd})(\text{ppm})$	Functional group
CdS_6	177(s)-238, 277 ¹⁰¹	thioxanthate
$\text{CdS}_4\text{N}_{2(\text{s})}$	325 ¹⁰²	thionate
CdS_3O_3	409 ¹⁰⁹	thiol
$\text{CdS}_2\text{N}_2\text{O}_2$	304 - 280 - 245 ¹⁰³ 354 ¹⁰⁴ 178	thioether thioacetate thiosemicarbazone
CdSN_3O_2	262 ¹⁰⁵	thiolate
CdSN_3O_2	281 ¹⁰⁶	thioether
CdS_5	277-325, 377 ¹¹¹	thionate, thiolate
$\text{CdS}_4\text{O}_{(\text{tbp})}$	502 ¹⁰⁹	thiol
CdS_2NO_2	442 ¹⁰⁷	thiolate
CdSN_4	361	thione
$\text{CdS}_{4(T_d)}$	687 ¹⁰⁸ 673 ¹⁰⁹ 586 ¹¹⁰ 445, 414 ¹¹¹ 557 604-670 ^{3,112}	sulfide thiolate thioazoline-2- thione thionate thioazoline-2- thione thiolate
$\text{CdS}_{4(sp)}$	258 ²	thiolate
CdS_3N	637-659 ¹¹³	thiolate
$\text{CdS}_2\text{N}_{2(\text{CDCl}_3)}$	475 ^{114,99}	thionate
$\text{CdS}_2\text{N}_{2(\text{s})}$	421-426 ¹⁰¹	
CdS_2NO	483 ¹¹⁵	thiolate
$\text{CdN}_3\text{O}_{4(\text{pentagonal bipyrimidal})}$	61 _(s) - 4.9 _(Sol.) ¹¹⁶	
$\text{CdN}_2\text{O}_{5(\text{pentagonal bipyrimidal})}$	34 _(s) ¹⁰⁰	
CdN_6	380 ¹¹¹ 272 _(s) , 238 ¹¹¹	
$\text{CdN}_{6(\text{CDCl}_3)}$	274 ⁹⁷ , 287 _(1 M) ⁴ 198-221 ⁴	

$\text{CdN}_{6(s)}$	230-238 ¹¹⁷	
$\text{Cd N}_4\text{O}_2$	122, 172 _(aq.) ¹¹⁸ 51 _(s) ⁵	
$\text{CdN}_4\text{O}_{2(\text{DMF/MeOH})}$	66 ¹⁰⁰	
CdN_2O_4	117, 107, 97 ¹¹¹	
$\text{CdN}_{5(\text{square pyramid})}$ $\text{CdN}_{5(\text{CDCl}_3)}$	432 418-498 ¹¹⁹	
$\text{Cd N}_{4(\text{sp})}$ $\text{CdN}_{4(\text{CDCl}_3)}$	399 ¹²⁰ 298-303 ¹⁰⁰	
CdO_8	-100 ¹¹¹	
CdO_7	-31 to -58 ¹¹¹	

Table 1-5 ¹¹³Cd Chemical shifts of different selenium coordination number.

Coordination Environment	$\delta(^{113}\text{Cd})(\text{ppm})$	Compound
CdSe_4	597 587 ¹²¹	$[\text{Cd}(\text{SePPh}_3)_4]^{2+}$ $[\text{Cd}(\text{SeP}(\text{C}_6\text{H}_{11})_3)_4]^{2+}$
CdSe_3	505 (198 K) 515 (213 K) ¹²¹	$[\text{Cd}(\text{SeP}(o\text{-C}_6\text{H}_4\text{Me})_3)_3]^{2+}$ $[\text{Cd}(\text{SeP}(\text{C}_6\text{H}_{11})_3)_3]^{2+}$
CdSe_2	195 ^{121*} (198 K)	$[\text{Cd}(\text{SeP}(o\text{-C}_6\text{H}_4\text{Me})_3)_2]^{2+}$
CdSe_4 (selenol)	541 ¹²²	$[\text{Cd}(\text{SePh})_4]^{2-}$
CdSe_4 (tetrahedral)	545 ¹⁰⁸ 541-590 ¹²²	CdSe $[\text{Cd}(\text{SePh})_4]_{\text{sol.}}^{2-}$
CdSe_2N_4 (solid)	472,460 ¹²³	$\text{Cd}(\text{Se}-2,4,6\text{-}^i\text{Pr}_3\text{-C}_6\text{H}_2)_2$ (bpy)
CdSe_3	250 ¹²⁴	$[\text{Cd}(\text{SeC}\{\text{O}\}\text{Tol})_3]^-$

* values recorded in liq. SO_2 and relative to 4M $\text{Cd}(\text{NO}_3)_2$

Table 1-6 ^{113}Cd coupling constants.

J	Compound	Range (Hz)
$^2J(^{113}\text{Cd}^1\text{H})$	Alkyl ^{125,126}	49-90
$^3J(^{113}\text{Cd}^1\text{H})$	O-alkyl, alkyl ^{125,126}	6-70
$^1J(^{113}\text{Cd}^{15}\text{N})$	TPP ^{*127,128} , amine ¹²⁹	75-150
$^1J(^{113}\text{Cd}^{17}\text{O})$	$[\text{Cd}(\text{OD}_2)_6]^{2+}$ ¹³⁰	248
$^1J(^{113}\text{Cd}^{77}\text{Se})$	$[\text{Cd}(\text{SePh})_m(\text{SPh})_{4-m}]^{2-}$ ¹²²	46-126
$^2J(^{113}\text{Cd}^{113}\text{Cd})$	Metallothionein ¹³¹	30-50

One of the characteristics of ^{113}Cd NMR is its sensitivity towards any change in the measurement condition: the ^{113}Cd chemical shift can change drastically by changing solvent,⁹⁷ temperature or concentration (Table 1-7 and Table 1-8).

Table 1-7 The effect of solvent on the ^{113}Cd chemical shift of 1.0 M $\text{Cd}(\text{CH}_3)_2$. (adapted from [97]). All chemical shifts were referenced to $\text{Cd}(\text{CH}_3)_2$ where $\delta_{\text{Cd}(\text{CH}_3)_2(\text{neat})} = \delta_{0.1\text{M}\text{Cd}(\text{ClO}_4)_2} + 642.93$. Positive values mean more shielding here.

Solvent	$\delta_{^{113}\text{Cd}}$, ppm	Solvent	$\delta_{^{113}\text{Cd}}$, ppm
$\text{Cd}(\text{CH}_3)_2$	0.0	Ethyl acetate	33.25
THF	66.65	Pyridine	28.26
Diglyme	65.93	Diethyl ether	5.32
N,N-DMF	55.18	Benzene	-2.03
Dioxane	50.77	Toluene	-2.03
Acetone	40.94	Methylene chloride	-3.13
acetonitrile	37.38	Cyclopentane	-33.08
Methyl formate	36.29	Cyclohexane	-34.67

* meso-tetraphenylporphyrin

Table 1-8 The effect of concentration on the ^{113}Cd chemical shift of $\text{Cd}(\text{ClO}_4)_2$ in water.

(adapted from [98]). Positive values mean more shielding here. All chemical shifts were referenced to 0.1M $\text{Cd}(\text{ClO}_4)_2$ in water.

$\text{Cd}(\text{ClO}_4)_2$ Concentration (M)	$\delta_{^{113}\text{Cd}}$ (ppm)
0.1	0.0
0.5	0.75
1.0	2.0
1.5	3.6
2.0	5.9
2.5	9.1
3.0	13.4

1.4.2.4 Advantages and Limitations of NMR Spectroscopy

NMR is a very effective technique for studying the coordination chemistry and geometry around a metal center. The chemical shift values are an important piece of information in investigating the metal coordination environment. As mentioned before ^{113}Cd NMR is sensitive to the change of solvent (Table 1-7), and temperature. As the temperature changes the equilibrium among different species, and also the rate of chemical exchange among them, affect the observed chemical shift. Although NMR solves many problems in modern chemistry, it has some limitations too. The best type of nuclei for NMR studies are those with nuclear spin $I = 1/2$. For nuclei with $I > 1/2$, there is always the quadrupole effect and line broadening problem. Additionally nuclei with $I = 0$ are not NMR active. The other problem is the concentration issue, especially for isotopes with low abundance.

Chapter Two: Comparative Study of Cadmium Complex Formation with Selenourea and its Analogue Thiourea

2.1 Introduction

In recent years many studies were focused on the complex formation of heavy metals such as cadmium with different ligands especially those of biological importance. Cadmium is considered as one of the environmental pollutants,¹³² at the same time it is one of the precursors in semiconductor production. Complex formation between cadmium (II) and selenourea or thiourea has attracted a great deal of interest in the field of nanoparticle chemistry. Cadmium (II)-selenourea has been used in the past decade as the precursor in the making of cadmium selenide (CdSe) quantum dots.⁴⁴

Considering the similarities and dissimilarities between thiourea and selenourea, their complex formation with cadmium (II) is the focus of this part of this thesis. The biological importance of selenoureas and thioureas as antioxidants¹³³ and radical scavengers⁴⁷ also makes them interesting ligands for investigation.

There are few articles available on selenourea-Cd(II) coordination. In a polarographic study, it was shown that selenourea can react more strongly than selenomethionine with cadmium (II) ions.⁷¹ This study shows that there is a solubility limit to cadmium-selenourea complexes in water. In the presence of 0.01 mM Cd(II) with selenourea concentrations higher than 1 mM, a Cd(II)-selenourea complex with limited solubility is formed.

In another study, vibrational spectra of $[\text{Cd}(\text{SeU})_2]\text{X}_2$, $\text{X} = \text{Cl}, \text{Br}, \text{I}$ ¹³⁴ complexes were discussed, showing that low frequency Cd-Se stretching ($<200 \text{ cm}^{-1}$) appears rather close to Cd-X stretching frequencies. The coordination chemistry of cadmium chloride with

selenourea and thiourea was studied using multinuclear NMR techniques and labeled ligands, which showed the formation of $\text{Cd}(\text{SeU})_2\text{Cl}_2$ and $\text{Cd}(\text{TU})_2\text{Cl}_2$, respectively.⁴³ The structure of a selenourea analogue with Cd(II), $[\text{Cd}(\text{dmise})_4][\text{PF}_6]_2$ (dmise = 1,3-dimethyl-2(3H)-imidazoleselone), showed the existence of a CdSe_4 core with average Cd-Se bond distance of 2.623 Å.⁴² None of the above mentioned studies provide direct information about the coordination geometry of cadmium (II) selenourea complexes.

Thermal decomposition of Cd(II) thiourea complexes are used as a precursor to make CdS semiconductors.⁵⁶ Unlike selenourea, there are many known crystal structures of thiourea with different metals, including 4-coordinated and 6-coordinated cadmium crystal structures.³³

In this chapter, complex formation between cadmium (II) and selenourea (SeU) and thiourea (TU) complexes in methanol solution is detailed. The study was carried out using a combination of methods: Cd K-edge XAS, ^{113}Cd NMR. Different solvents were chosen for these syntheses, such as water, 1-butanol, and methanol. Selenourea can rapidly go through redox reactions in water and decompose. H_2CN_2 , Se^{2-} , and HSe^- are the products of this decomposition.¹³⁵ Eventually methanol was chosen as the best solvent because of the stability of selenourea in methanol, as well as the ease of measuring low temperature NMR spectra.

2.2 Experimental Methods

2.2.1 Sample Preparation

Selenourea, thiourea, $\text{Cd}(\text{NO}_3)_2 \cdot 4\text{H}_2\text{O}$, triflic acid, methanol and methanol- d_4 were purchased from Sigma-Aldrich and used without further purification. All sample preparations were carried out under inert Ar atmosphere in a glove box using dried, deoxygenated methanol to avoid oxidation and decomposition of selenourea. Although thiourea solutions were more stable, the process of synthesis remained the same as the selenourea solutions. Methanol was dried over 4 Å molecular sieves (Sigma-Aldrich) and then distilled twice from magnesium turnings under Ar until the excess amount of magnesium was left unreacted.

2.2.2 Synthesis of $\text{Cd}(\text{CF}_3\text{SO}_3)_2$

Dehydrated cadmium(II) triflate salt was prepared following an earlier report.¹³⁶ 6 M triflic acid solution was added to freshly prepared $\text{Cd}(\text{OH})_2$, which was synthesized prior to the addition of triflic acid by reaction of $\text{Cd}(\text{NO}_3)_2$ and NaOH in water, under a fume hood at 40°C until all $\text{Cd}(\text{OH})_2$ was dissolved. Then the solution was heated to 60°C to reduce the volume to ~ 5mL, which was followed by cooling in the refrigerator in order to crystallize. The crystals were filtered and dried in oven at 160°C for 24 hrs, yielding a white dehydrated powder, $\text{Cd}(\text{CF}_3\text{SO}_3)_2$. The thermal gravimetry (TG) data did not show any mass loss between 25 and 500°C, which confirmed the absence of any coordinated water molecules.

2.2.3 Synthesis of Cd(II)-selenourea 100 mM solutions in methanol

Cd(II)-selenourea solutions were prepared in O₂ – free dry methanol using Cd(CF₃SO₃)₂ as the starting material, with a total cadmium concentration of 100 mM, and different SeU / Cd(II) ratios of 1.0 (A₁), 2.0 (B₁), 3.0 (C₁), 4.0 (D₁), and 5.0 (E₁) (see Table 2-1). All syntheses were carried out inside a glove box to avoid selenourea decomposition. An excess amount of ligand was used (L / M > 4.0) to ensure formation of a Cd(II) complex with the highest feasible number of selenourea ligands coordinated.

2.2.4 Synthesis of Cd(II)-thiourea 100 mM solutions in methanol

Cd(II)-thiourea solutions containing C_{Cd(II)} ~ 100 mM were synthesized by dissolving thiourea (1.0 - 10.0 mmol) in O₂ – free dry methanol, followed by the addition of Cd(CF₃SO₃)₂ (1.0 mmol) while stirring. Seven solutions with TU / Cd(II) molar ratios of 1.0 (A₂), 2.0 (B₂), 3.0 (C₂), 4.0 (D₂), 5.0 (E₂), 8.0 (F₂), and 10.0 (G₂) were prepared (see Table 2-2)

Table 2-1 Composition of SeU / Cd(II) solutions in MeOH.

Cd(II)-SeU solution	SeU / Cd(II) mole ratio	C _{Cd(II)} mM	C _{SeU} mM
A ₁	1.0	100	100
B ₁	2.0	100	200
C ₁	3.0	100	300
D ₁	4.0	100	400
E ₁	5.0	100	500

Final volume = 10 mL

Table 2-2 Composition of TU / Cd(II) solutions in MeOH.

Cd(II)-TU solution	TU / Cd(II) mole ratio	C_{Cd(II)} mM	C_{TU} mM
A ₂	1.0	100	100
B ₂	2.0	100	200
C ₂	3.0	100	300
D ₂	4.0	100	400
E ₂	5.0	100	500
F ₂	8.0	100	800
G ₂	10.0	100	1000

Final volume = 10 mL

2.2.5 Synthesis and Crystal Structure of $\text{cis-[Cd(TU)}_2(\text{OH}_2)_4]^{2+}$ and $\text{fac-[Cd(TU)}_3(\text{OH}_2)_3]^{2+}$ disulfate

Thiourea and $\text{CdSO}_4 \cdot 8/3(\text{H}_2\text{O})$ with molar ratio of (3.8 : 1.0) were added to 10 ml of hot water, after slow evaporation of the solution at constant temperature (35 °C) following a reported procedure for preparing $\text{Cd(TU)}_3(\text{SO}_4)$.¹³⁷ A mixture of colorless crystals, mainly consisting of $[\text{Cd(TU)}_3(\text{SO}_4)]$ and minor amount of $\text{cis-[Cd(TU)}_2(\text{OH}_2)_4]$ and $\text{fac-[Cd(TU)}_3(\text{OH}_2)_3]$ disulfate complexes were obtained. Figure 2-1 shows the resolved crystal structure for octahedral species $\text{cis-[Cd(TU)}_2(\text{OH}_2)_4]^{2+}$ and $\text{fac-[Cd(TU)}_3(\text{OH}_2)_3]^{2+}$ disulfate.¹³⁸

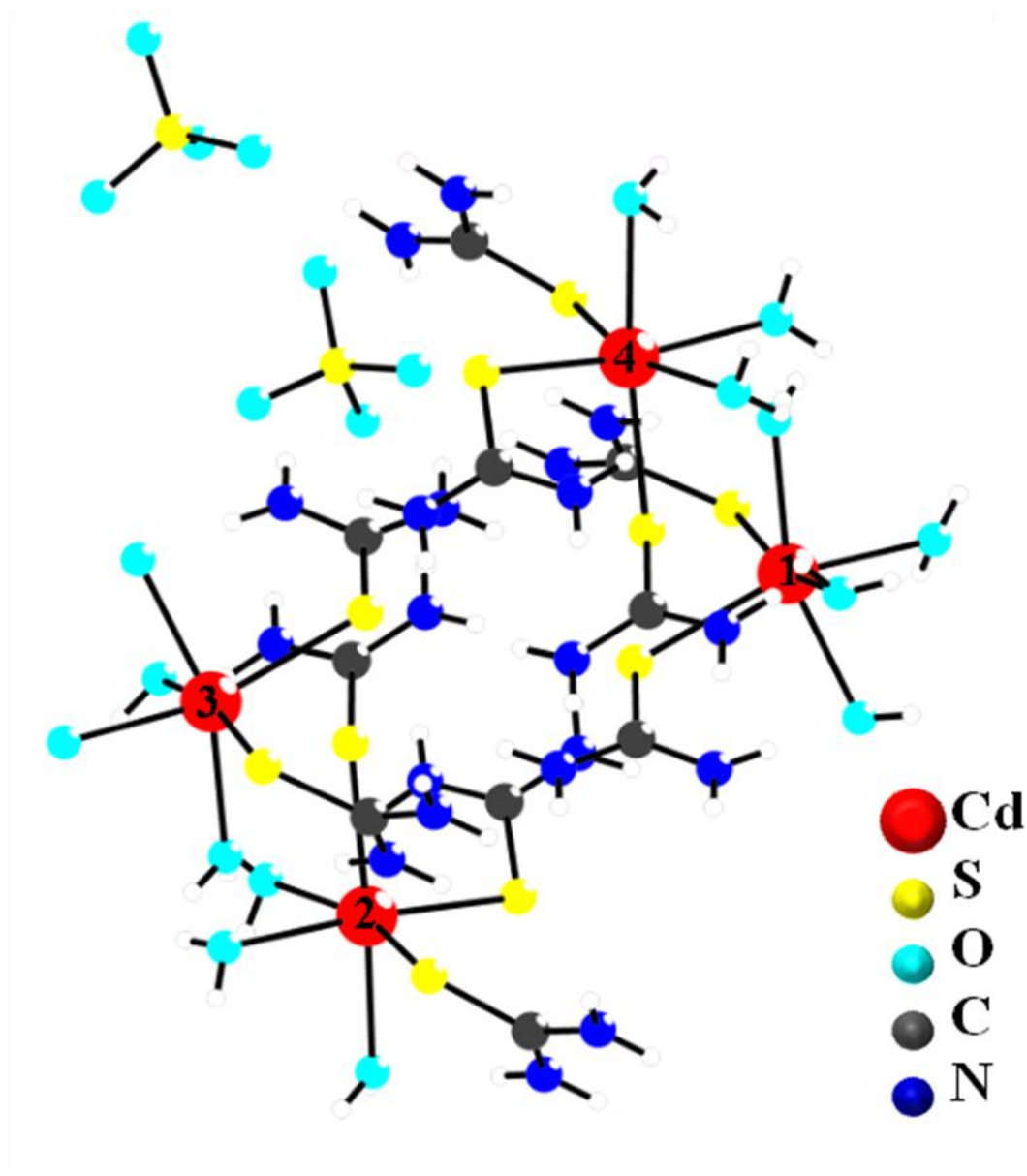


Figure 2-1 a) The molecular structure of *cis*-[Cd(TU)₂(OH₂)₄]²⁺ and *fac*-[Cd(TU)₃(OH₂)₃]²⁺ disulfate with Cd-O and Cd-S bond distances in the ranges of 2.323(8) - 2.421(9) Å and 2.580(4) - 2.599(4) Å respectively for Cd1 and Cd2 atoms in bis(thiourea) complex, *cis*-[Cd(TU)₂(OH₂)₄]²⁺, and 2.303(7) - 2.480(10) Å and 2.559(4) - 2.706(3) Å for Cd3 and Cd4 atoms in In the tris(thiourea) complex, *fac*-[Cd(TU)₃(OH₂)₃]²⁺ respectively¹³⁸

Table 2-3 Crystal data and structure refinement for *cis*-[Cd(TU)₂(OH₂)₄]²⁺ and *fac*-[Cd(TU)₃(OH₂)₃]²⁺ disulfateComplex

Empirical formula	C ₁₀ H ₆₈ Cd ₄ N ₂₀ O ₃₀ S ₁₄	
Formula weight	1847.28	
Temperature	173(2) K	
Wavelength	0.71073 Å	
Crystal system	Monoclinic	
Space group	Pc	
Unit cell dimensions	a = 10.9941(3) Å	α = 90°.
	b = 11.7602(3) Å	β = 98.9169(12)°.
	c = 24.0100(5) Å	γ = 90°.
Volume	3066.80(13) Å ³	
Z	2	
Density (calculated)	2.000 Mg/m ³	
Absorption coefficient	1.936 mm ⁻¹	
F(000)	1848	
Crystal size	0.07 x 0.06 x 0.05 mm ³	
Theta range for data collection	2.44 to 25.00°.	
Index ranges	-12 ≤ h ≤ 13, -13 ≤ k ≤ 13, -	
	28 ≤ l ≤ 28	
Reflections collected	16186	
Independent reflections	9995 [R(int) = 0.0367]	
Completeness to theta = 25.00°	99.3 %	
Absorption correction	Multi-scan method	
Max. and min. transmission	0.9094 and 0.8764	
Refinement method	Full-matrix least-squares on F ²	
Data / restraints / parameters	9995 / 44 / 675	
Goodness-of-fit on F ²	1.072	
Final R indices [I > 2σ(I)]	R1 = 0.0444, wR2 = 0.0840	
R indices (all data)	R1 = 0.0538, wR2 = 0.0918	
Absolute structure parameter	0.18(5)	
Largest diff. peak and hole	0.774 and -0.601 e.Å ⁻³	

2.2.6 ^{113}Cd NMR Spectroscopy

^{113}Cd NMR spectra of Cd(II)-selenourea and thiourea solutions were recorded at a resonance frequency of 88.6 MHz, using a Bruker DRX400 spectrometer (9.4 Tesla). The NMR spectrum for Cd(II)-selenourea SeU / Cd(II) = 2.0 solution was measured at different temperature (203K, 213K, and 223K); some of the peaks became broader as the temperature increased from 203K to 213K and disappeared at 223K. Therefore, the temperature was set at 203K for all measurements unless otherwise stated. Temperatures were calibrated using the ^1H NMR spectrum of MeOH.¹³⁹ All solutions contained ~ 70 % dry methanol and ~ 30 % dry methanol- d_4 . The ^{113}Cd chemical shifts were calibrated using as external reference 0.1 M $\text{Cd}(\text{ClO}_4)_2 \cdot 6\text{H}_2\text{O}$ in D_2O , resonating at 0 ppm at room temperature. Figure 2-2 shows the effect of different solvents and temperatures on the ^{113}Cd NMR spectra of 0.1 M $\text{Cd}(\text{ClO}_4)_2 \cdot 6\text{H}_2\text{O}$ solutions.

^{113}Cd solid state NMR spectra of standard were collected at a resonance frequency of 76.2 MHz, using a Bruker AMX300 spectrometer (7.2 Tesla). The spectrometer equipped with a BL4 MAS double-resonance broadband probe at resonance frequencies of 66.59 MHz for ^{113}Cd nuclei. The samples were packed into 4 mm ZrO rotors with different spin rate. Spectra were collected using a 4 ms contact time, and 10 s recycle delay. Solid $\text{Cd}(\text{ClO}_4)_2 \cdot 6\text{H}_2\text{O}$ was used as a reference resonating at 0 ppm at room temperature.

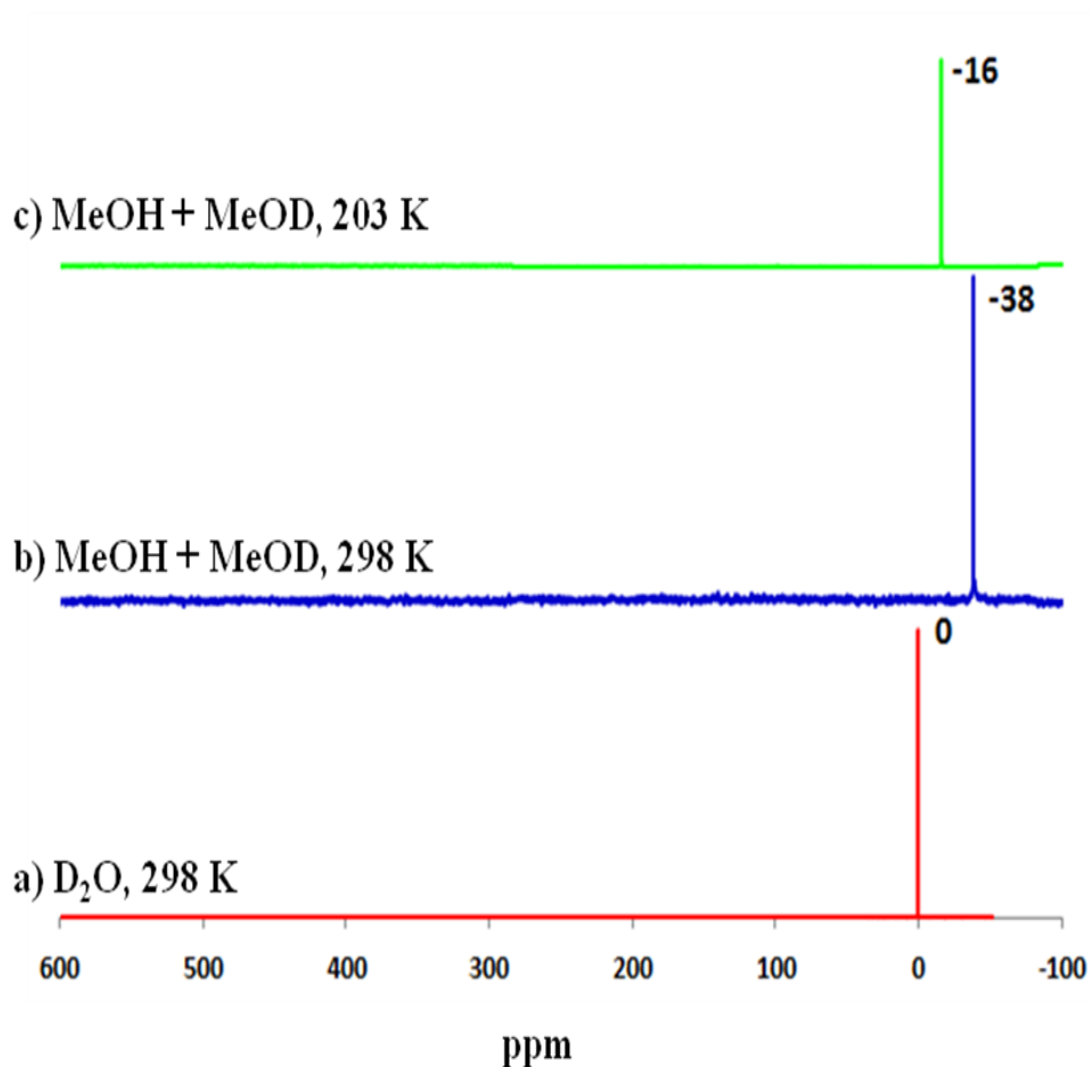


Figure 2-2 ^{113}Cd NMR sensitivity to solvent and temperature:^{140,97} 0.1 M $\text{Cd}(\text{ClO}_4)_2$ in - (a) D_2O at 298 K; (b) MeOH+ 30% MeOD at 298K; (c) MeOH+ 30% MeOD at 203 K.

2.2.7 Cd K- and L_{III} -edge X-ray absorption spectroscopy data collection

Cd K-edge X-ray absorption spectra were collected using beamline 7-3 at the Stanford Synchrotron Radiation Lightsource (SSRL) with storage ring containing 150-200 mA current at 3.0 GeV. Ion chambers I_0 , I_1 and I_2 were filled with Ar gas. The spectra were collected in transmission mode for MeOH solution containing

$C_{\text{Cd(II)}} \approx 100\text{mM}$ and SeU / Cd(II) mole ratios 1.0 (A_1), 2.0 (B_1), and 5.0 (E_1), and TU / Cd(II) mole ratios 1.0 (A_2) - 10.0 (G_2). These solutions were held in a 2 mm pinhole cell covered with Kapton windows; the sample temperature was maintained at : 200 K by means of an Oxford Instruments liquid helium flow cryostat. The Cd K-edge of the Cd-TU system was measured also at room temperature. Harmonic rejection was achieved by detuning the Si (220) double crystal monochromator to $\approx 50\%$ of the maximum I_0 intensity at the end of the scan (27735 eV). The energy of the X-rays was calibrated by assigning the first inflection point of a Cd foil to 26711 eV. Between two and five scans were collected for each sample and those that were overlapping were averaged after energy calibration.

Cd L_{III} -edge XANES spectra for solutions $A_2 - G_2$ containing $C_{\text{Cd(II)}} \approx 100\text{mM}$ and TU / Cd(II) mole ratios 1.0 to 10.0 and various references with known crystal structures were measured at room temperature in fluorescence mode using a PIPS detector on BL 4-3 at SSRL. Ion chamber I_0 was filled with He gas. Solutions were held in a 2 mm Teflon spacer with $5\mu\text{m}$ polypropylene film as the window material and kept under He atmosphere during the measurements. Higher harmonics from the Si (111) double crystal monochromator were rejected with a nickel and rhodium coated mirror. The energy was calibrated by assigning the first inflection point of a cadmium foil to 3537.6 eV. Either 2 or 3 scans were collected for each sample.

2.2.8 X-ray absorption spectroscopy data analysis

The Cd K-edge X-ray absorption data were calibrated and averaged using the EXAFSPAK program.⁹⁰ For each sample, individual scans were overlapped before averaging, to check that no radiation damage had occurred. The Cd K-edge EXAFS oscillation was extracted using the WinXAS 3.1 program.⁹¹ The background in the pre-edge region was removed using a first order polynomial. This was followed by normalization of the edge (in order to eliminate the effects of sample concentration and thickness), then conversion of the energy into k -space, where $k = \sqrt{[(8\pi^2 m_e / h^2)(E - E_0)]}$, using a threshold energy of $E_0 = 26710.0 - 26710.6$ eV. The atomic contribution was removed, using a cubic spline method. The $\chi(k)$ models were constructed by means of *ab initio* calculation of the effective amplitude function $|f_{\text{eff}}(k)|_i$, the total phase-shift $\phi_{ij}(k)$, and photoelectron mean free path $\lambda(k)$, using the FEFF 8.1 program⁹³ for the atomic coordinates of the crystal structure for octahedral $\text{Cd}(\text{TU})_4(\text{OReO}_3)_2$ ¹⁴¹ with CdS_4O_2 geometry, and tetrahedral $\text{Cd}(\text{TU})_4(\text{ONO}_2)_2$ ⁶⁰ with CdS_4 geometry as a model for thiourea system (see Appendix B), and tetrahedral $\text{Cd}(\text{dmise})_4(\text{PF}_6)_2$ (dmise = 1,3-dimethyl-2(3H)imidazoleselone)⁴² as a model for selenourea system (see Appendix B).

The structural parameters of the model function were refined by least squares curve-fitting to the k^3 -weighted experimental EXAFS data using the Win XAS 3.1 program, by fixing the S_0^2 (1.0), and/or coordination number (N), and allowing distance (R), Debye-Waller parameter (σ^2), and ΔE_0 to float. The estimated error of the refined

Cd-S/Se coordination numbers, bond distances and disorder parameters are within $\pm 20\%$, $\pm 0.02 \text{ \AA}$, and $\pm 0.001 \text{ \AA}^2$, respectively.

2.3 Result

2.3.1 Speciation of Cd(II)-selenourea complexes in methanol solution

In order to investigate the coordination environment of Cd in the Cd(II)-selenourea system, a series of Cd(II)-selenourea methanol solutions (A₁-E₁, see Table 2-1) containing 0.1 M Cd²⁺ and various selenourea concentrations were studied using ¹¹³Cd NMR and Cd K-edge XAS at low temperature. Measuring the EXAFS data at low temperature has two benefits: avoiding any photo reduction and increasing k-range of data by decreasing the thermal disorder.

Figure 2-3 shows the ¹¹³Cd NMR, the Cd K-edge EXAFS spectra, and their corresponding Fourier transforms of Cd(II)-selenourea solutions with different SeU / Cd(II) ratios at 203K. Figure 2-4 shows the result of EXAFS curve fitting for Cd(II)-SeU solutions A₁, B₁, and E₁. EXAFS spectra of solution C₁ was not measured since there was a mixture of species in the solution. Based on the ¹¹³Cd NMR spectra of solution D₁ and its similarity to solution E₁, the EXAFS spectra of Solution D₁ was not measured.

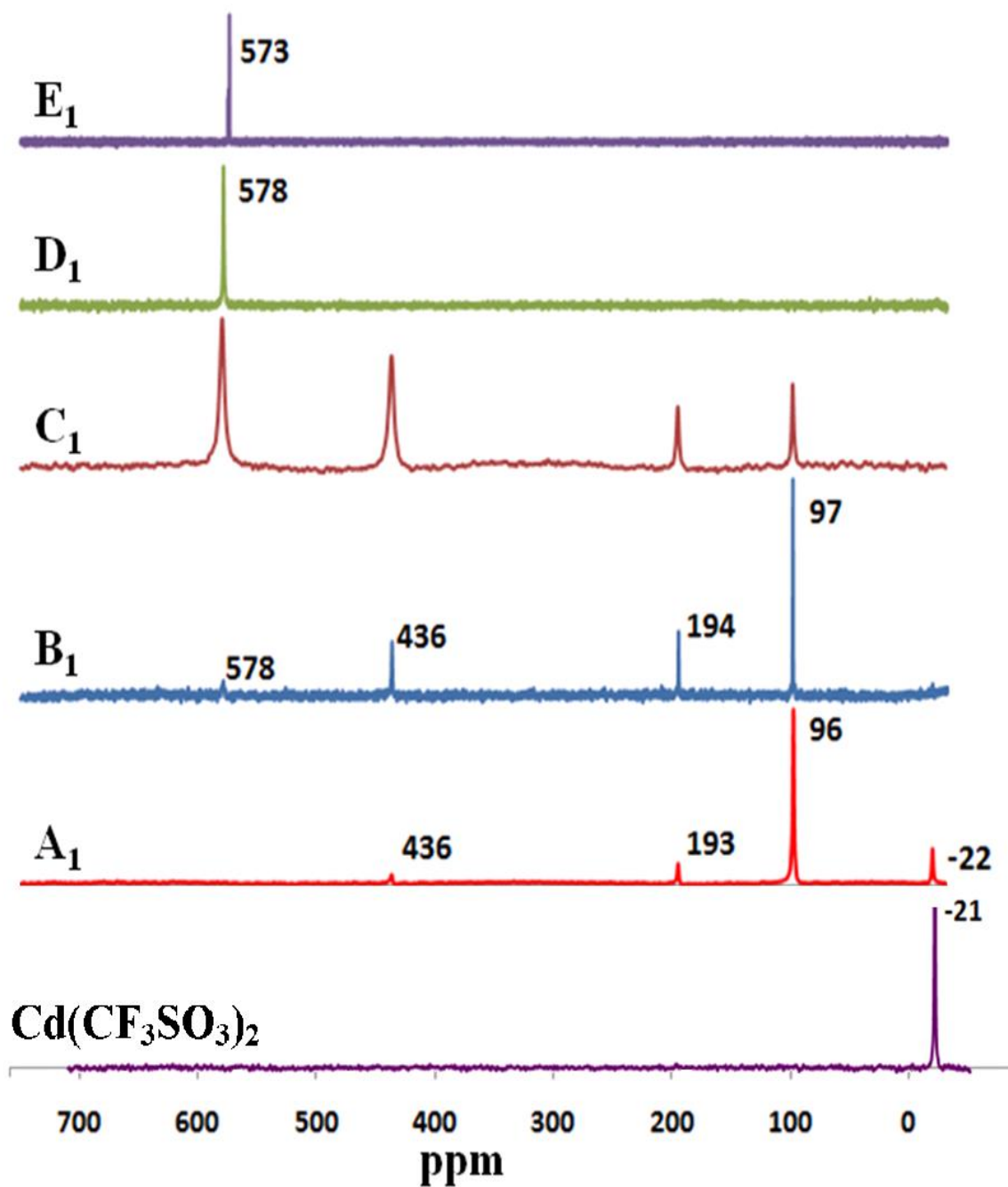


Figure 2-3 ^{113}Cd NMR spectra for Cd(II)-selenourea MeOH solutions A₁ – E₁ containing $C_{\text{Cd(II)}} \sim 100$ mM with varying SeU / Cd(II) molar ratios, measured at 203K.

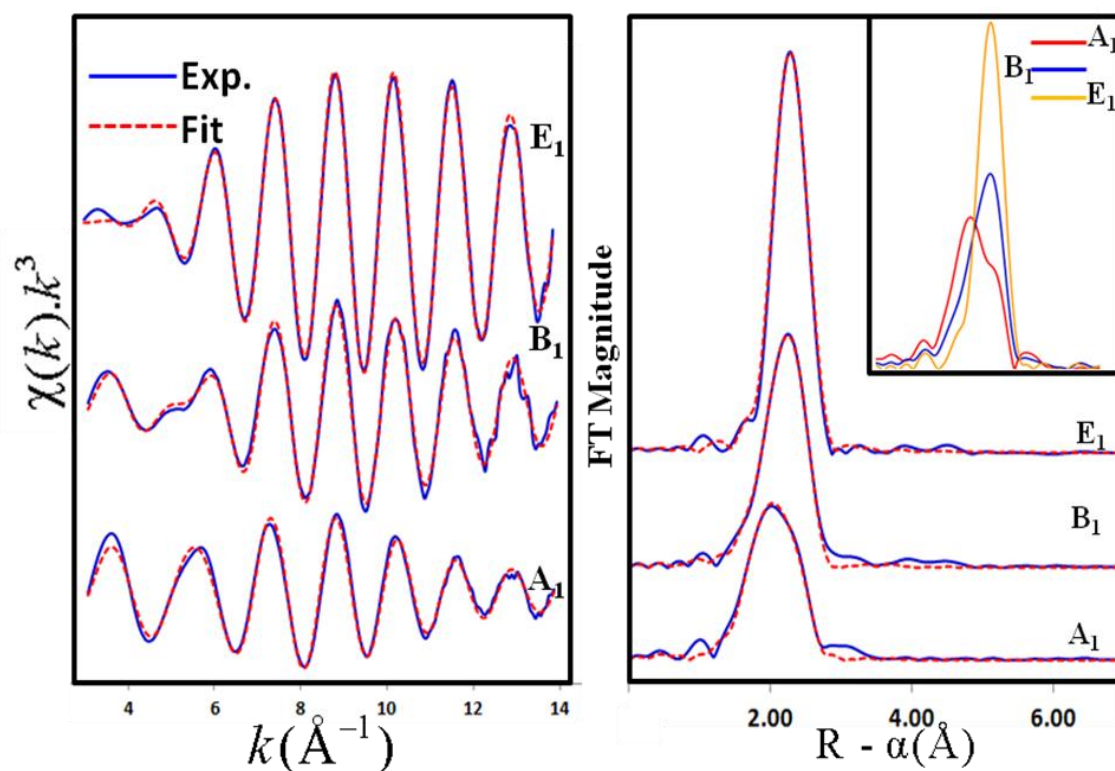


Figure 2-4 (Left) Cd K-edge EXAFS spectra and (Right) corresponding Fourier transforms for Cd(II)-SeU solution A₁, B₁, and E₁ SeU / Cd(II) molar ratios 1.0, 2.0, and 5.0, $C_{\text{Cd(II)}} \sim 100$ mM.

Table 2-4 EXAFS curve fitting results for Cd(II)-SeU solution A₁, B₁, and E₁ at : 200 K and fixed $S_0^2 = 1.0$.

Solution	Cd-Se			Cd-O			Residual
	<i>N</i>	<i>R</i> (Å)	σ^2 (Å ²)	<i>N</i>	<i>R</i> (Å)	σ^2 (Å ²)	
A ₁	0.9	2.62	0.0032	5f	2.31	0.0052	15.2
B ₁	2.8	2.62	0.0057	4f	2.36	0.0089	13.8
E ₁	4.3	2.63	0.0047				8.2

In the ¹¹³Cd NMR spectra of Cd(II)-selenourea solutions A₁ – C₁ with lower SeU / Cd(II) mole ratios (1.0, 2.0, and 3.0) (Figure 2-3), multiple peaks were observed which

show a mixture of species. For solutions B₁ and C₁ containing SeU / Cd(II) = 2.0 and 3.0 (Figure 2-3), four signals appeared at different ¹¹³Cd chemical shifts. Although their positions remained the same, their intensities changed, showing that the equilibrium between the dominant species has changed as the selenourea concentration increased from 0.2 M to 0.3 M. As the amount of selenourea increases, the peaks in the more deshielded region gain in intensity, indicating a higher concentration of Cd(II) complexes with more selenourea in their coordination shell. For solution D₁ and E₁ with a SeU / Cd(II) mole ratio ≥ 4.0 , a single peak appeared at 573 – 578 ppm, showing a dominating CdSe₄ species in these solutions.

As was shown in Figure 2-4, the shape of the EXAFS envelope changes from A₁ solution to E₁ solution with the EXAFS amplitude increasing at higher *k* values, which indicates there is a higher contribution of heavier atoms (i.e., Se vs. O) as the SeU / Cd(II) mole ratio increases. The latter was also observed in the corresponding Fourier Transforms (FT) of these solutions (Figure 2-4), which shows a distinctive shift of maximum peak position between A₁ and E₁ solutions from shorter to longer bond distances (i.e., Cd-O vs. Cd-Se). Superimposing the FT spectra of these solutions also shows an increase in the amplitude as the SeU / Cd(II) mole ratio increases, which indicates an increase in selenium coordination. As shown in Figure 2-3, the four ¹¹³Cd NMR peaks of solution C₁ have similar intensity which makes it impossible to get any useful data from EXAFS measurement of this solution. Additionally, based on the similarities of the ¹¹³Cd NMR spectra of solutions D₁ and E₁, only the EXAFS spectrum of solution E₁ (SeU / Cd(II) = 5.0) was measured.

For the peak assignment, the ^{113}Cd NMR chemical shifts of the Cd(II)-selenourea solutions were compared with the ^{113}Cd NMR chemical shifts reported in the literature for cadmium complexes with either sulfur or selenium coordination (Table 1-4 and Table 1-5), knowing that selenium is more shielding than sulfur. Since there was a limited number of reported $\delta_{\text{Cd-Se}}$ values in the literature, the EXAFS results for Cd(II)-selenourea solutions, and also comparison with ^{113}Cd NMR spectra of Cd(II)-thiourea solutions helped us to assign the ^{113}Cd NMR peak positions shown in Figure 2-3.

For SeU / Cd(II) ratio = 1.0, the ^{113}Cd NMR spectrum of solution A₁ showed three minor and one major peaks (Figure 2-3). A minor peak at -22 ppm is assigned to $\text{Cd}(\text{CF}_3\text{SO}_3)_2$ in MeOH (Figure 2-5), with CdO_6 coordination in the solution. The EXAFS spectrum of solution A₁ (Figure 2-4) was well modeled by 1 Cd-Se bond with a mean distance of $2.62 \pm 0.02 \text{ \AA}$ and 5 Cd-O bonds with mean distances of $2.31 \pm 0.02 \text{ \AA}$ (see Table 2-4). The EXAFS spectrum shows the average of the bond distances for all species present in solution. According to the ^{113}Cd NMR spectrum of solution A₁, almost 90% of the Cd species have $\delta_{\text{Cd}} = 96 \text{ ppm}$ and form the major contribution in EXAFS oscillation. Therefore the ^{113}Cd NMR peak at 96 ppm represents CdSeO_5 (O = triflate or MeOH). There are two other minor peaks at 193 and 436 ppm. ^{113}Cd solid state NMR spectra of *cis*- $[\text{Cd}(\text{TU})_2(\text{OH}_2)_4](\text{SO}_4)$ and $[\text{Cd}(\text{TU})_3(\text{SO}_4)]$ crystal shows two peaks at 148 ppm and 346 ppm which were assigned to CdS_2O_4 and CdS_3O_3 respectively. Based on the ^{113}Cd NMR of *cis*- $[\text{Cd}(\text{TU})_2(\text{OH}_2)_4](\text{SO}_4)$ and $[\text{Cd}(\text{TU})_3(\text{SO}_4)]$ the two peaks at 193 and 436 ppm were assigned to CdSe_2O_4 and CdSe_3O , respectively. Based on the ^{113}Cd

chemical shift and the EXAFS spectrum, a mixture of Cd(II) complexes with CdO_6 , CdSeO_5 , CdSe_2O_4 , and CdSe_3O coordination environment is proposed for solution A_1 with $\text{Cd}(\text{SeU})(\text{MeOH})_m(\text{CF}_3\text{SO}_3)_2$ ($m = 3-5$) as the dominant species.

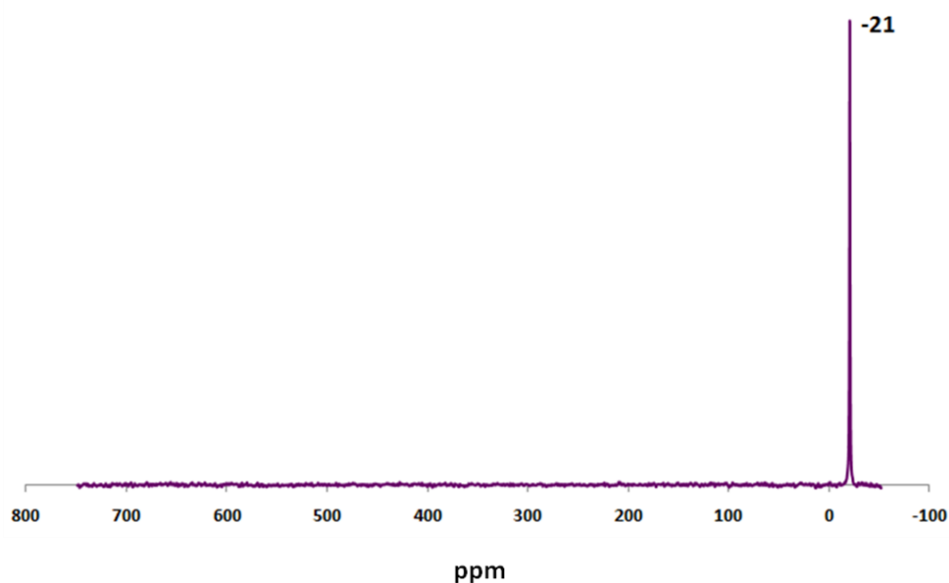


Figure 2-5 ^{113}Cd NMR spectra for $\text{Cd}(\text{CF}_3\text{SO}_3)_2$ in MeOH solutions at 203 K.

For **SeU / Cd(II) ratio = 2.0**, the ^{113}Cd NMR spectrum of solution B_1 (SeU / Cd(II) = 2.0) showed three minor and one major ^{113}Cd resonances (Figure 2-3). The peak at 97 ppm is assigned to CdSeO_5 , which was the major species in solution A_1 (SeU / Cd(II) ratio = 1.0). The peaks at 194 and 436 ppm have the same assignments as for solution A_1 . There is a minor peak at 578 ppm which was absent for solution A_1 . This peak gains intensity as $[\text{SeU}]$ increases in solutions $C_1 - E_1$. Chemical shifts for mononuclear CdSe_4 species have been observed at 541 ppm for CdSe_4 species in $[\text{Cd}(\text{SePh})_4]^{2-}$ and at 587 to 597 ppm for $[\text{Cd}(\text{SeP})_4]^{2+}$ complex ion (see Table 1-5). The CdSe_3 species is observed at 250 ppm for $[\text{Cd}(\text{SeC}\{\text{O}\}\text{Tol})_3]$ species. Based on

the above reported values, the small, broad peak at 578 ppm is associated with a small amount of four coordinated species, $\text{Cd}(\text{SeU})_4^{2+}$. The EXAFS spectrum of solution B₁ (Figure 2-4) was well modeled (see Table 2-4) with 2 or 3 Cd-Se bonds with mean bond distance of $2.62 \pm 0.02 \text{ \AA}$, and 4 Cd-O bonds with mean distances of $2.36 \pm 0.02 \text{ \AA}$. Based on the ^{113}Cd chemical shifts, a mixture of CdSeO_5 , CdSe_2O_4 and CdSe_3O with a small percentage of CdSe_4 coordination environments are proposed for solution B₁ with $\text{Cd}(\text{SeU})\text{O}_5$ dominating.

For SeU / Cd(II) ratio = 3.0, the ^{113}Cd NMR spectrum for solution C₁ composed of $C_{\text{SeU}} \sim 300 \text{ mM}$ and $C_{\text{Cd(II)}} \sim 100 \text{ mM}$ at 203 K showed four distinguishable peaks consistent with those that were observed for SeU / Cd(II) ratio = 2.0 (Figure 2-3), with significant differences in their intensities. Since the chemical shift positions remain the same, we propose that the species are the same in both B₁ and C₁ solutions. The obvious changes in their intensity show that the equilibrium among these species changed from solution B₁ to C₁. In solution C₁ with higher selenourea concentration, species with higher number of selenourea coordination gain more intensity.

For SeU / Cd(II) ratio = 4.0 and 5.0, the ^{113}Cd NMR spectrum for solution D₁ composed of $C_{\text{SeU}} \sim 400 \text{ mM}$ and $C_{\text{Cd(II)}} \sim 100 \text{ mM}$ at 203 K showed a single sharp peak at 578 ppm (Figure 2-3). Even after hours of data collection, no other peaks were observed. The ^{113}Cd NMR spectrum for solution E₁ composed of $C_{\text{SeU}} \sim 500 \text{ mM}$ and $C_{\text{Cd(II)}} \sim 100 \text{ mM}$ at 203 K also showed a single sharp peak at 573 ppm. The EXAFS

spectrum of solution E₁ was well modeled (see Figure 2-4 and Table 2-4) by 4 Cd-Se bonds with mean distances of $2.63 \pm 0.02 \text{ \AA}$ which is similar to the Cd-Se bond distance (2.6227 \AA) obtained from $\text{Cd}(\text{dmise})_4(\text{PF}_6)_2$ (dmise = 1,3-dimethyl-2(3H)imidazoleselone) (see Appendix B). Therefore, a $\text{Cd}(\text{SeU})_4^{2+}$ with CdSe_4 coordination environment is proposed for both solutions D₁ and E₁.

Attempts to measure the ^{113}Cd NMR spectra of solutions with a SeU / Cd(II) mole ratio > 5.0 failed due to the formation of excess selenourea crystals inside the NMR tube, as a result of saturation and lower solubility of selenourea than thiourea in methanol at 203 K.

The Cd(II) coordination environment was studied by means of ^{113}Cd NMR spectroscopy, Cd K-edge, and Cd L_{III}-edge XAS in a series of Cd(II)-thiourea solutions at both low temperature (: 200 K) and room temperature.

2.3.2 Speciation of Cd(II)-thiourea complexes in methanol solution at low temperature

Figure 2-6 and Figure 2-11 show the ^{113}Cd NMR spectra and the EXAFS spectra and their corresponding Fourier transforms of different L / M ratios of Cd(II)-thiourea solutions at 203K and room temperature, respectively.

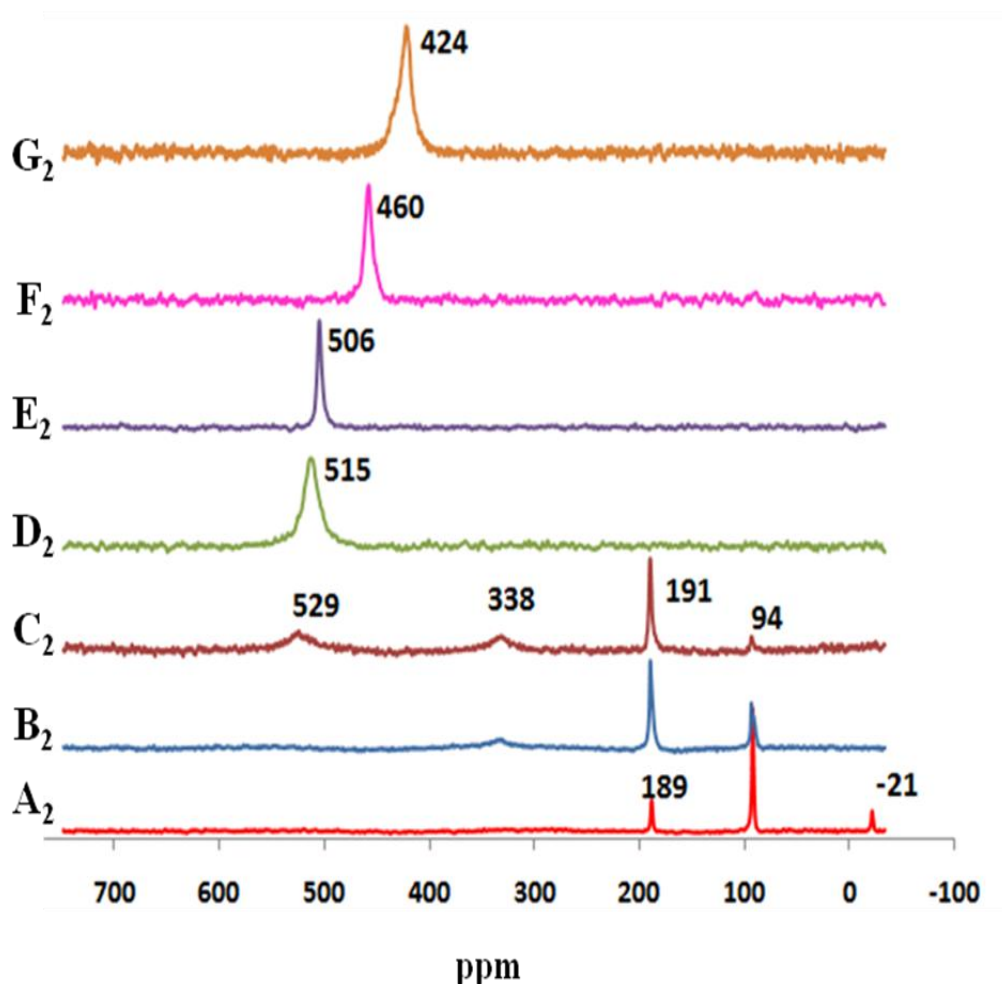


Figure 2-6 ^{113}Cd NMR spectra of Cd(II)-thiourea solutions $\text{A}_2 - \text{G}_2$ $C_{\text{Cd(II)}} \sim 100 \text{ mM}$. All spectra were measured in a mixture of : 70% methanol and : 30% methanol- d_4 at 203 K.

In order to interpret the δ_{Cd} observed for Cd(II)-thiourea solutions, a series of Cd-thione complexes was synthesized according to a previously reported procedure and their solid state ^{113}Cd NMR were measured. (Figure 2-7 to Figure 2-9). These complexes are: tetrathiourea-cadmium dinitrate, $[\text{Cd}(\text{TU})_4](\text{NO}_3)_2$, with coordination environment of CdS_4 ⁶⁰ (see Appendix B), tetrakis(N,N-Dimethylthioformamide)-bis(trifluoromethanesulfonato-O)-cadmium(II), $[\text{Cd}(\text{SCHN}(\text{CH}_3)_2)_4(\text{O}_3\text{SCF}_3)_2]$, with

coordination environment of CdS_4O_2 ¹⁴² (see Appendix B), hexakis(*N,N*-Dimethylthioformamide)-cadmium(II) diperchlorate, $[\text{Cd}(\text{SCHN}(\text{CH}_3)_2)_6](\text{ClO}_4^-)_2$, ($\text{SCHN}(\text{CH}_3)_2 = N,N$ -dimethylthioformamide) with coordination environment of CdS_6 ¹⁴² (see Appendix B), and a sample containing mainly $[\text{Cd}(\text{TU})_3(\text{SO}_4)]$ with coordination environment of CdS_3O and minor amount of *cis*- $[\text{Cd}(\text{TU})_2(\text{OH}_2)_4]^{2+}$ and *fac*- $[\text{Cd}(\text{TU})_3(\text{OH}_2)_3]^{2+}$ disulfate, with coordination environment of $\text{CdS}_2\text{O}_4 + \text{CdS}_3\text{O}_3$ were measured. The crystal structures of these complexes was confirmed by X-ray crystallography and their solid state NMR were measured at a resonance frequency of 66.6 MHz using AMX 300 spectrometer (7.2 Tesla).

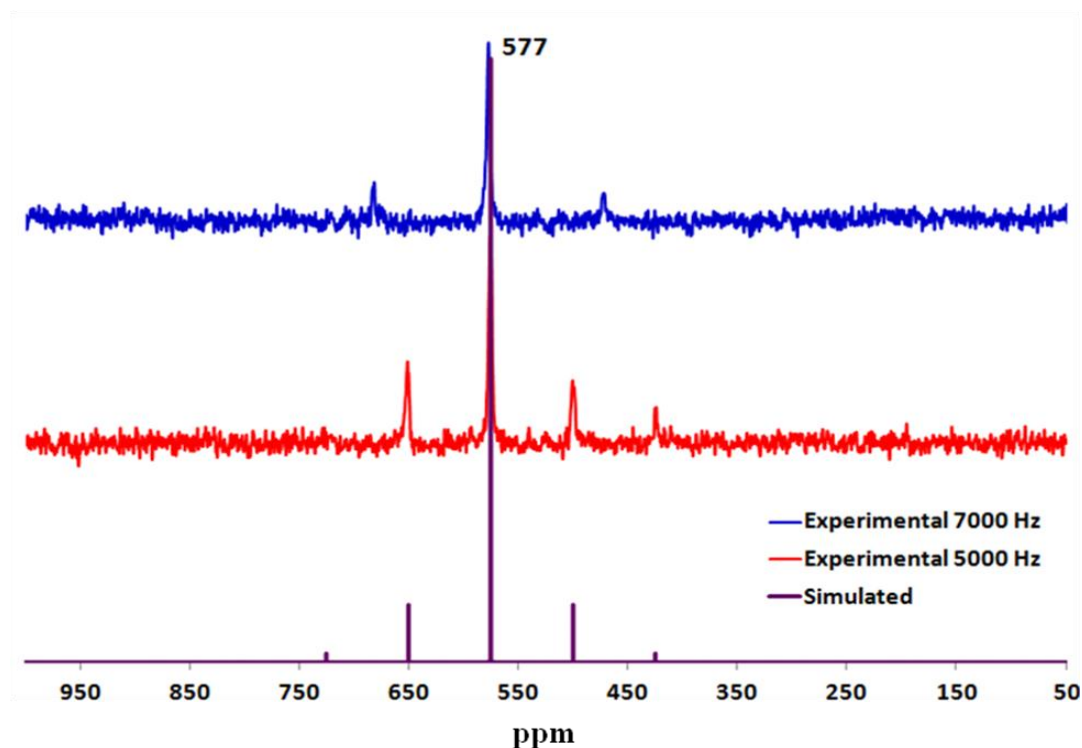


Figure 2-7 Solid state ^{113}Cd NMR spectra of $\text{Cd}(\text{SCN}_2\text{H}_4)_4(\text{NO}_3)_2$ at different spin rate at room temperature (CdS_4 , $\delta_{\text{iso}} = 577$ ppm, with $\delta_{11} = 651$ ppm, $\delta_{22} = 576$ ppm, and $\delta_{33} = 501$ ppm).

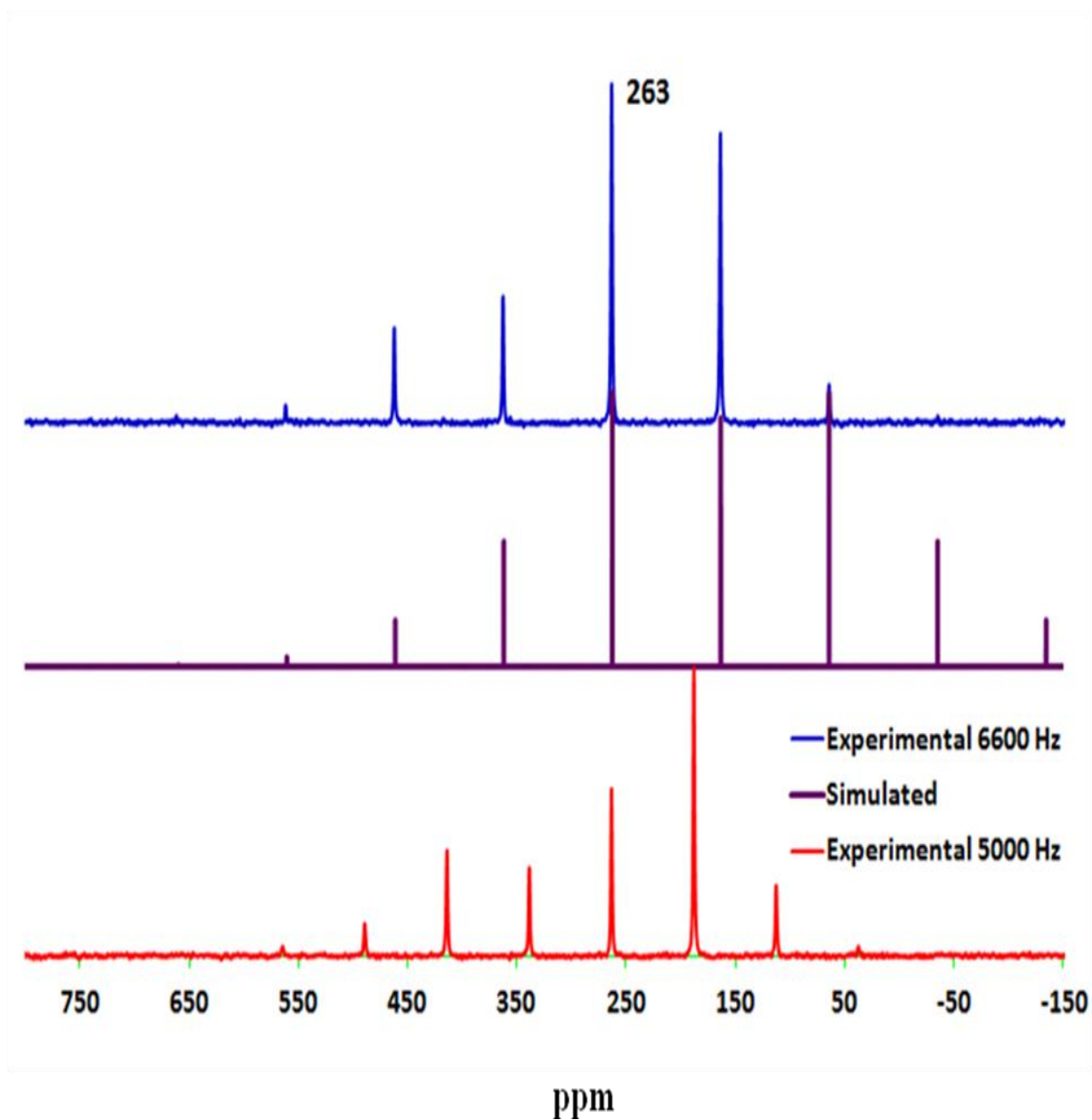


Figure 2-8 Solid state ^{113}Cd NMR spectra of $\text{Cd}(\text{SCHN}(\text{CH}_3)_2)_4(\text{O}_3\text{SCF}_3)_2$ at different spin rate at room temperature (CdS_4O_2 , $\delta_{\text{iso}} = 263$ ppm, with $\delta_{11} = 562$ ppm, $\delta_{22} = 263$ ppm, and $\delta_{33} = -35$ ppm).

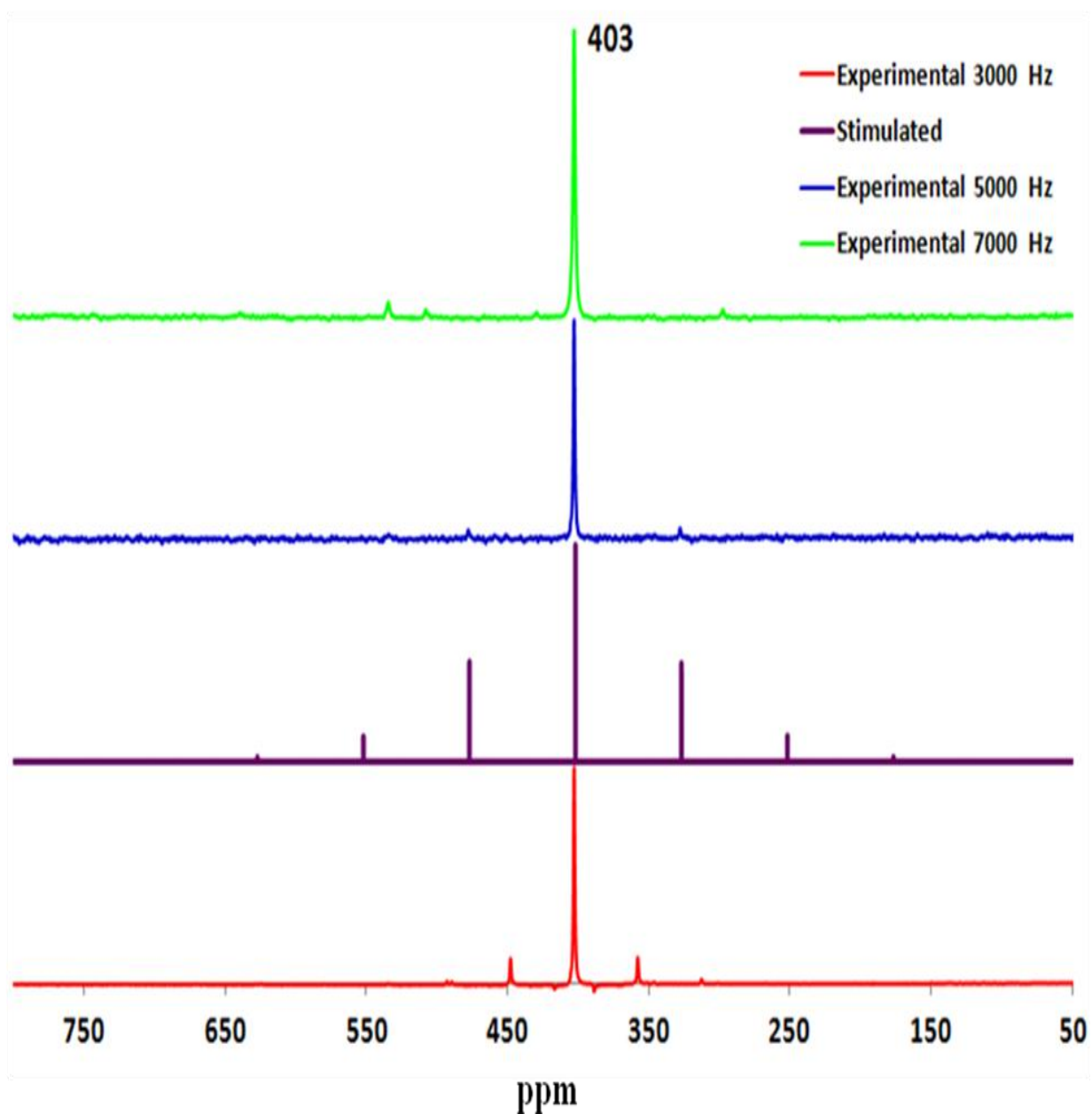


Figure 2-9 Solid state ^{113}Cd NMR spectra of $\text{Cd}(\text{SCHN}(\text{CH}_3)_2)_6](\text{ClO}_4)_2$ at different spin rate at room temperature (CdS_6 , $\delta_{\text{iso}} = 403$ ppm, with $\delta_{11} = 553$ ppm, $\delta_{22} = 403$ ppm, and $\delta_{33} = 250$ ppm).

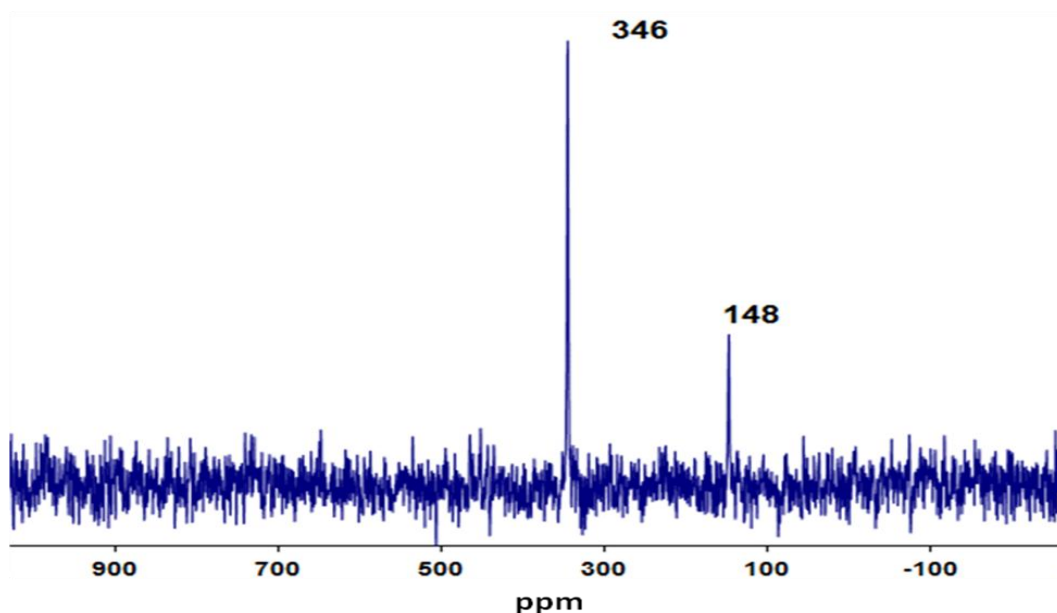


Figure 2-10 Solid state ^{113}Cd NMR spectra of $\text{cis-}[\text{Cd}(\text{TU})_2(\text{OH}_2)_4]^{2+}$ and $[\text{Cd}(\text{TU})_3(\text{SO}_4)]$ at 8000 Hz spin rate at room temperature (CdS_2O_4 and CdS_3O , $\delta = 148$ and 346 ppm respectively).

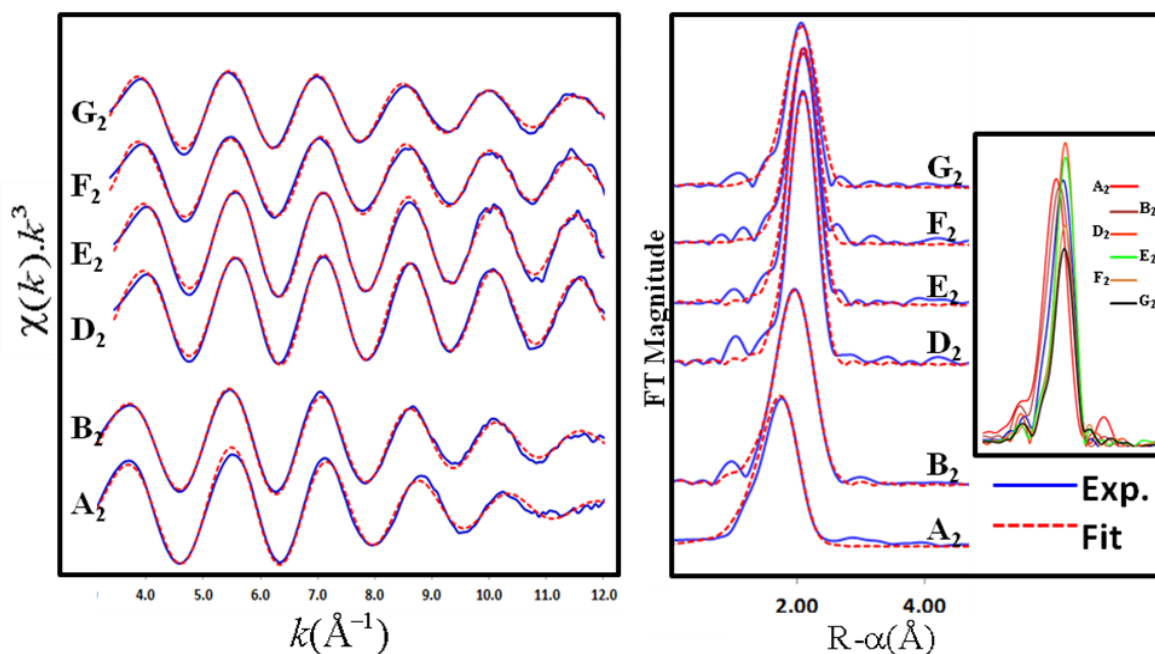


Figure 2-11 (Left) Cd K-edge EXAFS spectra and (Right) corresponding Fourier transforms for Cd(II)-TU solutions A₂-G₂ with TU / Cd(II) molar ratios 1.0 to 10.0, $C_{\text{Cd(II)}} \sim 100$ mM at 200-205 K.

Table 2-5 EXAFS curve fitting results for Cd(II)-TU solution A₂-G₂ at 200 – 205 K.
 $S_0^2 = 1.0$ fixed.

Solution	$\delta(^{113}\text{Cd})$ ppm	Cd-S			Cd-O			ΔE_0	Residual
		N	R(Å)	$\sigma^2(\text{\AA}^2)$	N	R(Å)	$\sigma^2(\text{\AA}^2)$		
A ₂	-21, 94, 189	1f	2.53	0.0049	5.6	2.29	0.0079	-3.3	15.2
B ₂	94, 191, 338	2f	2.53	0.0050	4.1	2.31	0.0107	-3.8	10.1
D ₂	515	3.7	2.53	0.0050				-1.7	15.6
E ₂	506	3.7	2.53	0.0053				-0.9	11.6
F ₂	460	3.5	2.54	0.0066				-3.3	19.4
G ₂	424	3.9	2.54	0.0088				-4.4	20.3

For TU / Cd(II) ratio = 1.0, the ^{113}Cd NMR spectrum of solution A₂ showed two minor and one major peaks (Figure 2-6). The peak at -21 ppm, is related to $\text{Cd}(\text{CF}_3\text{SO}_3)_2$ in MeOH with CdO_6 coordination in the solution (Figure 2-5). Two other peaks appeared at 94 and 189 ppm and are similar to the peaks observed in Cd(II) – selenourea solution A₁ at 96 and 193 ppm (Figure 2-3). Based on reported values for ^{113}Cd NMR chemical shifts in the literature, it can be assumed that the observed peak is in the octahedral species region with high coordination number of oxygen. The Fourier transforms for Cd(II)-TU solutions gives one single broad peak, corresponding to the Cd-S and Cd-O paths. The small peaks below 1.5 Å in some of the samples are spurious peaks, generated from the background removal procedure. The EXAFS spectrum of solution A₂ was well modeled (see Table 2-5) by 1 Cd-S bond with mean distance of 2.53 ± 0.02 Å and 5 Cd-O bonds with mean distances of 2.29 ± 0.02 Å using CdSO_5 model (Table 2-5). The obtained bond distances are in the range of bond distances obtained for octahedral crystal structures (see Appendix A₁). Using models with higher sulfur coordination numbers resulted in either small amplitude reduction factor, S_0^2 , or

unreasonable bond distances or coordination number. The S_0^2 was fixed at 1.0, the value obtained by EXAFS curve fitting of models with known crystal structure used as Feff fitting models. Information about the coordination environment of solution A₂ was obtained from Cd K-edge EXAFS, ¹¹³Cd NMR, also by comparisons of Cd L_{III}-edge XANES spectra of solution A₂ with structurally known cadmium(II) complexes. The peak at 94 ppm is assigned to CdSO₅ and the one at 189 ppm is assigned to CdS₂O₄. Since the EXAFS spectrum shows only average bond distances and the dominant ¹¹³Cd NMR peak is at 94 ppm, which represents CdSO₅, therefore a mixture of CdO₆, CdSO₅, and CdS₂O₄ coordination environment is proposed for solution A₂.

For TU / Cd(II) ratio = 2.0, the minor peak at 94 ppm, which was also observed for solution A₂, is assigned to CdSO₅ species. A major peak appeared at 191 ppm, and a minor peak at 338 ppm. Based on available ¹¹³Cd chemical shifts in the literature and also values obtained from SS NMR of mixture of [Cd(TU)₃(SO₄)] and *cis*-[Cd(TU)₂(OH₂)₄]²⁺ and *fac*-[Cd(TU)₃(OH₂)₃]²⁺ disulfate (see Figure 2-10), the peak at 191 ppm which is the dominant peak is assigned to CdS₂O₄ and the broad peak observed at 338 ppm for solution B₂ is assigned to CdS₃O coordination environment. The EXAFS spectrum of solution B₂ was well modeled (see Table 2-5) by 2 Cd-S bonds with mean distance of 2.53 ± 0.02 Å and 4 Cd-O bonds with mean distances of 2.31 ± 0.02 Å.

For TU / Cd(II) ratio = 3.0, the ¹¹³Cd NMR spectrum for solution C₂ composed of C_{TU} ~ 300 mM and C_{Cd(II)} ~ 100 mM at 203 K showed (Figure 2-15) four distinguishable peaks at 94, 191, 338, and 529 ppm, of which the first three peaks are similar to those in solution B₂ with significant differences in their intensities.

Additionally, a broad peak appeared at 529 ppm, which was absent in solution B₂. Since the chemical shift positions remained the same in both solutions B₂ and C₂, we propose that the types of species are the same but the changes in their intensity shows that the equilibrium amongst these species have changed from solution B₂ to C₂ as the ligand concentration increased from 0.2 M to 0.3 M. At the new equilibrium, species with higher thiourea coordination numbers gained more intensity. Since the ¹¹³Cd solid state NMR spectrum of the reference compound tetrathiourea-cadmium dinitrate (CdS₄) showed a peak at 577 ppm at room temperature, we conclude that the small, broad peak at 529 ppm is associated with a mixture of CdS₃O₃ and CdS₄ species. The EXAFS spectrum of this solution (C₁) does not give any useful information as it shows only a mixture of species and the dominant ¹¹³Cd NMR peak is at 191 ppm which represents CdS₂O₄. A mixture of 6-coordinated CdSO₅, CdS₂O₄, and CdS₃O₃ and a small percentage of 4-coordinated CdS₄ is proposed for solution C₂.

For TU / Cd(II) ratio = 4.0 – 10.0, for solutions D₂ to G₂ (TU / Cd(II) = 4.0 - 10.0), the ¹¹³Cd NMR peaks appeared between 424 and 515 ppm. The peaks moved downfield as a single broad peak, comparing with dominant peaks for solutions A₂ to C₂ (TU / Cd(II) = 1.0 - 3.0). The peaks were broad, indicating fast ligand exchange between mixtures of species. This downfield shift of the ¹¹³Cd NMR peak shows that a higher number of sulfur atoms are coordinated as thiourea concentration increases. The EXAFS fitting of these solutions show an increase in the S coordination number.

The ¹¹³Cd NMR spectrum for solution D₂ composed of C_{TU} ~ 400 mM and C_{Cd(II)} ~ 100 mM at 203 K showed a single broad peak at 515 ppm. This shows that, as

the TU / Cd(II) ratio increases, the of species in the solution are changing, towards 4-coordinated species. This peak (515 ppm) can be associated with a mixture of CdS₄O and CdS₄ species. This information was confirmed with the EXAFS spectrum of solution D₂, which was well modeled (see Table 2-5) by 3.7 Cd-S bonds with mean distance of 2.53 ± 0.02 Å. This average Cd-S bond distance is in the range expected for tetrahedral species in solution. Considering the lower sensitivity of EXAFS compared to NMR, the error range of 20% for coordination number measurement in EXAFS, and also, since it is harder to detect the existence of light atoms such as oxygen in the presence of a heavier backscatterer such as sulfur, also considering the facts that ¹¹³Cd NMR of Cd(TU)₄(NO₃)₂ shows a peak at $\delta_{\text{iso}} = 577$ ppm, the observed $\delta = 541$ ppm for: TU / Cd(II) = 10.0 mole ratio, and the chemical shift change from 529 ppm (TU / Cd(II) = 3.0) to 515 ppm (TU / Cd(II) = 4.0), we conclude that the single ¹¹³Cd NMR peak at 515 ppm represents minor CdS₄O and CdS₄. These are the only species in solution D₂.

For TU / Cd(II) ratio = 5.0, the ¹¹³Cd NMR spectrum for solution E₂ composed of C_{TU} ~ 500 mM and C_{Cd(II)} ~ 100 mM at 203 K showed a single peak at 506 ppm. This peak can be associated with a mixture of CdS₄O and CdS₄ species (Figure 2-6). The EXAFS spectrum of solution E₂ was well modeled (see Table 2-5) by 3.7 Cd-S bonds with mean distance of 2.53 ± 0.02 Å. Compared to the ¹¹³Cd NMR value for previous ratio (solution A₂-D₂), the chemical shift moved to lower values, by looking at the value resulted from measuring CdS₄ (577 ppm) and CdS₆ (403 ppm) references, it seems that as ligand ratio increases, the coordination number tends to go to higher value (i.e., 6), therefore the possible species in solution E₂ are CdS₄ and CdS₄O and minor

amount of CdS_6 since chemical shift changes to more shielded region comparing to previous ratio (from 515 ppm to 506 ppm).

For TU / Cd(II) ratio = 8.0, the ^{113}Cd NMR spectrum for solution F_2 composed of $C_{\text{TU}} \sim 800 \text{ mM}$ and $C_{\text{Cd(II)}} \sim 100 \text{ mM}$ at 203 K showed a single peak at 460 ppm. This shows that the ^{113}Cd NMR peak is shifted to more shielded areas; in other words, it shows an increase in coordination number. This peak is consistent with a mixture of four-coordinated species CdS_4 , and small portion of 6-coordinated species $\text{CdS}_5(\text{S/O})$ and CdS_6 (Figure 2-6). The EXAFS spectrum of solution F_2 was well modeled (see Table 2-5) by 3 to 4 Cd-S bonds with mean distance of $2.54 \pm 0.02 \text{ \AA}$. Based on slight increase in the obtained bond distance for solution F_2 and the fact that δ_{Cd} is shifting toward more shielded region and comparing the value with 403 ppm as standard CdS_6 , there is a mixture of species (CdS_4 , $\text{CdS}_5(\text{S/O})$ and CdS_6) in solution F_2 .

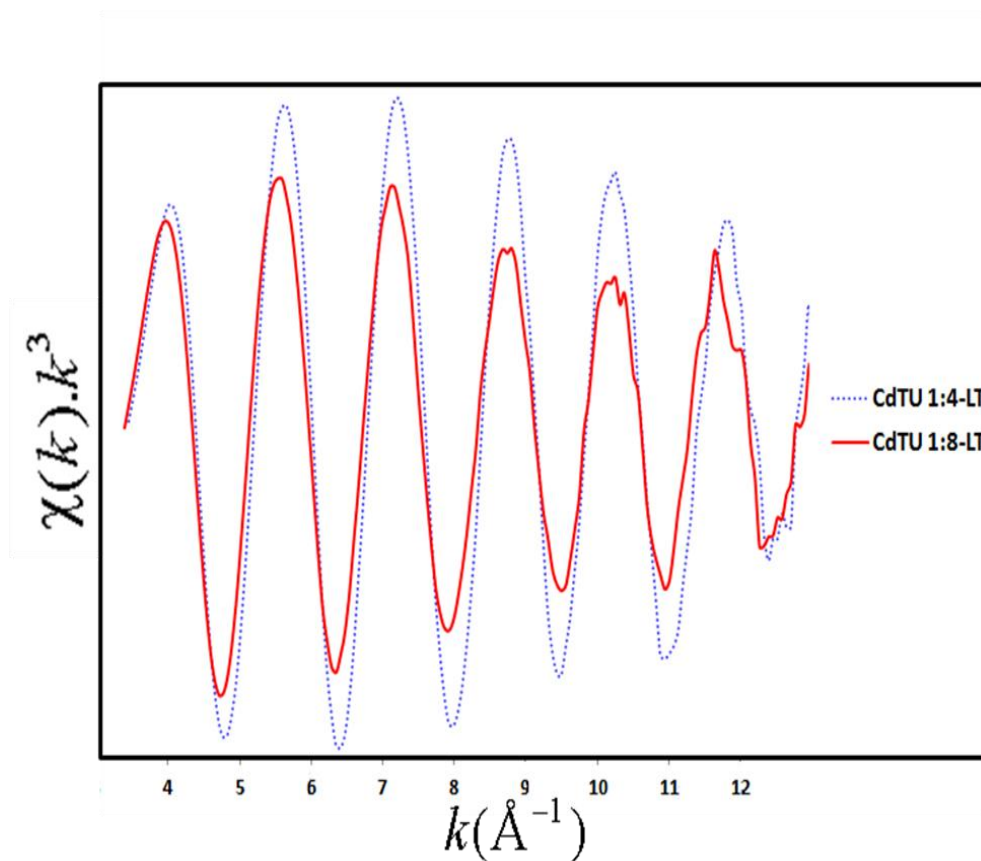


Figure 2-12 Comparison between k^3 -weighted EXAFS spectra of solutions D₂ and F₂.

Figure 2-12 shows that the EXAFS amplitude for solution F₂ (TU / Cd(II) = 8.0) is smaller than the EXAFS amplitude for solution D₂ (TU / Cd(II) = 4.0). This decrease in the EXAFS amplitude is opposite to what is expected (i.e., the EXAFS amplitude increases as coordination number increases). This could be explained by the fact that if the EXAFS oscillation of existing species in the solution (CdS_4 , $\text{CdS}_5(\text{S/O})$, and CdS_6) have different phase shifts, they will cancel each other, causing the amplitude to be lower than expected.

For TU / Cd(II) ratio = 10.0, the ^{113}Cd NMR spectrum for solution G₂ composed of $C_{\text{TU}} \sim 1000 \text{ mM}$ and $C_{\text{Cd(II)}} \sim 100 \text{ mM}$ at 203 K showed only one single

peak at 424 ppm, which can be assigned to CdS_4 , $\text{CdS}_5(\text{S/O})$ and CdS_6 , with the 4-coordinated species dominant. The EXAFS spectrum of solution G_2 was well modeled (see Table 2-5) by 4 to 5 Cd-S bonds with mean distance of $2.54 \pm 0.02 \text{ \AA}$. Additionally, the EXAFS spectrum of this solution was measured at 160-170 K (sample is frozen at this temperature), and was well-modeled with 6-coordinated species with Cd-S bonds with mean distance of $2.75 \pm 0.02 \text{ \AA}$, which matches with the value that were obtained for 6-coordinated complexes in the (see Appendix A₁).

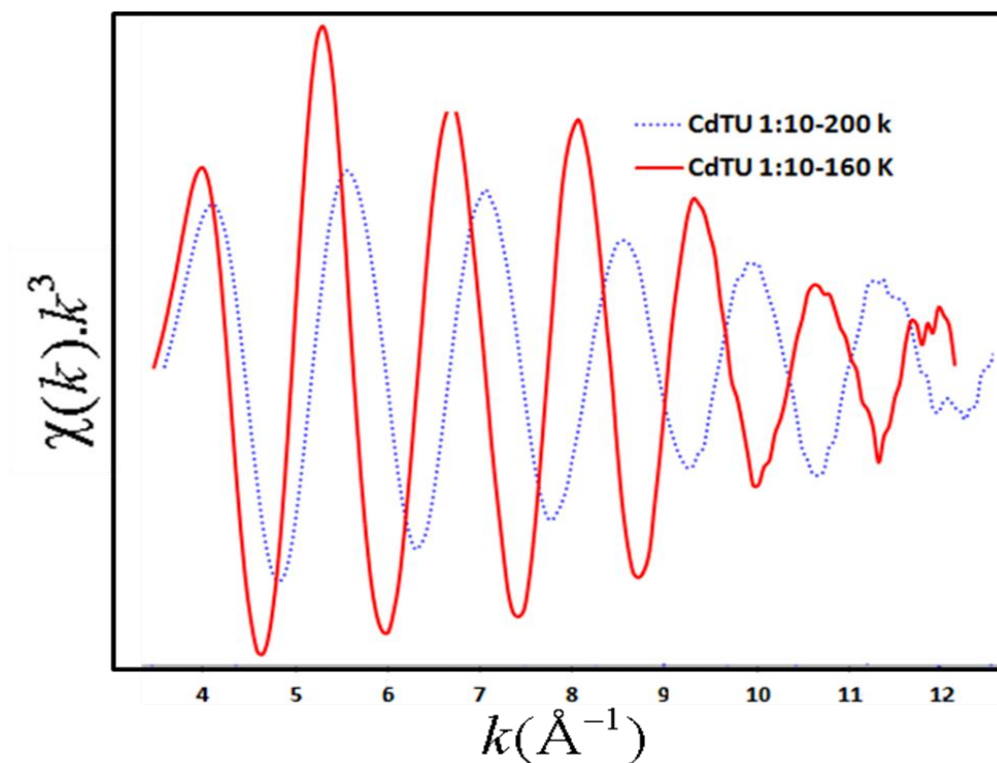


Figure 2-13 Comparison between k^3 -weighted EXAFS spectra of solutions G_2 at 160 K and 200 K.

The comparison of EXAFS amplitude of G_2 solution at 160 K and 200 K shows an increase in the EXAFS amplitude, which proves the formation of higher coordination number (Figure 2-23).

2.3.3 Speciation of Cd(II)-thiourea complexes in methanol solution at room temperature

In order to confirm the ^{113}Cd NMR peak assignments of Cd(II)-thiourea solutions at low temperature (i.e., the peak appeared at 529 ppm in Figure 2-6), ^{113}Cd NMR and EXAFS spectra of Cd(II)-thiourea solutions were also measured at room temperature. Figure 2-14 and Figure 2-15 show the results of these measurements. For TU / Cd(II) ratios from 1.0 to 3.0 (solution A₂-C₂), attempts to measure their ^{113}Cd NMR failed and no signal was obtained due to the fast exchange of species in the NMR time scale. For TU / Cd(II) ratios from 4.0 to 10.0 solutions (solution D₂-G₂), we were able to get NMR signals in the range of 503 to 541 ppm. As was shown in Figure 2-14, as the ligand ratio increase, the resonances shifted downfield, indicating a higher contribution of S coordination.

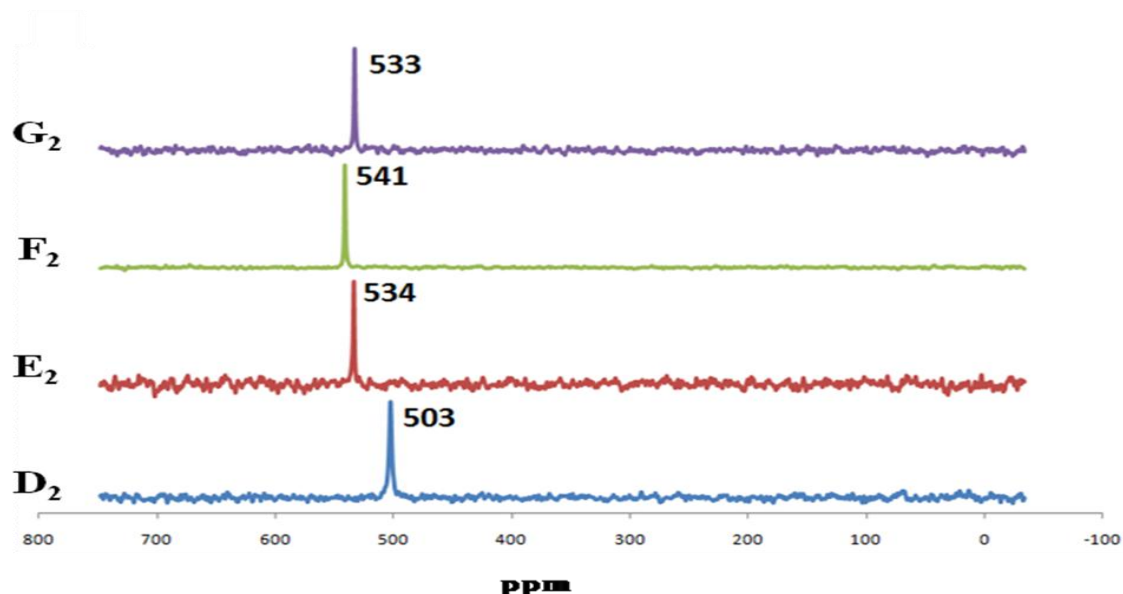


Figure 2-14 ^{113}Cd NMR spectra of Cd(II)-thiourea solutions D₂ – G₂ $C_{\text{Cd(II)}} \sim 100 \text{ mM}$ in : 70 % methanol and : 30 % methanol - d₄ at 298 K.

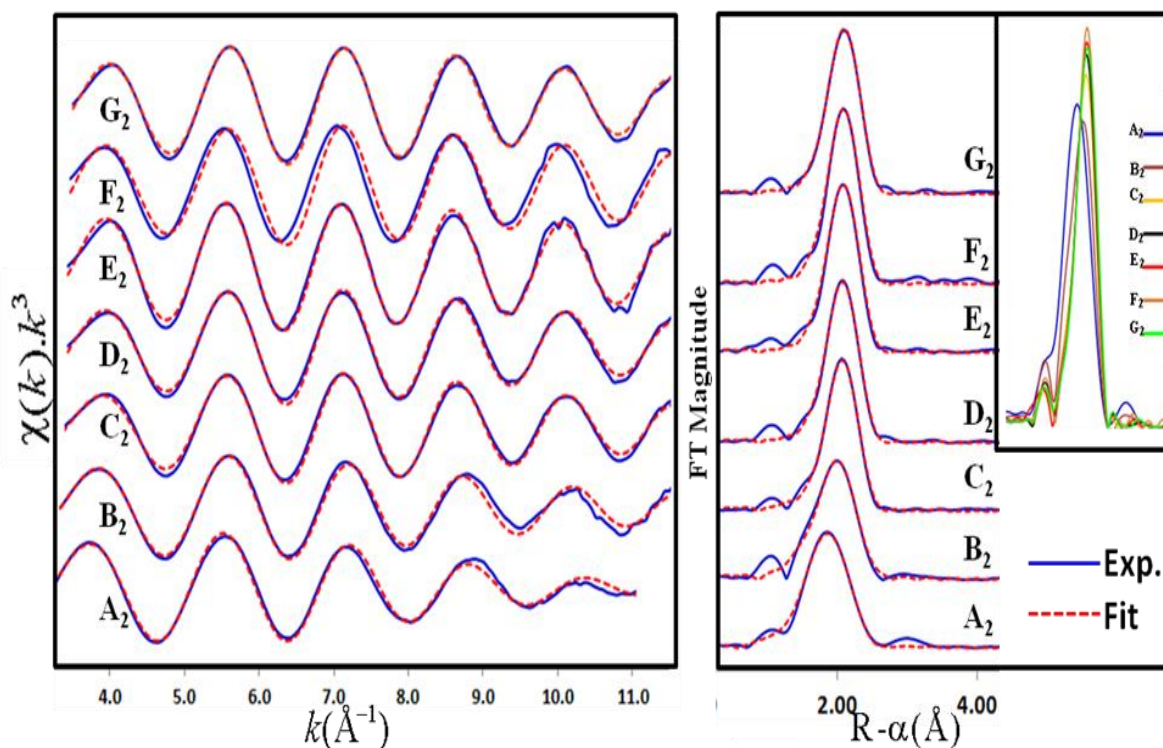


Figure 2-15 (Left) Cd K-edge EXAFS spectra and (Right) corresponding Fourier transforms for Cd(II)-TU solutions A₂-G₂ with TU / Cd(II) molar ratios 1.0 to 10.0, $C_{\text{Cd(II)}} \sim 100$ mM at room temperature.

Table 2-6 EXAFS curve fitting results for Cd(II)-TU solution A₂-G₂ at room temperature. S_0^2 value was fixed at 1.0.

Solution	$\delta(^{113}\text{Cd})$ ppm	Cd-S			Cd-O			ΔE_0	Residual
		<i>N</i>	<i>R</i> (Å)	σ^2 (Å ²)	<i>N</i>	<i>R</i> (Å)	σ^2 (Å ²)		
A ₂	N/A	1.0f	2.52	0.0058	4.3	2.28	0.0087	-3.2	11.2
B ₂	N/A	1.5f	2.52	0.0039	4.0	2.28	0.0135	-1.6	17.2
C ₂	N/A	3.0f	2.52	0.0056	1.2	2.26	0.0216	-3.2	11.1
D ₂	503	3.3	2.53	0.0066	0.5f	2.26	0.0014	-0.2	11.0
		3.5	2.52	0.0062				-2.5	12.2
E ₂	534	3.9	2.54	0.0056				-1.0	13.5
F ₂	541	3.3	2.53	0.0052				-1.3	14.0
G ₂	533	3.7	2.53	0.0062				0.7	10.7

For TU / Cd(II) ratio = 1.0, although no ^{113}Cd NMR signal was observed for this solution at room temperature, we know from ^{113}Cd NMR spectra of solution A₂ at 203 K that there is a mixture of species in the solution, The EXAFS spectrum of solution A₂ was well modeled (see Table 2-6) by 1 to 1.5 Cd-S bonds with mean distance of 2.52 ± 0.02 Å and 4 to 5 Cd-O bonds with mean distances of 2.28 ± 0.02 Å. Therefore, a mixture of minor CdS₂O₄, CdO₆ and major CdSO₅ species exists in solution A₂ at room temperature, as observed in ^{113}Cd NMR of A₂ at 203 K.

For TU / Cd(II) ratio = 2.0, the EXAFS spectrum of solution B₂ was well modeled (see Table 2-6) by 1.5 Cd-S bonds with mean distance of 2.52 ± 0.02 Å and 4 Cd-O bonds with mean distances of 2.28 ± 0.02 Å. Since there is no ^{113}Cd NMR for this solution at room temperature, based on ^{113}Cd NMR of this solution at 203 K, there is a mixture of CdSO₅ and CdS₂O₄ species in solution B₂.

For TU / Cd(II) ratio = 3.0, the EXAFS spectrum of solution C₂ was well modeled (see Table 2-6) by 3 Cd-S bonds with mean distance of 2.52 ± 0.02 Å and 1 Cd-O bond with mean distance of 2.26 ± 0.02 Å. Considering the fact that EXAFS only provide information on average bond distance and also based on the ^{113}Cd NMR spectrum of solution C₂ at 203 K, there is a mixture of 4-coordinated species CdS₄ and CdS₃O₃ and possibly CdS₂O₄ (based on LT ^{113}Cd NMR) in solution C₂.

For TU / Cd(II) ratio = 4.0, the ^{113}Cd NMR spectrum for solution D₂ composed of C_{TU} ~ 400 mM and C_{Cd(II)} ~ 100 mM at room temperature showed a single peak at 503 ppm. This value is near 577 ppm at room temperature, which is the measured value for solid state NMR for CdS₄ reference confirming that there are 4-coordinated

species, i.e., CdS_3O_3 and CdS_4 (Figure 2-14). The EXAFS spectrum of solution D_2 was well modeled (see Table 2-6) by 3 to 4 Cd-S bonds with mean distance of $2.52 \pm 0.02 \text{ \AA}$.

For TU / Cd(II) ratio = 5.0, the ^{113}Cd NMR spectrum for solution E_2 composed of $C_{\text{TU}} \sim 500 \text{ mM}$ and $C_{\text{Cd(II)}} \sim 100 \text{ mM}$ at room temperature showed a single peak at 534 ppm. This peak is associated with a mixture of species; minor CdS_3O_3 and major CdS_4 (Figure 2-14). This value is higher than the value obtained for solution D_2 , which indicates higher fractionation of CdS_4 species, but lower than the reference value which indicate the existence of CdS_3O_3 species in the solution. The EXAFS spectrum of solution E_2 was well modeled (see Table 2-6) by 4 Cd-S bonds with mean distance of $2.54 \pm 0.02 \text{ \AA}$. Therefore, the single ^{113}Cd NMR peak at 534 ppm represents a mixture of broad CdS_3O_3 and CdS_4 in solution E_2 .

For TU / Cd(II) ratio = 8.0, the ^{113}Cd NMR spectrum for solution F_2 composed of $C_{\text{TU}} \sim 800 \text{ mM}$ and $C_{\text{Cd(II)}} \sim 100 \text{ mM}$ at room temperature showed a single peak at 541 ppm. This shows that the ^{113}Cd NMR peak is shifted to more deshielded area, in other words, it shows an increase in the percentage of CdS_4 species in solution (Figure 2-14). The EXAFS spectrum of solution F_2 was well modeled (see Table 2-6) by 3 to 4 Cd-S bonds with mean distance of $2.53 \pm 0.02 \text{ \AA}$. Both the EXAFS spectrum and ^{113}Cd NMR show there is a dominant CdS_4 species in the solution.

Finally, For TU / Cd(II) ratio = 10.0, the ^{113}Cd NMR spectrum for solution G_2 composed of $C_{\text{TU}} \sim 1000 \text{ mM}$ and $C_{\text{Cd(II)}} \sim 100 \text{ mM}$ at room temperature showed only one peak at 533 ppm (Figure 2-14), which can be assigned to mixture of 4-coordinated

species, CdS_4 and CdS_4O , with CdS_4 as dominant species. The EXAFS spectrum of solution G_2 was well modeled (see Table 2-6) by 4 Cd-S bonds with mean distance of $2.53 \pm 0.02 \text{ \AA}$. Comparing this result to the EXAFS of this solution measured at 160-170 K and 200 K, it shows that as the temperature decrease from 298 K to 160 K, the coordination number increases from 4 to 6, which is also consistent with a change in Cd-S bond distance from 2.53 at room temperature to 2.75 \AA at 160-170 K.

2.3.4 X-ray Absorption Near Edge Structure of Cd(II)-thiourea Solutions at room temperature

Figure 2-16 shows Cd L_{III} -edge XANES spectra of model compounds containing O and S ligands (i.e., CdO_6 , CdS_4O_2 , CdS_6 , CdS_3O , and CdS_4) and Cd(II)-thiourea solutions (TU / Cd(II) ratios = 1.0 – 10.0). Cd L_{III} -edge X-ray absorption spectra are sensitive to changes in coordinating atom (i.e., O vs. S) and geometry or symmetry of the complex, therefore comparison of the corresponding spectra with reference models will help to confirm the coordination of Cd(II)-thiourea complexes in solutions. As was shown in the corresponding 2nd derivative of the XANES spectrum of reference models with high O coordination, a clearly resolved feature appears at 3567.5 eV, the minima position change to area around 3560.5 eV for CdS_4O_2 , CdS_6 . As the coordination environment changed to tetrahedral species (CdS_3O , and CdS_4) the main minima appear at 3539.0 eV with smaller feature at 3541.0 eV, which is more obvious for CdS_4 model. In comparison, the corresponding 2nd derivative of tetrahedral reference models (CdS_3O ,

and CdS_4) and Cd(II) -thiourea solutions ($A_2 - G_2$) at room temperature shows high similarities in the observed features.

These similarities indicate the presence of mainly tetrahedral species in solutions F_2 ($\text{TU} / \text{Cd(II)} = 8.0$) and G_2 ($\text{TU} / \text{Cd(II)} = 10.0$), which support the results obtained from EXAFS and ^{113}Cd NMR measurements at room temperature.

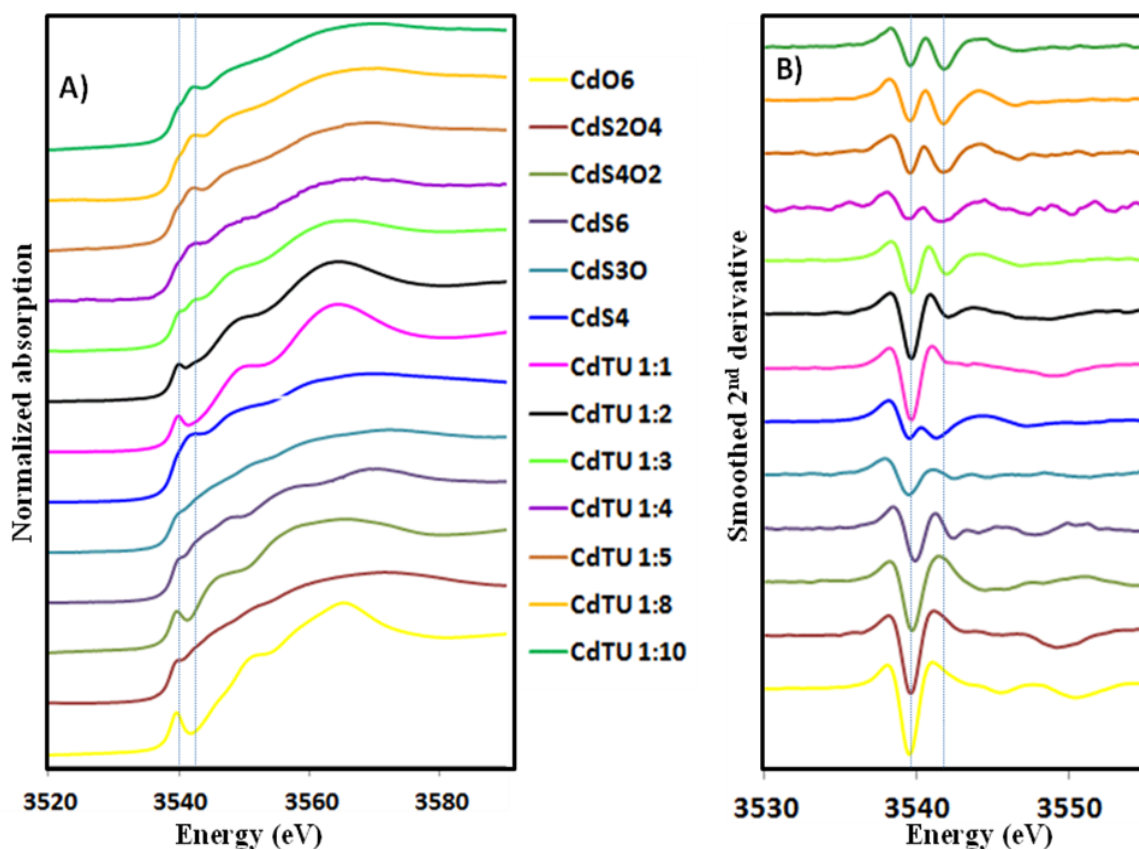


Figure 2-16 (A) Cadmium L_{III} -edge XAS of cadmium(II) perchlorate hydrate $\text{Cd}(\text{ClO}_4)_2 \cdot 6\text{H}_2\text{O}$ (CdO_6 model), tetrakis(*N,N*-dimethylthioformamide) bis(trifluoromethanesulfonato) cadmium(II) $[\text{Cd}(\text{SCHN}(\text{CH}_3)_2)_4(\text{O}_3\text{SCF}_3)_2]$ (CdS_4O_2 model), hexakis(*N,N*-dimethylthioformamide) cadmium(II) perchlorate $[\text{Cd}(\text{SCHN}(\text{CH}_3)_2)_6](\text{ClO}_4)_2$ (CdS_6 model), imidazolium tris(thiosaccharinato)aqua cadmate(II) $(\text{HIm})[\text{Cd}(\text{tsac})_3(\text{H}_2\text{O})]$ (CdS_3O model), cadmium adamantane cage $(\text{Et}_3\text{NH})_4\text{[S}_4\text{Cd}_{10}(\text{SPh})_{16}]$ (CdS_4 model) and Cd(II) -thiourea solutions $A_2 - G_2$ at room temperature, and (B) corresponding smoothed second derivatives; dotted lines correspond to 3539.2 eV and 3541.3 eV.

2.4 Conclusion and Future Work

Based on a combination of Cd K-edge EXAFS, and ^{113}Cd NMR spectroscopy, the speciation in 0.1 M Cd(II)-selenourea with different selenourea concentrations at a temperature around 200 K have been structurally characterized. Due to the unstable nature of selenourea solutions, the limited number of studies focused on the coordination environment in these systems, and to the best of our knowledge, there is no extended study on the possible coordination number of this ligand with Cd(II) in solution.

For Cd(II)-selenourea, at lower ratios a mixture of species with major amount of octahedral species (CdSeO_5 , CdSe_2O_4 , CdSe_3O) and a minor percentage of tetrahedral species (CdSe_4) were found, as selenourea concentration increases, the equilibrium moves toward tetrahedral species, CdSe_4 , which confirmed to be the only species in the solution E_1 ($\text{SeU} / \text{Cd(II)} = 5.0$). From Cd K-edge EXAFS spectroscopy of Cd(II)-selenourea in methanol solution containing 0.1 M Cd(II) and 0.5 M SeU, the presence of tetrahedral CdSe_4 species was confirmed with Cd-Se bond distance of 2.64 ± 0.02 Å. ^{113}Cd NMR measurements of this solution show a single sharp peak at 573 ppm, which is in agreement with reported CdSe_4 values (see Table 1-5). Attempt to investigate the coordination environment of ratios higher than 5.0 failed due to saturation and crystallization of excess selenourea in the NMR tube.

To make a comparison between coordination of Cd(II) with selenourea and thiourea, we studied a series of similar Cd(II)-thiourea solutions. These studies reveal the differences between coordinating character of selenourea and thiourea ligand, which shows the ability of thiourea to form higher coordination number complexes with Cd(II)

than selenourea under similar conditions. Despite the above mentioned fact, $\text{Cd}(\text{SeU})\text{O}_5$ and $\text{Cd}(\text{TU})\text{O}_5$ and also $\text{Cd}(\text{SeU})_2\text{O}_4$ and $\text{Cd}(\text{TU})_2\text{O}_4$ show similar peak positions due to the high contribution of O coordination.

^{113}Cd NMR of Cd(II)-Thiourea solutions $\text{A}_2 - \text{G}_2$ (thiourea/Cd(II) ratio 1.0-10.0) were measured showing a mixtures of species with major octahedral species of CdSO_5 , CdS_2O_4 , CdS_3O_3 at lower ratios (solutions $\text{A}_2 - \text{C}_2$) which shifted to CdS_4O and CdS_4 species in higher thiourea ratios (solutions D_2 and E_2), the ^{113}Cd NMR peaks at 515 ppm and 506 ppm, respectively are in agreement with the value obtained from solid state ^{113}Cd NMR measurements of $\text{Cd}(\text{SCN}_2\text{H}_4)_4(\text{NO}_3)_2$ crystal at 577 ppm. Finally by increasing thiourea ratios to values higher than 8.0 (solutions F_2 and G_2), the ^{113}Cd NMR spectra moved to more shielded area indicating the presence of octahedral CdS_6 species which shows a ^{113}Cd chemical shift near the value obtained for the solid state $\text{Cd}(\text{SCHN}(\text{CH}_3)_2)_6](\text{ClO}_4)_2$ crystal structure at 403 ppm. The formation of CdS_6 generated an EXAFS oscillation with different phase shift than CdS_4 which causes dumping the amplitude of overall EXAFS.

Based on the results obtained from Cd K-edge EXAFS, Cd L_{III} -edge XANES, and ^{113}Cd NMR spectroscopy at room temperature, Cd(II)-thiourea solutions containing excess thiourea form $\text{Cd}(\text{TU})_4$ species with $\delta_{\text{Cd}} = 541$ ppm and Cd-S bond distance of 2.53 ± 0.02 Å. We confirmed that the speciation in the solution is mostly CdS_4 species.

Considering that the current study provides a library of chemical shifts for Cd(II)-thiourea in solutions, for future studies, EXAFS and ^{113}Cd NMR of structurally important Cd-thione complexes should be measured and compared with the present

results. Also, Cd(II) complex formation with bulkier selenone ligands with known crystal structure such as (1,3-dimethyl-2(3H)-imidazoleselenone, or new Se-containing drugs such as Ebselen, and also their sulfur analogues should be investigated and the result compared with our findings to find out the effect of different variables such as ligands' size, side chains, or nature of donor atoms on coordination chemistry of Cd(II) ions or other heavy metals such as Hg(II) and Pb(II).

Chapter Three: Structure of Cadmium (II) N-Acetylcysteine Complex

3.1 Introduction

Cadmium exposure causes hepatotoxicity and nephrotoxicity. The main target organs of cadmium are the liver and, to some extent, kidneys and other tissues. One of the detoxification mechanisms in the body is the formation of a nontoxic CdMT (MT = metallothionein) complex in the liver. Metallothionein is a cysteine-rich protein with 30 % cysteine (20 aminoacids residues out of the 60 are cysteines). Stored CdMT is later transferred to the kidneys. Cadmium toxicity happens when there is not enough MT to prevent cadmium from binding to thiol groups of other proteins, including enzymes. There are also reports on an increase in tissue glutathione (GSH) levels when cadmium exposure happens.¹⁴³

The chelating property of N-acetylcysteine (NAC) in excreting toxic metals has been studied by different groups. Ottenwälder and co-workers¹⁴⁴ showed that using N-acetylcysteine increases the excretion of Pb, Cd, and Au, but has no effect on Hg. Another study by Shaikh and co-workers¹⁴⁵ showed that N-acetylcysteine can affect Cd-induced nephrotoxicity and hepatotoxicity through one or more of the following processes: 1) by reducing CdMT release from the liver by either forming a complex with cadmium directly or by acting as a radical scavenger, 2) by providing cysteine for glutathione synthesis.

Understanding the nature of complexes formed between free Cd(II) ions in extracellular media is the purpose of this part of our study. This investigation follows the previous studies in our group, which were focused on structural studies on Cd(II)

complex formation with natural ligands such as cysteine and glutathione¹⁴⁶, or drugs such as penicillamine.¹⁴⁷

In this Chapter, complex formation between 0.1 M Cd(II) and NAC in aqueous solution was studied. The effect of changing pH (7.5 and 11.0) on the speciation in solution was investigated using different ligand concentrations (Cd(II)-NAC L / M = 2.0 to 20.0) at room temperature (RT) 298 K. This study was carried out using different methods, i.e., Cd K- and L_{III}-edge XAS, ¹¹³Cd NMR, as well as ESI-MS. The reason for choosing a rather high concentration of Cd(II) is to enable ¹¹³Cd NMR studies of these solutions.

$$[\text{Cd}^{2+}]_{\text{TOT}} = 100.00 \text{ mM}$$

$$[\text{NAC}^{2-}]_{\text{TOT}} = 200.00 \text{ mM}$$

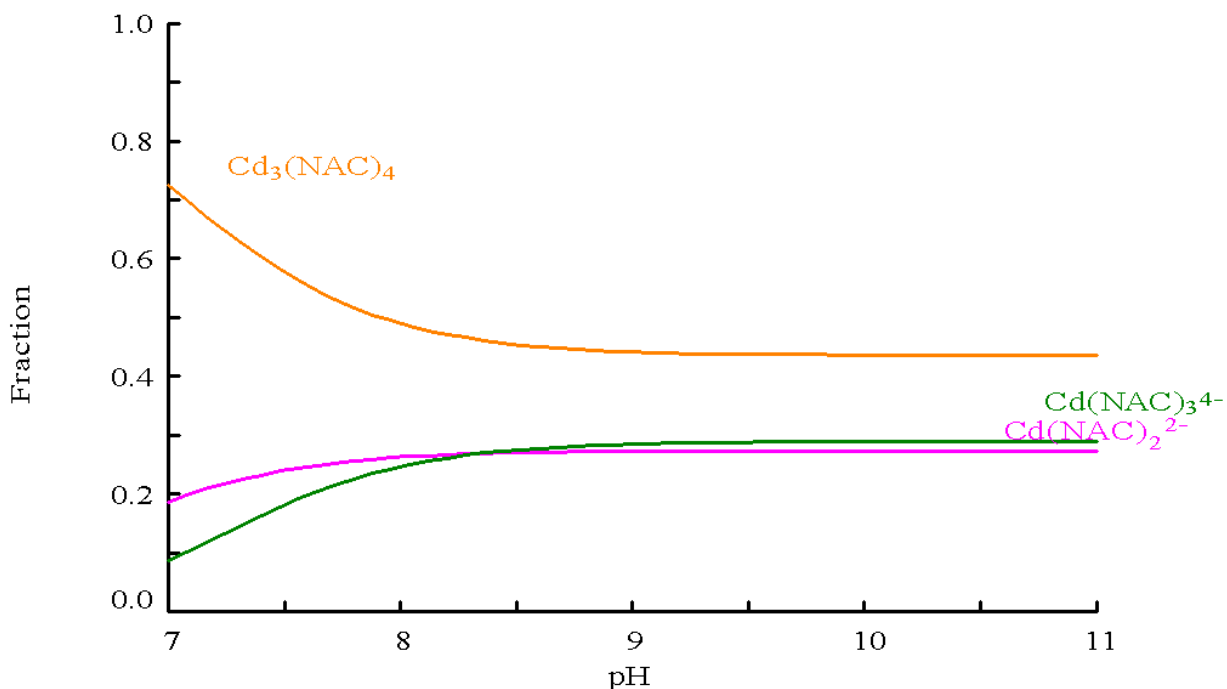


Figure 3-1 Fraction diagram of Cd(II)-N-acetylcysteine complexes in aqueous solution as a function of pH at $[\text{Cd}^{2+}] = 0.1 \text{ M}$ and $[\text{NAC}^{2-}] = 0.2 \text{ M}$.^{14,21,148}

Table 3-1 Stability constants for Cd^{2+} complexes with N-acetylcysteine (NAC).¹⁴⁸

<i>log β</i>			
$\text{Cd}(\text{NAC})$	$[\text{Cd}(\text{NAC})_2]^{2-}$	$[\text{Cd}(\text{NAC})_3]^{4-}$	$[\text{Cd}_3(\text{NAC})_4]^{2-}$
7.05	13.49	17.41	35.53

The stability constants for cadmium complexes of N-acetyl cysteine¹⁴⁸ are shown in Table 3-1.

The fraction diagram of Cd(II)-N-acetylcysteine complexes in aqueous solution is shown in Figure 3-1. This diagram is more accurate at low concentrations because the stability constants were measured at $[\text{Cd}^{2+}] : 1 \text{ mM}$ and there is a limitation in estimating the number of coordinating ligands especially with ligands that have two or more coordinating functional groups.¹⁴⁹

Based on the fraction diagram of N-acetylcysteine (Figure 1-5), it is obvious that near physiological pH ($\text{pH} = 7.5$) the thiol group is only slightly deprotonated. However, in the presence of heavy metals such as mercury, cadmium, or lead, there is a competition between H^+ and these M^{2+} ions to coordinate to the sulfur atom, leading to M-NAC coordination. Under alkaline conditions ($\text{pH} = 11.0$), the thiol group is fully deprotonated and, therefore, there is a higher possibility for species with higher coordination to form.

3.2 Experimental Methods

3.2.1 Sample Preparation

In order to avoid N-acetylcysteine oxidation, all samples were prepared under inert atmosphere using oxygen-free boiled water. Cadmium perchlorate hexahydrate $\text{Cd}(\text{ClO}_4)_2 \cdot 6\text{H}_2\text{O}$, sodium hydroxide, and N-acetylcysteine were purchased from Sigma Aldrich and used without further purification. The pH of the solutions was measured using a Corning semi-micro electrode.

3.2.2 Synthesis of Cd(II)-N-Acetylcysteine 100 mM Solutions in Water

Solutions containing $C_{\text{Cd(II)}} \sim 100 \text{ mM}$ were synthesized by dissolving N-acetylcysteine (2.0 - 20.0 mmol) in O_2 -free water, followed by the addition of $\text{Cd}(\text{ClO}_4)_2 \cdot 6\text{H}_2\text{O}$ (1.0 mmol) while stirring. Seven solutions with NAC / Cd(II) molar ratios of 2.0 (A_1), 3.0 (B_1), 4.0 (C_1), 5.0 (D_1), 10.0 (E_1), 15.0 (F_1) and 20.0 (G_1) were prepared at pH = 11.0 (see Table 3-2); in order to adjust the pH of the solutions, sodium hydroxide solution was used. The same method was used to synthesize seven solutions with NAC / Cd(II) molar ratios of 2.0 (A_2), 3.0 (B_2), 4.0 (C_2), 5.0 (D_2), 10.0 (E_2), 15.0 (F_2) and 20.0 (G_2) at pH = 7.5. For the ^{113}Cd NMR measurements, all of the above solutions contained ~10 % D_2O . For all above mentioned solution the total volume was 10.0 mL.

Table 3-2 Composition of Cd(II)-N-acetylcysteine solutions.

Solution (pH = 11.0)	Solution (pH = 7.5)	[Cd²⁺] (ppm)	L / M
A₁	A₂	100	2.0
B₁	B₂	100	3.0
C₁	C₂	100	4.0
D₁	D₂	100	5.0
E₁	E₂	100	10.0
F₁	F₂	100	15.0
G₁	G₂	100	20.0
I₁	I₂	500	2.0
A'₁	A'₂	10	2.0
B'₁	B'₂	10	3.0
C'₁	C'₂	10	4.0
D'₁	D'₂	10	5.0

In order to investigate the metal complex formation with N-acetylcysteine, combination of the following spectroscopic methods were used:

3.2.3 ¹¹³Cd NMR Spectroscopy

¹¹³Cd NMR spectra of Cd(II)-NAC solutions A₁ – G₁ and A₂ – G₂ were recorded at 298 K and a resonance frequency of 88.6 MHz using a Bruker DRX400 spectrometer (9.4 T). A 0.1 M solution of Cd(ClO₄)₂·6H₂O in D₂O was used as the external reference at room temperature and the chemical shift calibrated to 0.0 ppm.¹⁵⁰ A 60° pulse program (zgdc) was used with a sweep width between -50 to 750 ppm using a 5 mm broad band (BBO) probe with a two second delay. The NMR spectrum for 0.5 M Cd(II)-N-acetylcysteine solution NAC / Cd(II) = 2.0 (I₁, pH = 11.0) was measured at different temperatures (288 K, 298 K, 310 K, 320 K, 330 K, and 341 K).

3.2.4 X-ray Absorption Spectroscopy Data Collection

Cd K-edge X-ray absorption spectra were collected using beamlines 7-3 at the Stanford Synchrotron Radiation Lightsource (SSRL) with storage ring operating with 150 - 200 mA current at 3.0 GeV. Ion chambers I_0 , I_1 and I_2 were filled with Ar gas. Spectra for solutions $A_1 - G_1$ and $A_2 - G_2$ were measured in transmission mode. These solutions were held in 5 mm Teflon spacer with 5 μ m polypropylene films as window material. Harmonic rejection was achieved by detuning the Si (220) double crystal monochromator to $\approx 50\%$ of the maximum I_0 intensity at the end of the scan (27735 eV). The energy of the X-rays was calibrated by assigning the first inflection point of a Cd foil to 26711 eV. Either 2 or 3 scans were collected and averaged. Cd L_{III} -edge XANES spectra for solutions $A_1 - G_1$ (pH = 11.0) were measured in fluorescence mode using a PIPS solid state detector on BL 4-3 at SSRL. Ion chamber I_0 was filled with He gas. Solutions containing $C_{Cd(II)} \approx 100$ mM ($A_1 - G_1$, pH = 11.0) were held in 2 mm Teflon spacer with 5 μ m polypropylene film as window material. Higher harmonics from Si (111) double crystal monochromator were rejected with a nickel and rhodium coated mirror. The energy was calibrated by assigning the first inflection point of a cadmium foil to 3537.6 eV. Either 2 or 3 scans were collected for each sample.

3.2.5 X-ray Absorption Spectroscopy Data Analysis

Cd K-edge X-ray absorption data were calibrated and averaged using the EXAFSPAK program.⁹⁰ Individual scans were overlapped before averaging the scans, to ensure that no radiation damage had occurred. The EXAFS oscillations were extracted using the WinXAS 3.1 program.⁹¹ The background in the pre-edge region was removed

using a first order polynomial. This was followed by normalization of the edge (in order to delete the effect of sample concentration and thickness), then conversion of the energy into k -space, where $k = \sqrt{[(8\pi^2 m_e / h^2)(E - E_0)]}$, using a threshold energy of $E_0 = 26710.0 - 26710.6$ eV. Above the edge the atomic background contribution was removed by subtracting a 7-segment cubic spline. The $\chi(k)$ models were constructed by means of *ab initio* calculation of the effective amplitude function $|f_{\text{eff}}(k)|_i$, the total phase-shift $\phi_{ij}(k)$, and photoelectron mean free path $\lambda(k)$, using the FEFF 8.1 program. The atomic coordinates of the crystal structure of imidazolium aquatris(thiosaccharinato)-cadmium(II) with CdS_3O geometry was used as a FEFF model (Figure 3-2).

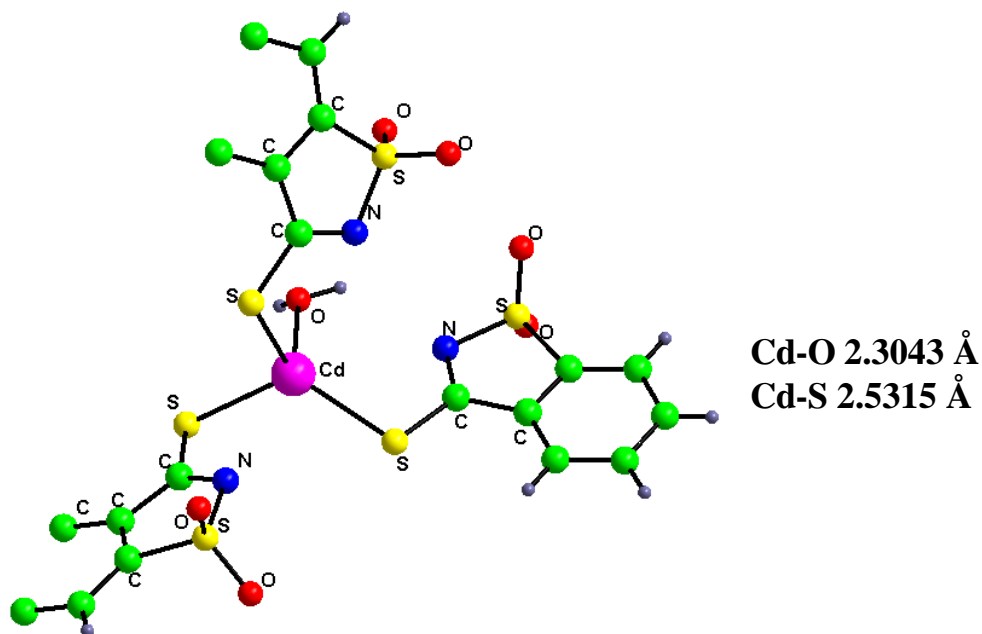


Figure 3-2 Structure of $\text{Cd}((\text{tsac})_3(\text{H}_2\text{O}))$ (tsac = anion of thiosaccharine) used as a FEFF model to simulate EXAFS spectra¹⁵¹.

The structural parameters of the model function were refined by least squares curve-fitting to the k^3 -weighted experimental EXAFS data using the Win XAS 3.1 program, by fixing the S_0^2 (≈ 0.87), and/or N , allowing R , σ^2 , and ΔE_0 to float. The estimated error of the refined Cd-S coordination numbers, bond distances and disorder parameters are within $\pm 20\%$, $\pm 0.02 \text{ \AA}$, and $\pm 0.001 \text{ \AA}^2$, respectively. Due to the difficulty in separating the lighter Cd-(O/N) contribution in the presence of heavier scatterers (like sulfur), the obtained results for structural parameters are less accurate, with the estimated error of the bond distances within $\pm 0.04 \text{ \AA}$, and $\pm 0.003 - 0.005 \text{ \AA}^2$ for the disorder parameters.¹⁴⁶

3.3 Result and Discussion

3.3.1 ^{113}Cd NMR Spectroscopy of Cd(II)-N-Acetylcysteine Solutions at pH = 11.0

There are two possibilities for N-acetylcysteine coordination to cadmium: it can either coordinate through oxygen of the carboxylate group or sulfur of the thiolate group. Coordination through sulfur will show more deshielding than through oxygen.¹⁵² The deshielding trend for ^{113}Cd is $\text{S} > \text{N} > \text{O}$, where S is the most deshielding.

^{113}Cd NMR spectra of solutions B₁ – G₁ are shown in Figure 3-3 and Figure 3-4. The changes in the chemical shift suggest the existence of different species in the solution. No ^{113}Cd NMR signal could be obtained for solution A₁ (after more than 72 hours of measurement) at room temperature. This may be because of the low

concentration of species and/or fast exchange between different species existing in the solution.

For 0.1 M Cd(II)-NAC solution B₁ L / M = 3.0 (Figure 3-3), a broad peak was observed at 630 ppm; this peak is related to the CdS₃O as a dominant species. CdS₃O₃ is much more shielded also Cd(Pen)₃ appeared at 607 ppm, therefore a mixture of CdS₃O and CdS₄ in intermediate ligand exchange is more feasible.

For solution C₁ (L / M = 4.0), a sharper signal at 659 ppm was observed (Figure 3-3), which is shifted more toward the CdS₄ chemical shift region, although the broadness of the peak and the chemical shift position may be related to a mixture of CdS₃O and CdS₄ species. For Cd(II)-NAC solutions D₁ – G₁, L / M > 4.0, a sharp signal around 677 ppm indicates that the dominant species is a CdS₄¹¹⁵ coordinated environment.

Table 3-3 ¹¹³Cadmium chemical shifts for various thiolate coordination environments.
147, 153

Coordination environment	Chemical Shift (δppm)
CdS ₄ (mono nuclear)	650, 680, 704-751
CdS ₄ (multi nuclear)	600-707
CdS ₃	572, 684-690
CdS ₃ O	560-645
CdS ₃ O ₃	391-409

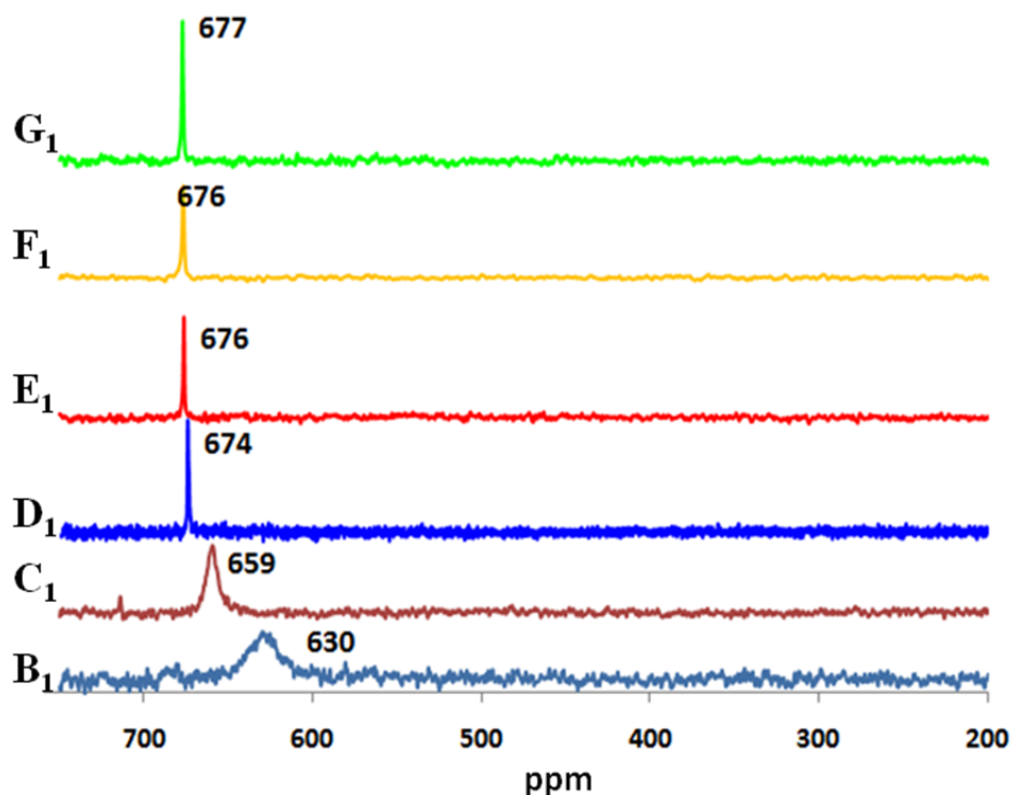


Figure 3-3 ^{113}Cd NMR spectra of 0.1 M Cd(II)-NAC solutions $\text{B}_1 - \text{G}_1$ at pH = 11.0 and 298 K.

In order to observe a ^{113}Cd NMR signal for solution A_1 , the temperature was raised to 341 K. The spectrum shows a signal at 487 ppm (Figure 3-4). In order to understand the nature of species present in A_1 ($\delta = 487$ ppm), a 0.5 M solution (I_1) of Cd(II)-NAC with L / M ratio = 2.0 was synthesized and corresponding ^{113}Cd NMR spectra were measured at variable temperature. By decreasing the temperature to 288 K, three peaks appeared for solution I_1 that become more obvious at 423, 585, and 643 ppm, that can be related to CdS_3O_3 , CdS_3O (S = thiolate, O = hydroxyl, carboxylate or aqua) and CdS_4 coordination sites respectively. The reported chemical shifts in literature are usually based on RT measurements. The ^{113}Cd chemical shift is temperature dependent

because of the effects on the dynamic exchange processes. Considering the NAC / Cd(II) ratio = 2.0, formation of complexes with CdS_3O_3 , CdS_3O , and CdS_4 requires multinuclear complexes with single Cd-S-Cd bridging groups. By increasing the temperature from 288 K to 341 K for solution I_1 , a broad peak around 515 ppm was observed that is in the region between CdS_3O_3 and CdS_3O , showing a possible balance between these two species or just an average of three signals at 288 K. Comparison between ^{113}Cd NMR of solution A_1 and I_1 at 341 K shows a difference of 27 ppm in chemical shift. Since chemical shift for I_1 is slightly more deshielded, this might be due to less concentration of CdS_3O_3 in I_1 relative to A_1 .

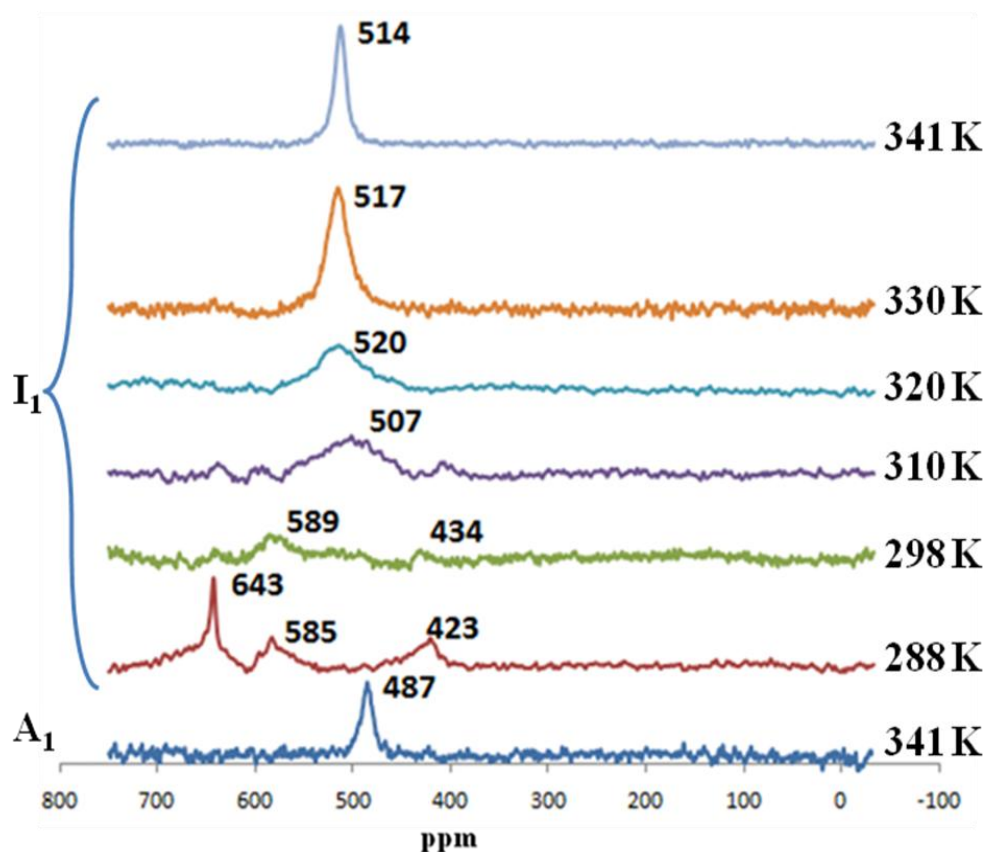


Figure 3-4 ^{113}Cd NMR spectra for Cd(II)-NAC solutions A_1 and I_1 at pH = 11.0

3.3.2 Extended X-ray Absorption Fine Structure of Cd(II) N-Acetylcysteine Solutions at pH = 11.0

The EXAFS spectroscopy results (Figure 3-5) showed an average Cd-S bond distance of 2.53(2) Å for Cd-NAC in solutions A₁ – G₁.

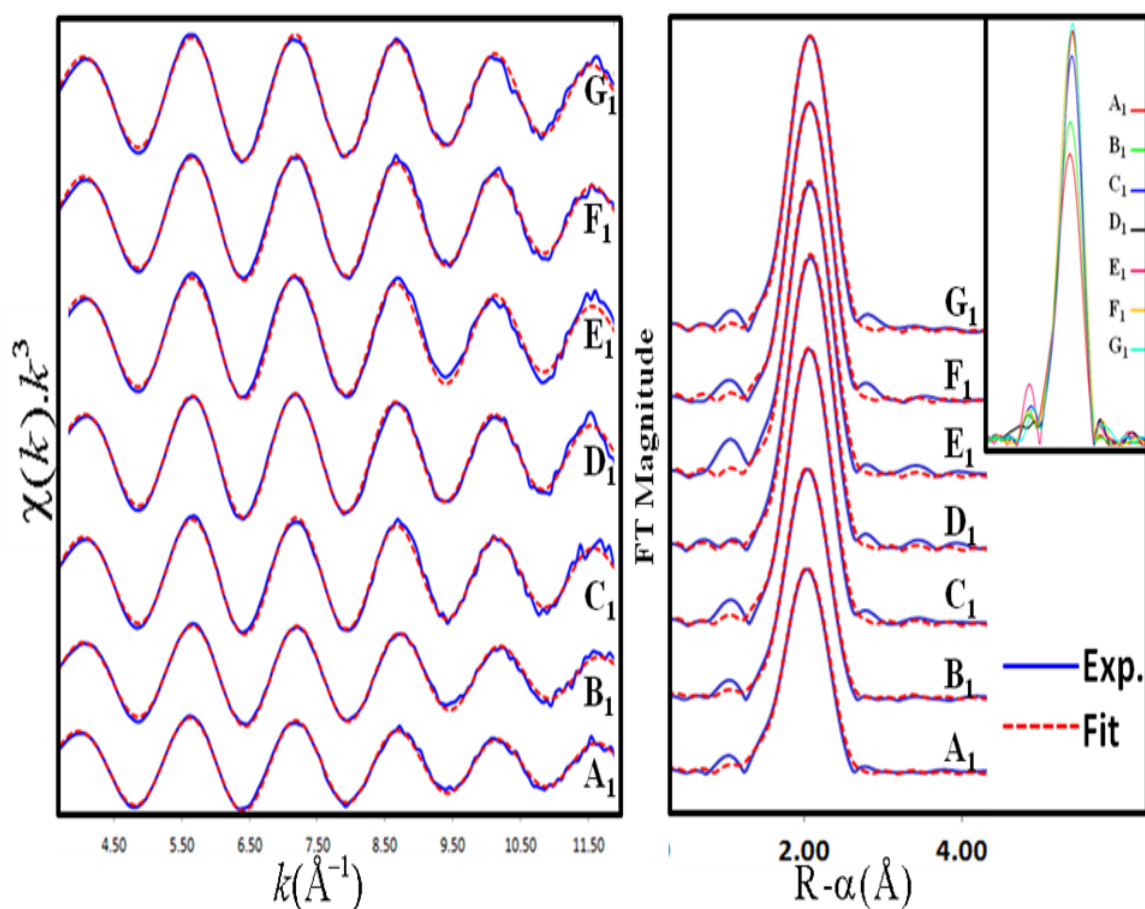


Figure 3-5 (Left) Cd K-edge EXAFS least-squares curve fitting of 0.1M Cd(II)-NAC solutions A₁ – G₁ at pH = 11.0 and (Right) their corresponding Fourier-transforms.

Table 3-4 EXAFS curve-fitting results for Cd(II)-NAC solutions $A_1 - G_1$ at pH = 11.0.

Solution	Path	C.N.	R(Å)	$\sigma^2(\text{Å}^2)$	Residual
A₁	Cd-S	3.2	2.53	0.0066	15.0
	Cd-O	1.1	2.31	0.0062	
B₁	Cd-S	3.0f	2.53	0.0067	9.7
	Cd-O	1.2	2.35	0.0037	
C₁	Cd-S	4.0f	2.52	0.0058	14.8
	Cd-S	2.9	2.53	0.0041	9.59
	Cd-O	1.2	2.33	0.0066	
D₁	Cd-S	4.2	2.53	0.0053	9.1
E₁	Cd-S	4.0	2.53	0.0049	14.5
F₁	Cd-S	4.1	2.53	0.0050	9.2
G₁	Cd-S	4.2	2.53	0.0053	10.0

A survey of Cd-S bond distances in compounds with known crystal structures in the Cambridge Structural Database (CSD)³³ reveals the average Cd(II)-thiolate bond distance for different octahedral (CdS_6 , CdS_4O_2 , and CdS_3O_3) and tetrahedral (CdS_4 and CdS_3O) coordination (Table 3-5).³³

Table 3-5 A survey of Cd(II)-S bond distance available in CSD for thiolate complexes.³³

Coordination Environment	Cd-O R(Å) distance range	Cd-O R(Å) average	Cd-S R(Å) distance range	Cd-S R(Å) average
CdSO_6	2.36-2.67	2.42	2.77	2.77
CdS_2O_4	2.37-2.41	2.39	2.62	2.62
CdS_3O_3	2.29-2.75	2.50	2.54-2.60	2.57
CdS_3O	2.30	2.30	2.49-2.57	2.53
CdS_4			2.52-2.61	2.55
CdS_6			2.69-2.73	2.71

The EXAFS spectra of the Cd(II)-NAC solution A_1 and B_1 were modeled to 1 Cd-O and 3 Cd-S bonds with the mean distances of 2.33 ± 0.04 Å and 2.53 ± 0.02 Å,

respectively. In the presence of sulfur (a heavier backscatterer), the presence of oxygen (a lighter backscatterer) is harder to detect. The large σ^2 value, $0.006 \pm 0.001 \text{ \AA}^2$ (Cd-S), indicates the distribution of Cd-S distances.

The average Cd-S bond distance in B_1 , 2.53 \AA , indicates tetrahedral species in solution, with the possibility of CdS_4 and CdS_3O coordination environments. This is in agreement with $\delta_{\text{Cd}} = 659 \text{ ppm}$ (Figure 3-3). As was shown by both ^{113}Cd NMR and EXAFS measurements, there is a mixture of species, mainly CdS_3O and CdS_3O_3 , which is the reason for broader peaks at lower ratios in the ^{113}Cd NMR spectrum.

As it was shown in Table 3-4, with the S_0^2 factor fixed at 0.9 (the fixed value for S_0^2 obtained from curve fitting of standard models), the results show that the Cd-S coordination number increases as the N-acetylcysteine concentration increases. By combining ^{113}Cd NMR chemical shifts with EXAFS bond distances, we can have a better idea of what the Cd-S coordination number is. As shown in Figure 3-5, the increase in the amplitude of the FT for solutions $A_1 - G_1$ shows an increase in the Cd-S contribution as the ligand to metal ratio increases from 2.0 to 20.0. Also, the Cd-S σ^2 decreases from 0.0066 \AA^2 to 0.0052 \AA^2 , indicating the presence of a dominant species. Presence of tetra thiolate CdS_4 complex can be confirmed with Cd L_{III} -edge.

3.3.3 X-ray Absorption Near Edge Structure of Cd(II) N-Acetylcysteine Solutions at $pH = 11.0$

The Cd L_{III} -edge X-ray absorption near edge structure (XANES) region is sensitive to the type of coordination environment around the absorbing atom. Cd L_{III} -edge spectra of several Cd complexes with known structure were previously measured in

our group (Figure 3-6) and demonstrate the sensitivity of Cd L_{III}-edge to coordination chemistry. In the case of the octahedral CdO₆ species, it can show a pre-peak at 3534.9 eV.¹⁵⁴

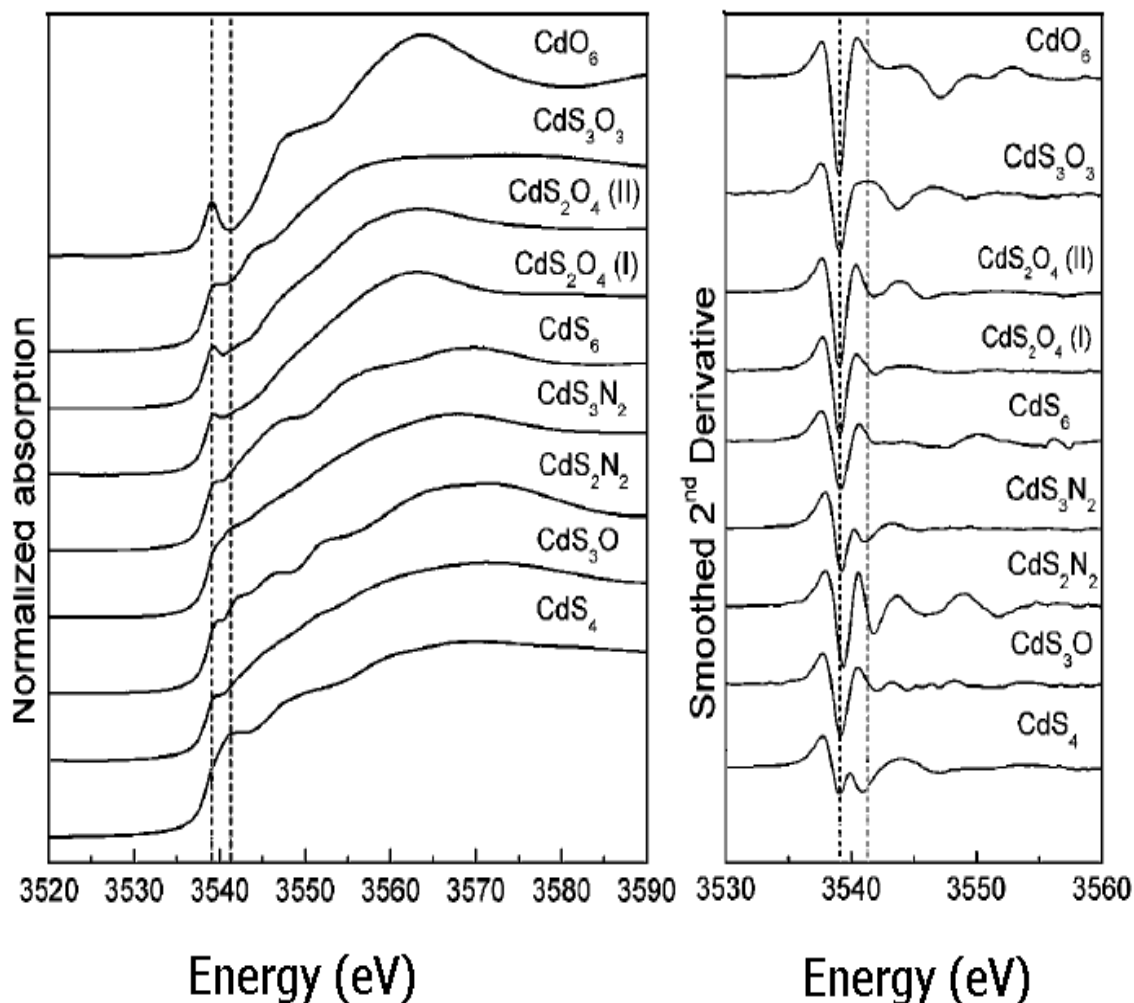


Figure 3-6 (Left) Cadmium L_{III}-edge XANES and (Right) corresponding second derivatives of (CdO₆), Cd(ClO₄)₂·6H₂O; (CdS₃O₃), [Ph₄P][Cd(SCO(CH₃))₃]; [CdS₂O₄(II)], [Cd(tu)₂(NO₃)₂]; [CdS₂O₄(I)], [Cd(tmtu)₂(NO₃)₂] tmtu = tetramethyl thiourea; (CdS₆), [Cd(SCHN(CH₃)₂)₆](ClO₄)₂; (CdS₃N₂), [Cd(SCH₂CH₂NH₂)₂]; (CdS₂N₂), [Cd(tsac)₂(Im)₂] Im = imidazole; (CdS₃O), (HIm)[Cd(tsac)₃(H₂O)] tsac = thiosaccharinato; and (CdS₄), (Et₃NH)₄[S₄Cd₁₀(SPh)₁₆].¹⁵⁵ Dotted lines are at 3539.1 and 3541.3 eV.

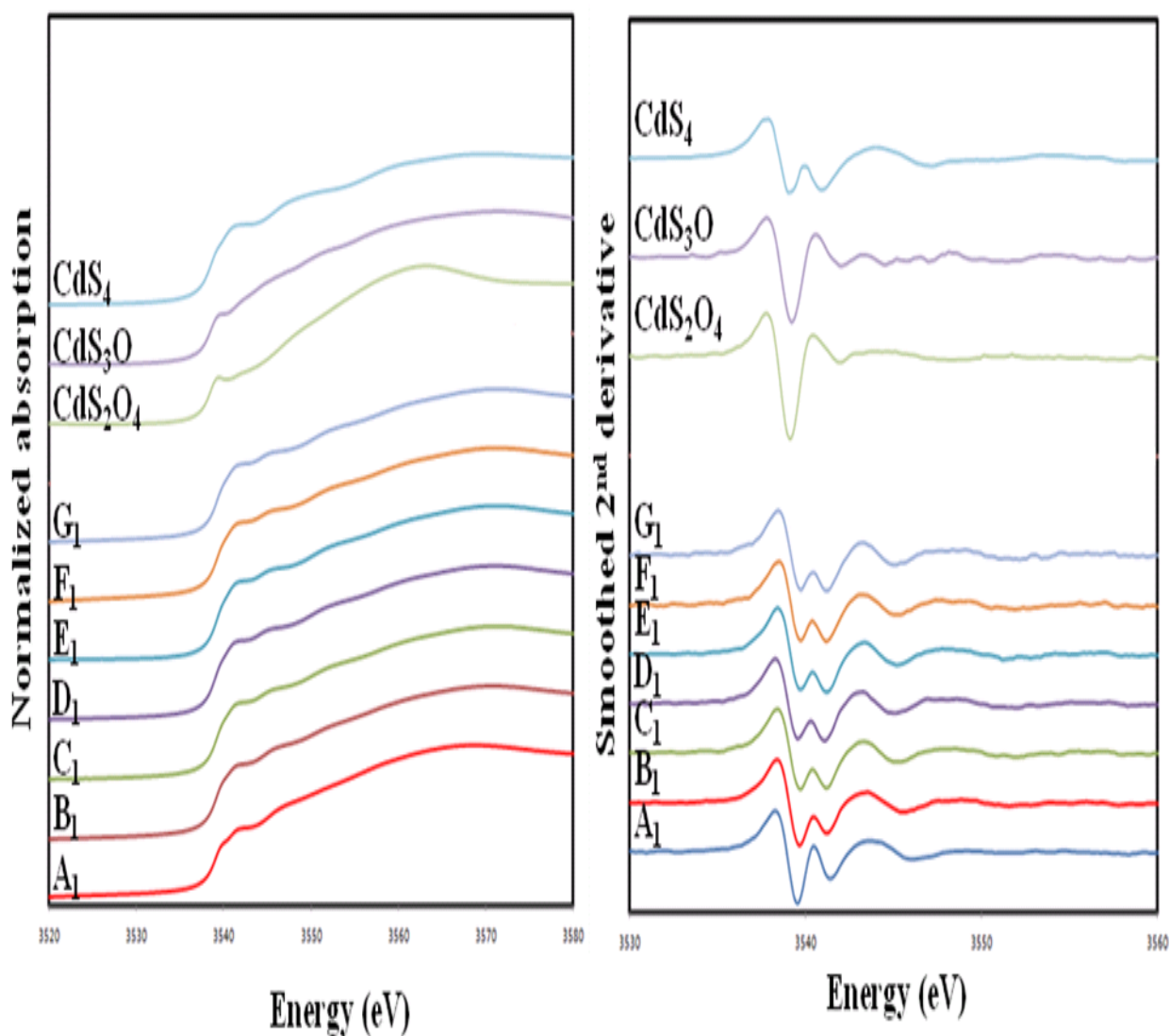


Figure 3-7 (Left) Cadmium L_{III}-edge XANES spectra Cd(II)-NAC solutions A₁ – G₁ and (Right) corresponding smoothed second derivatives.

In the tetrahedral CdS₃O model, having oxygen coordination gives rise to some features in the edge region; in the case of CdS₄ that has only sulfur coordination, the edge is smoother with fewer features (Figure 3-7). The differences between these structures are more obvious in their second derivative. In the octahedral model (CdS₂O₄), only one minimum is observed in second derivatives, while in the tetrahedral models, an additional

minimum appears in the region near 3541 -3543 eV, specifically at 3540.9 eV in the CdS₄ model. There is an obvious difference between second derivatives of the CdS₄ and CdS₃O models.

Cd L_{III}-edge of Cd(II)-NAC C₁ – G₁ solutions show more similarity to the CdS₄ model than the CdS₃O and based on the ¹¹³Cd NMR of these solutions, it seems that the dominant species in these solution is CdS₄.

3.3.4 ¹¹³Cd NMR Spectroscopy of Cd(II)-N-Acetylcysteine Solutions at pH = 7.5

For 0.1 M Cd(II)-NAC solutions at pH = 7.5, ¹¹³Cd NMR signal could be only observed at RT for solutions D₂-G₂ with NAC / Cd(II) ratios of 5.0-20.0, over the range of 629 - 659 ppm. Chemical shift for G₂ (L / M = 20.0, pH = 7.5) is the same as solution C₁ (L / M = 4.0, pH = 11.0), i.e. 659 ppm. This means that both solutions have similar Cd(II) speciation, and free thiolate concentration. Free ligand N-acetylcysteine is mainly present as HNAC⁻ at pH = 7.5 and only small percentage of it is in NAC²⁻ form. (Figure 1-5). At L / M < 5.0, the presence of different species (e.g. CdS₃O₃, CdS₃O, and CdS₄ as observed for ¹¹³Cd NMR of solution I₂ at 288 K; Figure 3-4) causes broadening of the ¹¹³Cd NMR signal and therefore no signals were observed at RT.

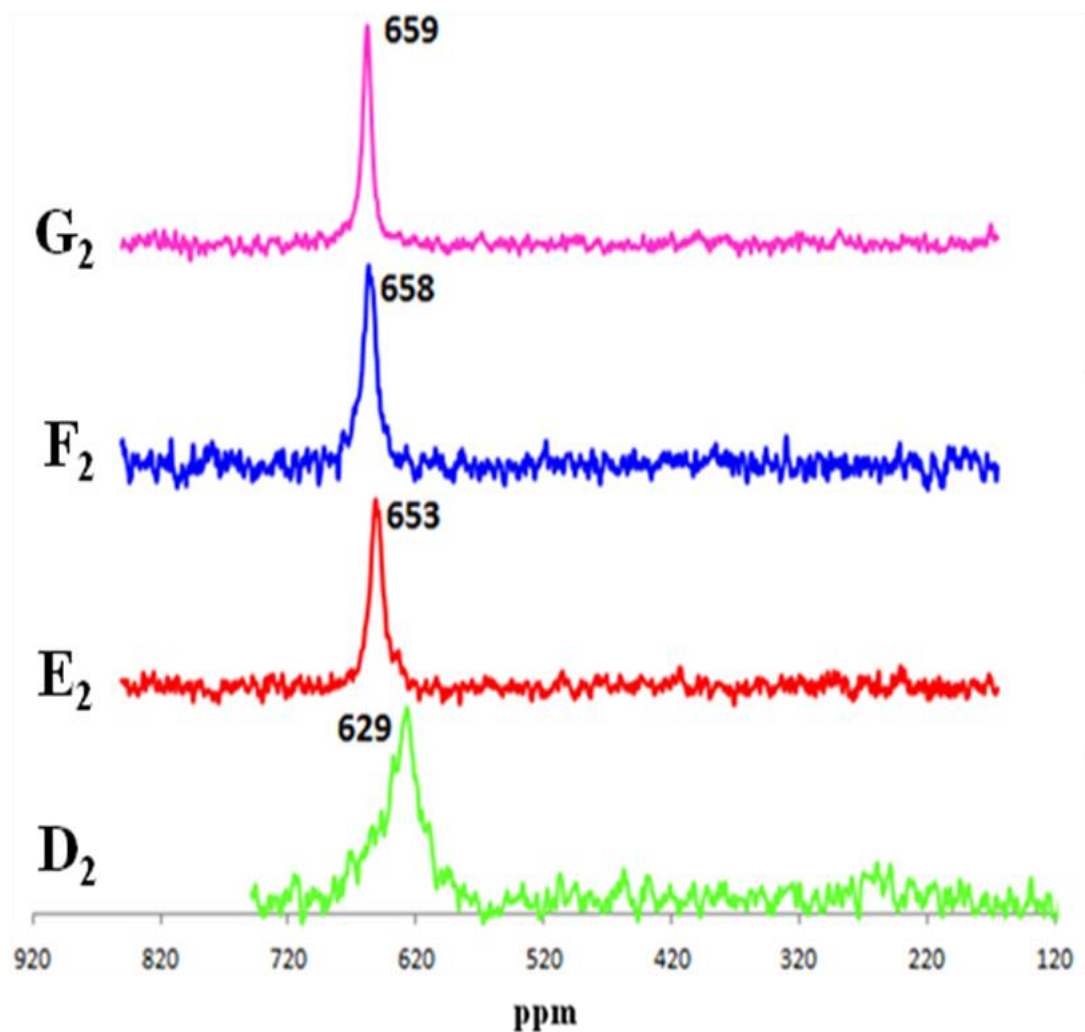


Figure 3-8 ^{113}Cd NMR spectra of 0.1M Cd(II) - NAC solutions $\text{D}_2 - \text{G}_2$ at 298 K (L / M mole ratio = 5.0 – 20.0 at pH = 7.5).

The broad NMR peak for solution D_2 reveals the presence of a mixture in the solution, which, based on chemical shift (629 ppm), shows the presence of major CdS_3O and minor CdS_4 species. Increasing the L / M ratio causes the the NMR peaks to become sharper and shift to higher chemical shift values (Figure 3-8) indicating an increase in the possibility of the formation of CdS_4 species. This indicates that as the concentration of

NAC^{2-} increases, there is a higher thiolate concentration in the solution and higher possibility of tetrathiolate $\text{Cd}(\text{NAC})_4$ formation. Comparison between the NMR spectra of solutions $\text{D}_1 - \text{G}_1$ in Figure 3-3 and $\text{D}_2 - \text{G}_2$ in Figure 3-8 indicates that in the first series ($\text{pH} = 11.0$), a sharp NMR signal at 677 ppm proved that the only species present in those solutions is CdS_4 , while in the latter ($\text{pH} = 7.5$), the broad NMR peak in more shielded regions shows the presence of CdS_3O and CdS_4 geometries.

In aqueous solution, for $\text{Cd}(\text{II})$ - N-acetylcysteine complexes, potentiometric titrations for 1 mM Cd^{2+} solutions have confirmed the existence of $[\text{Cd}(\text{NAC})_3]^{4-}$, $[\text{Cd}(\text{NAC})_2]^{2-}$, and $[\text{Cd}(\text{NAC})]$ at $[\text{Cd}^{2+}] = 0.1 \text{ M}$.¹⁴ However, in the current study $\delta_{^{113}\text{Cd}}$ is considerably deshielded for having CdS_2O_4 as $[\text{Cd}(\text{NAC})_2]^{2-}$ or CdSO_5 as $[\text{Cd}(\text{NAC})]$ complexes in solution.

However our ^{113}Cd NMR studies show the possibility of $[\text{Cd}(\text{NAC})_4]^{6-}$ species in these systems. According to our studies increasing the ligand concentration in these solutions at both pH values studied ($\text{pH} = 7.5$ and 11.0), increases the possibility of higher S-coordination in the $\text{Cd}(\text{II})$ -NAC system.

3.3.5 Extended X-ray Absorption Fine Structure of Cd(II) N-Acetylcysteine Solutions

at pH = 7.5

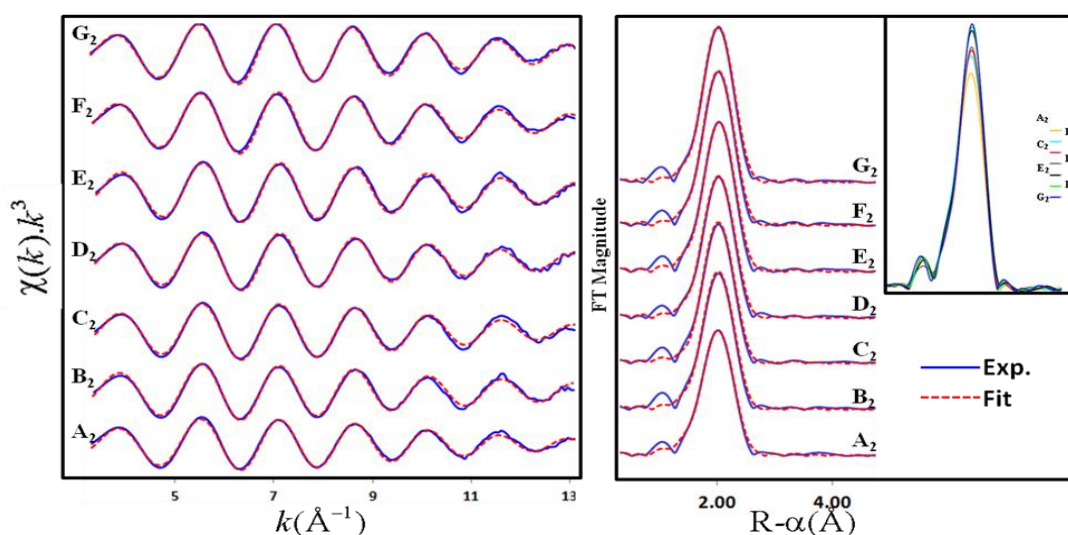


Figure 3-9 (Left) EXAFS fitting of 0.1M solution of Cd(II)-NAC solutions $A_2 - G_2$ at pH = 7.5 and (Right) their corresponding Fourier-transforms.

Table 3-6 EXAFS curve-fitting results for Cd(II)-NAC solutions $A_2 - G_2$ (pH = 7.5).

Solution	Path	C.N.	R(Å)	$\sigma^2(\text{Å}^2)$	Residual
A_2	Cd-S	2.94	2.52	0.0057	8.8
	Cd-O	1.0	2.25	0.011	
	Cd-S	3.7	2.51	0.0072	10.3
B_2	Cd-S	3.8	2.51	0.0066	10.6
	Cd-O	0.05	2.11	0.0077	
	Cd-S	3.7	2.51	0.0063	12.1
C_2	Cd-S	3.6	2.51	0.0061	11.1
	Cd-S	3.0f	2.53	0.0065	11.7
	Cd-O	1.0f	2.35	0.0023	
D_2	Cd-S	3.8	2.52	0.0063	9.5
E_2	Cd-S	3.8	2.52	0.0058	11.4
F_2	Cd-S	3.9	2.52	0.0059	9.3
G_2	Cd-S	4.0	2.52	0.0058	9.3

Cd K-edge spectra of solution A₂ – G₂ were measured at RT. The result (Table 3-6) showed an average Cd-S bond distance of 2.52 ± 0.04 Å for Cd-S and 2.25 ± 0.02 Å for Cd-O, which is in agreement with the reported values for CdS₃O. Appendix A₁ shows different bond distances for Cd-S and Cd-O based on the coordination environment. These bond distances are used to confirm the coordination number around the Cd(II) ion.

The large σ^2 value (0.007 ± 0.0002 Å²) for the Cd-S bond in solutions A₂ and B₂ indicates the possibility of having a distribution in Cd-S bond distance. In solutions with ligand to metal ratios higher than 5.0, the ¹¹³Cd NMR signal position shows a mixture of species with an increase in the proportion of CdS₄ species.

The same phenomena that happens in the amplitude of FT for solution at pH = 11.0 (see Figure 3-5), was observed for solution at pH = 7.5 (Figure 3-9) showing that as the ligand to metal ratio increases, a higher contribution of Cd-S bonds is observed.

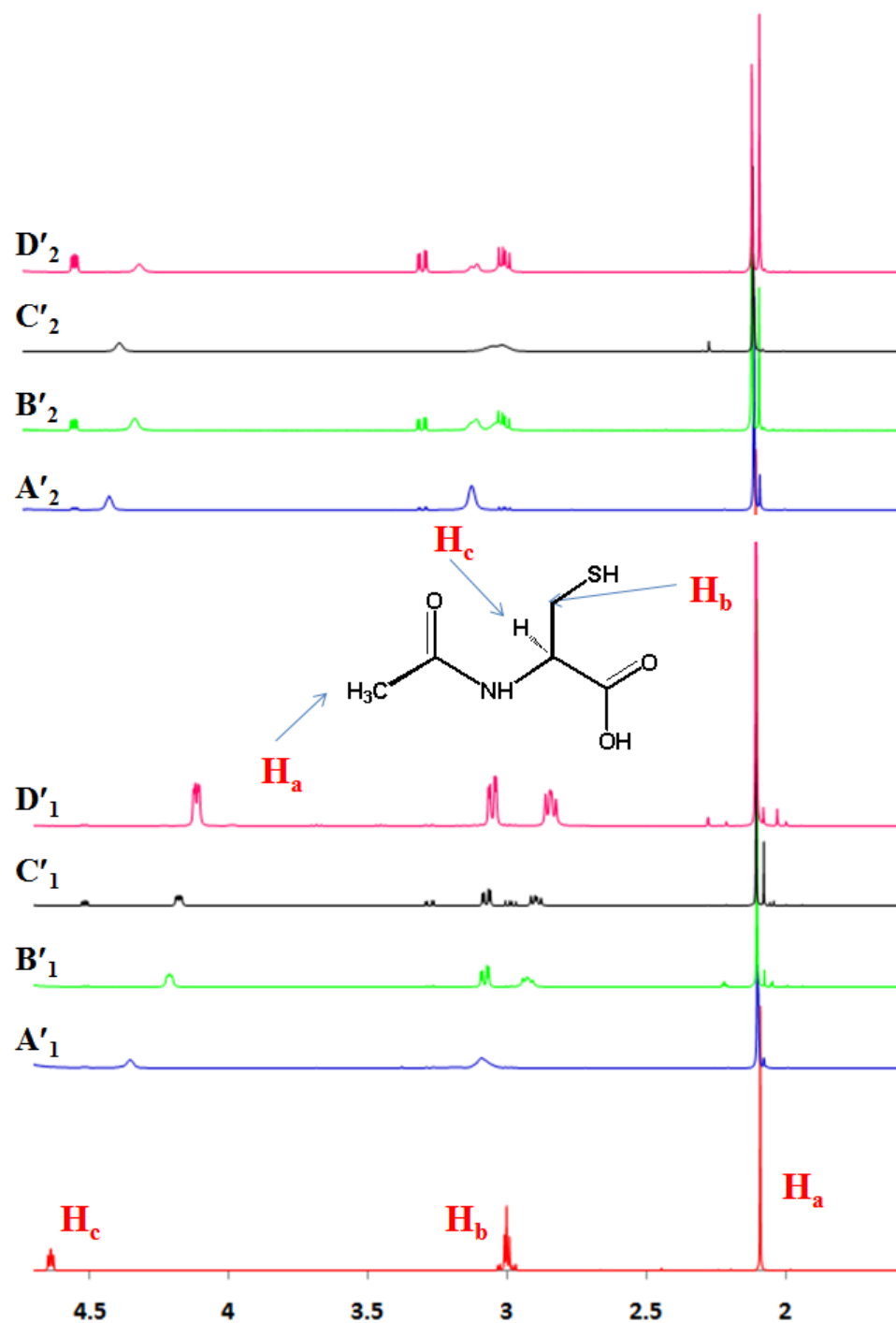


Figure 3-10 ^1H NMR spectra of 10 mM CdNAC solution A'₁ - D'₁ (pH 11.0) and A'₂ - D'₂ (pH 7.5) with NAC / Cd(II) = 2.0 – 5.0, comparing with free N-acetylcysteine.

As shown in Figure 3-10, the comparison between ^1H NMR spectra of 0.01 M Cd(II)-NAC solution and free N-acetylcysteine was made. As was mentioned before cadmium coordination to carboxylate group and thiolate group of N-acetylcysteine increases at $\text{pH} > 3.5$ and 9.0, respectively. The ^1H NMR spectra of Cd(II)-NAC solutions are somewhat broader than free N-acetylcysteine because of exchange between coordinated and free N-acetylcysteine molecules. Additionally, the ^1H NMR spectra showed that peak position of protons (i.e., H_b and H_c) near the N-acetylcysteine functional groups (i.e., carboxylate and thiolate) became more shielded upon complex formation.

3.4 Conclusion and Future Work

Based on potentiometric studies,^{19,148} the $\text{Cd}(\text{NAC})_3^{4-}$ complex, which has a high formation constant, is the highest reported coordination number in Cd(II)-N-acetylcysteine complex formation. A previous study in our group¹⁴⁷ showed that penicillamine cannot act as an effective chelator for cadmium removal due to its inability to form 4-coordinated CdS_4 species. N-acetylcysteine appears to have the ability to form $\text{Cd}(\text{NAC})_4^{6-}$ with average Cd-S bond distance of $2.53 \pm 0.02 \text{ \AA}$. Based on the following results obtained from ^{113}Cd NMR and XAS spectroscopy, we confirmed the formation of four-coordinated $\text{Cd}(\text{NAC})_4^{6-}$.

Cd(II) complexation with N-acetylcysteine at $\text{pH} = 7.5$ and $\text{pH} = 11.0$ and $[\text{Cd}^{2+}] = 0.1\text{M}$ shows the formation of $\text{Cd}(\text{NAC})_4^{6-}$ species at high free ligand concentration. This is the first report of this Cd(II) tetrathiolate complex with N-acetylcysteine. In Cd(II)-NAC solutions with $L / M < 3.0$ at $\text{pH} = 11.0$, a mixture of CdS_3O_3 , CdS_3O , and CdS_4

coordination sites within an oligomeric species with single thiolate bridges would be expected. As the ligand concentration increases, CdS_4 species concentration increases, which causes the NMR signals to shift to more deshielded regions. At $\text{pH} = 7.5$, less free thiolate ligand is present and therefore a mixture of CdS_3O and CdS_4 is formed even at very high N-acetylcysteine concentrations.¹⁵⁶

For future studies, the complex formation of N-acetylcysteine with lower concentrations of cadmium and under biological conditions and should be studied. This can be accomplished using XAS spectroscopy (Cd K-edge and Cd L_{III} -edge) to determine if the Cd speciation changes significantly when the Cd concentration change to lower values. Since one of the limits of ^{113}Cd NMR is concentration, XAS spectroscopy will be helpful at lower Cd concentration studies. These methods can be developed to investigate *in vivo* reactions of cadmium with N-acetylcysteine in the presence of other thiol-containing groups such as metallothionein, and glutathione.

Appendix A-1 Survey of Cd(II) complexes with thione (CdS₄, CdS₃O, CdSO₆, CdS₂O₄, CdS₃O₃, and CdS₆) ligands in CSD version 5.30 (November 2008).

CdS ₄		
	<i>CSD Code</i>	<i>Cd-S (Å)</i>
1	AYABIL	2.534
		2.532
		2.549
		2.553
2	CAFMEC	2.528
		2.516
		2.563
		2.526
3	CAGSEI	2.517
		2.562
		2.564
		2.496
4	GUFHIZ	2.541
		2.541
		2.541
		2.541
5	MAKVAV	2.525
		2.574
		2.530
		2.611
6	MAKVAV01	2.534
		2.552
		2.506
		2.582
7	XANHOJ	2.569
		2.569
		2.569
		2.569
Range		2.516 – 2.611
Average		2.546

Appendix A-1 (continued)

CdS ₃ O			
<i>CSD Code</i>		<i>Cd-S</i> (Å)	<i>Cd-O</i> (Å)
1	UKOTIX	2.573	2.304
		2.529	
		2.493	
Range		2.493 – 2.573	2.304
Average		2.532	

CdSO ₆			
	<i>CSD Code</i>	<i>Cd-S</i> (Å)	<i>Cd-O</i> (Å)
1	GECZOD	2.415	2.674
			2.276
			2.259
			2.360
			2.362
			2.561
	Range	2.773	2.360 – 2.674
Average	2.415		

CdS ₂ O ₄			
<i>CSD Code</i>		<i>Cd-S</i> (Å)	<i>Cd-O</i> (Å)
1	KASWOQ	2.617	2.374
		2.617	2.374
			2.408
			2.408
Range		2.617	2.374 – 2.408
Average			2.391

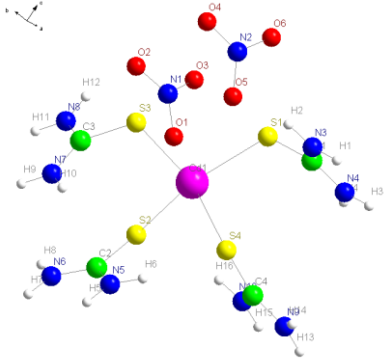
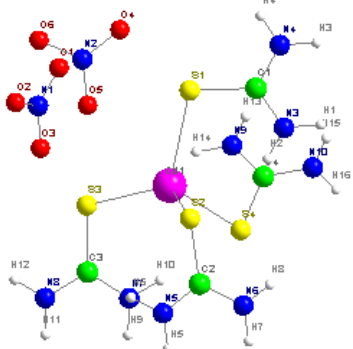
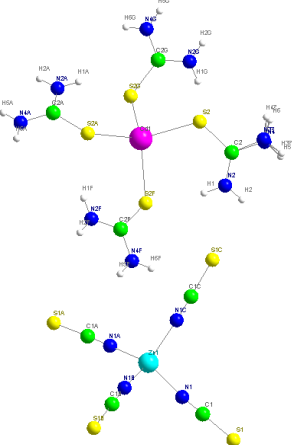
CdS ₃ O ₃			
<i>CSD Code</i>		<i>Cd-S</i> (Å)	<i>Cd-O</i> (Å)
1	NEMJEU	2.572	2.291
		2.536	2.446
		2.602	2.752
Range		2.536 – 2.602	2.291 – 2.752
Average		2.570	2.496

Appendix A-1 (*continued*)

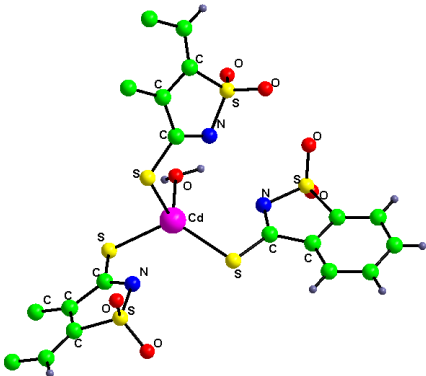
CdS ₆		
	<i>CSD Code</i>	<i>Cd-S</i> (Å)
1	RASQEH	2.714
		2.714
		2.686
		2.686
		2.734
		2.734
	Range	2.686 – 2.734
	Average	2.711

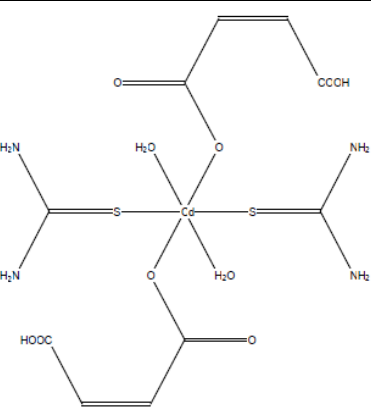
Appendix A-1 (continued)

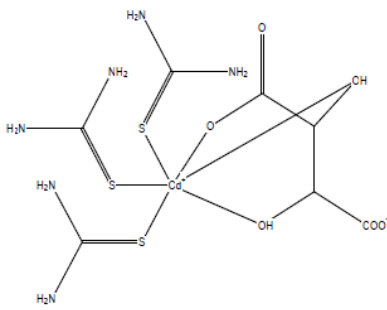
C.N.	Structure	Bond Distances	CSD Code
CdS ₄		Cd-S -2.5339(27) Cd-S -2.5317(26) Cd-S -2.5494(24) Cd-S -2.5527(23)	AYABIL
CdS ₄		Cd-S -2.5284(18) Cd-S -2.5159(12) Cd-S -2.5628(12) Cd-S -2.5261(17)	CAFMEC
CdS ₄		Cd-S -2.5171(7) Cd-S -2.5616(5) Cd-S -2.5643(7) Cd-S -2.4958(5)	CAGSEI
CdS ₄		Cd-S -2.5412(13) Cd-S -2.5412(12) Cd-S -2.5412(13) Cd-S -2.5412(12)	GUFHIZ

CdS ₄		<p> Cd-S -2.525(12) Cd-S -2.574(6) Cd-S -2.530(5) Cd-S -2.611(1) </p>	MAKVAV
CdS ₄		<p> Cd-S -2.534(20) Cd-S -2.552(3) Cd-S -2.506(2) Cd-S -2.582(4) </p>	MAKVAV0 1
CdS ₄		<p> Cd-S -2.569(4) Cd-S -2.569(4) Cd-S -2.569(4) Cd-S -2.569(4) </p>	XANHOJ

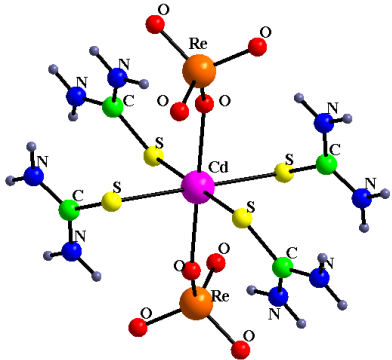
Appendix A-1 (continued)

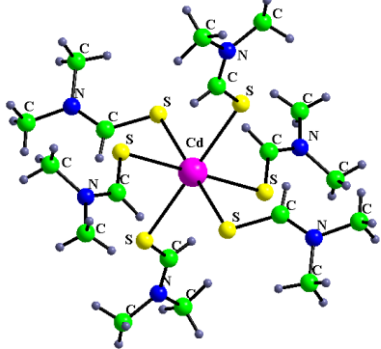
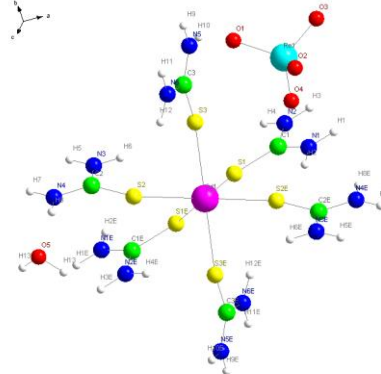
C.N.	Structure	Bond Distances	CSD Code
CdS ₃ O		Cd-S -2.5726(13) Cd-S -2.5293(17) Cd-S -2.4926(14) Cd-O -2.3043(23)	UKOTIX

C.N.	Structure	Bond Distances	CSD Code
CdS ₂ O ₄		Cd-S -2.6166(22) Cd-S -2.6166(22) Cd-O -2.3744(49) Cd-O -2.3744(49) Cd-O -2.4077(64) Cd-O -2.4077(64)	KASWOQ

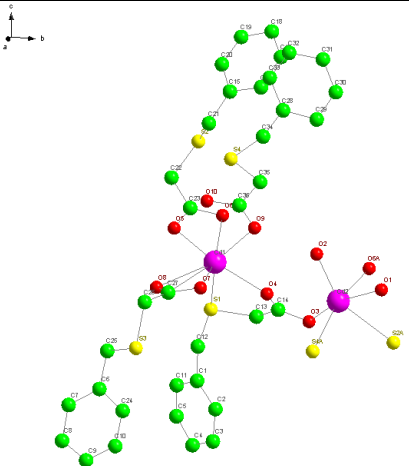
C.N.	Structure	Bond Distances	CSD Code
CdS ₃ O ₃		Cd-S -2.5721(19) Cd-S -2.5356(22) Cd-S -2.6015(19) Cd-O -2.2908(44) Cd-O -2.4456(40) Cd-O -2.7517(51)	NEMJEU

Appendix A-1 (continued)

C.N.	Structure	Bond Distances	CSD Code
CdS ₄ O ₂		Cd-S -2.7008(11) Cd-S -2.6462(87) Cd-S -2.7008(11) Cd-S -2.6462(87) Cd-O -2.4066(156) Cd-O -2.4066(156)	TEJZIR

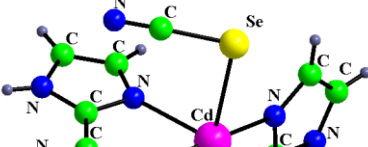
C.N.	Structure	Bond Distances	CSD Code
CdS ₆		Cd-S -2.6980(101) Cd-S -2.7135(116) Cd-S -2.7319(33) Cd-S -2.6980(101) Cd-S -2.7135(116) Cd-S -2.7319(33)	NEFXEB
CdS ₆		Cd-S -2.714(23) Cd-S -2.714(23) Cd-S -2.686(12) Cd-S -2.686(12) Cd-S -2.734(14) Cd-S -2.734(14)	RASQEH

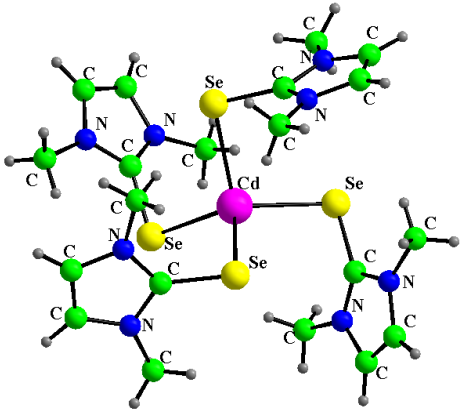
Appendix A-1 (continued)

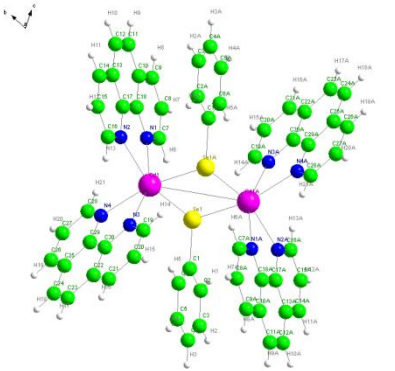
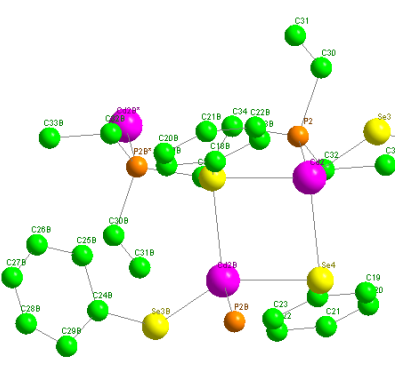
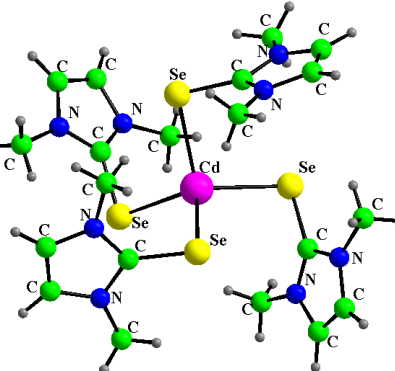
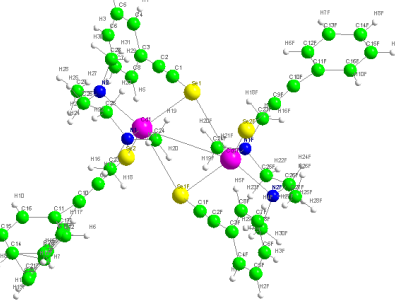
C.N.	Structure	Bond Distances	CSD Code
CdSO ₆		Cd-S -2.773(31) Cd-O -2.674(27) Cd-O -2.276(28) Cd-O -2.259(23) Cd-O -2.360(22) Cd-O -2.362(18) Cd-O -2.561(30)	GECZOD

Appendix A-2 Survey of Cadmium Complexes with selenone ligands in CSD version 5.30
(November 2008).

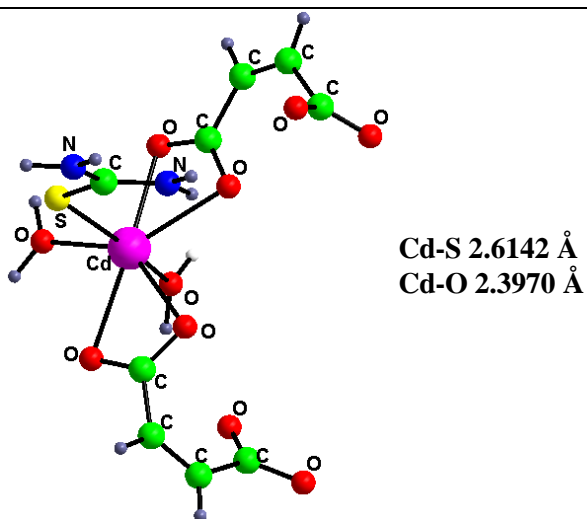
CdSe ₄		
	<i>CSD Code</i>	<i>Cd-Se (Å)</i>
1	DIRFIT	2.768
		2.776
		2.768
		2.776
2	JAMVAU	2.716
		2.708
		2.708
		2.716
3	IPZEQ	L2.636
		2.609
		2.636
		2.609
4	TENYAM	3.277
		2.629
		2.629
		3.277
Range		2.609 – 3.277
Average		2.718

C.N.	Structure	Bond Distances	CSD Code
CdSe ₂ N ₄		Cd-Se -2.8024(10) Cd-Se -2.8023(15) Cd-N -2.3507(91) Cd-N -2.3968(61) Cd-N -2.3968(82) Cd-N -2.3506(80)	KIBTAR

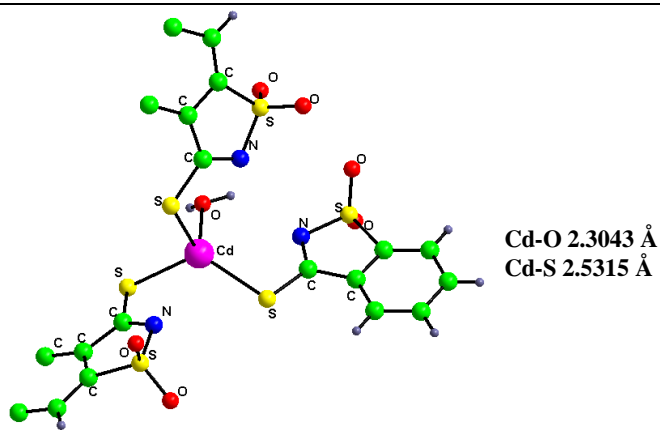
C.N.	Structure	Bond Distances	CSD Code
CdSe ₄		Cd-Se -2.6364(13) Cd-Se -2.6090(15) Cd-Se -2.6364(13) Cd-Se -2.6090(15)	LIPZEQ

CdSe ₄		Cd-Se -2.768(12) Cd-Se -2.776(18) Cd-Se -2.768(12) Cd-Se -2.776(18)	DIRFIT
CdSe ₄		Cd-Se -2.716(55) Cd-Se -2.708(7) Cd-Se -2.708(7) Cd-Se -2.716(55)	JAMVAU
CdSe ₄		Cd-Se -2.6364(13) Cd-Se -2.6090(15) Cd-Se -2.6364(13) Cd-Se -2.6090(15)	LIPZEQ
CdSe ₄		Cd-Se -3.277(43) Cd-Se -2.629(29) Cd-Se -2.629(29) Cd-Se -3.277(43)	TENYAM

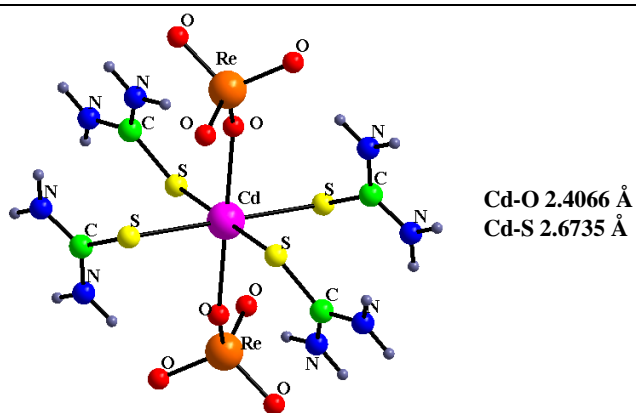
Appendix B- EXAFS Feff Model



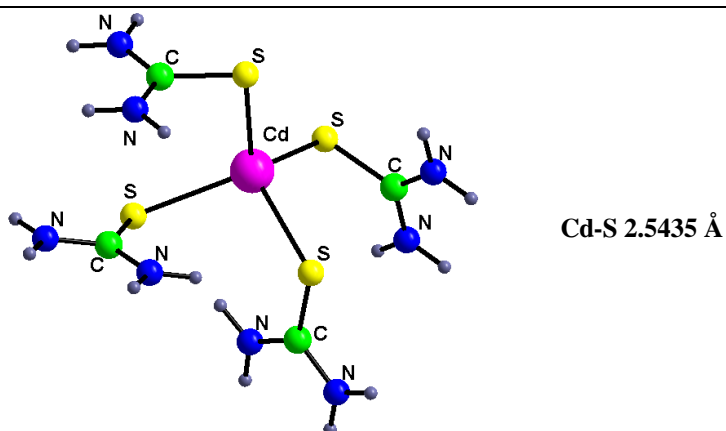
$(\text{Cd}_2\text{S}_3\text{C}_{11}\text{N}_6\text{O}_{10}\text{H}_{20})_n$ used as a fitting model for Cd(II)-thiourea solution A₂-C₂ at 200 K and room temperature.



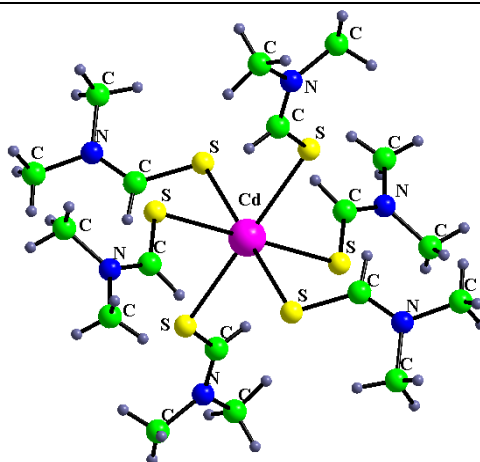
$\text{Cd}((\text{tsac})_3(\text{H}_2\text{O}))$ (tsac = anion of thiosaccharine) used as a fitting model for Cd(II)-thiourea solution D₂ and E₂ at room temperature.



$\text{Cd}(\text{TU})_4(\text{OReO}_3)_2$ used as a fitting model for Cd(II)-thiourea solution F₂ at 200K.

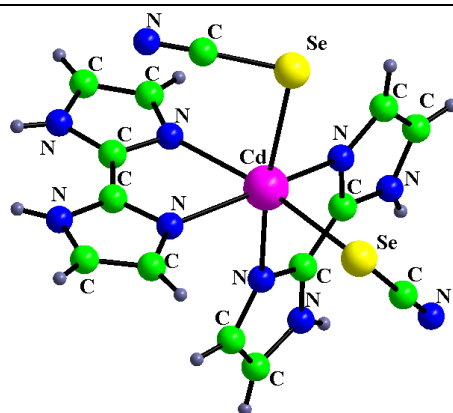


$\text{Cd}(\text{TU})_4(\text{NO}_3)_2$ used as a fitting model for Cd(II)-thiourea solutions D₂ and E₂ at 200 K,
and F₂ and G₂ at room temperature.



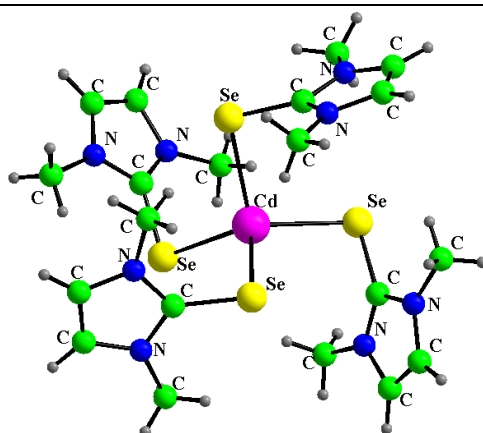
Cd-S 2.7145 Å

$\text{Cd}(\text{SC}_3\text{NH}_7)_6$ used as a fitting model for Cd(II)-thiourea solutions G_2 at 200 K



**Cd-N 2.3735 Å
Cd-Se 2.8023 Å**

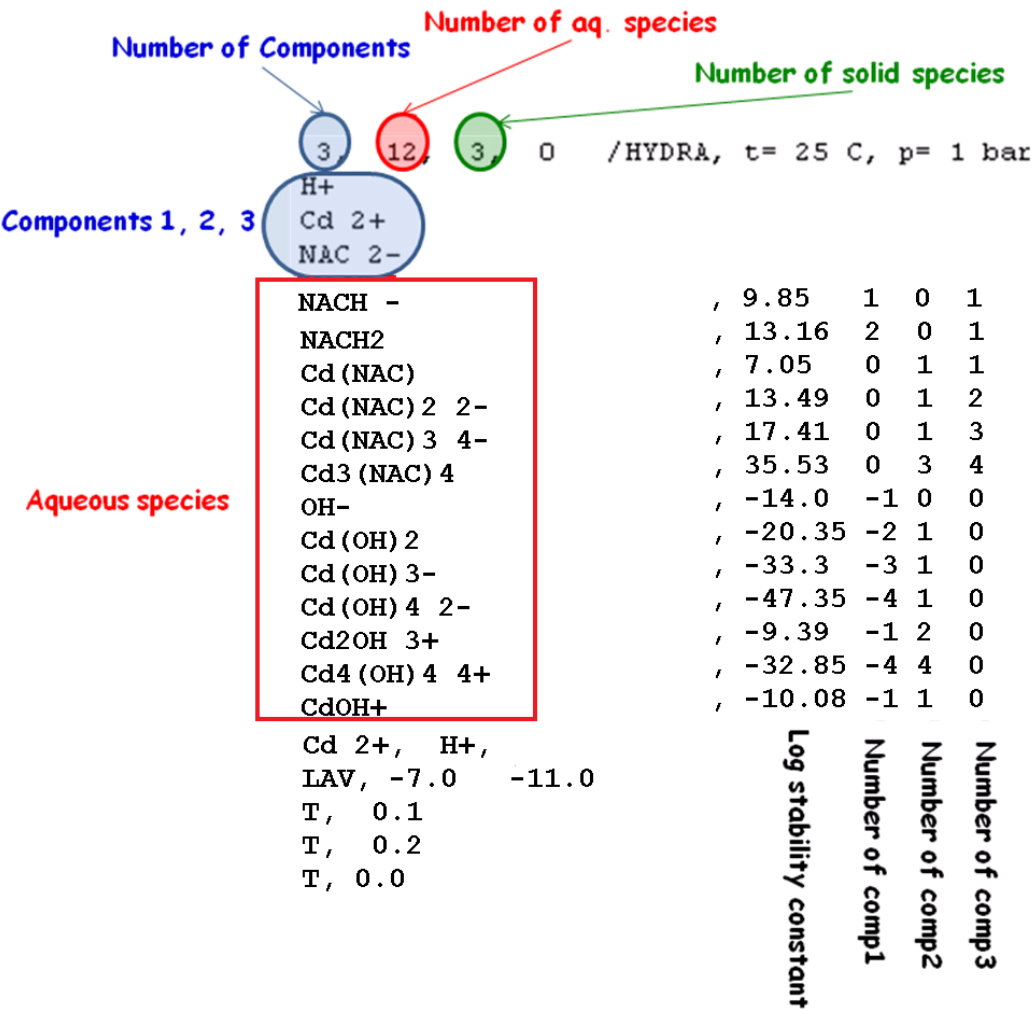
$\text{Cd}(\text{C}_6\text{N}_4\text{H}_6)_2(\text{SeCN})_2$ used as a fitting model for Cd(II)-selenourea solutions A_1 and B_1).



Cd-Se 2.6227 Å

$\text{Cd}(\text{dmise})_4(\text{PF}_6)_2$ (dmise = 1,3-dimethyl-2-(3H)imidazoleselone) used as a fitting model for Cd(II)-selenourea solution E_1 .

Appendix C Medusa input file



Medusa input file for Cd(II)-N-acetylcysteine solutions.

Appendix D Total number of scans collected during the ^{113}Cd NMR measurements

Cd(II)-SeU Solution	δ_{Cd}	No. of Scans
A ₁	-22, 96, 193, 436	26000
B ₁	97, 194, 436, 578	24652
C ₁	97, 194, 436, 578	49995
D ₁	578	4477
E ₁	573	2209

Cd-thiourea Coordination	Compound	Peak Position (ppm)	Spin Rates	No. of Scans
CdS ₄	[Cd(TU) ₄](NO ₃) ₂	577	5 KHz 7 KHz	20000 20000
CdS ₂ O ₄ & CdS ₃ O	<i>cis</i> -[Cd(TU) ₂ (OH ₂) ₄](SO ₄) and [Cd(TU) ₃ (SO ₄)]	148, 346	8 KHz	
CdS ₄ O ₂	[Cd(SCHN(CH ₃) ₂) ₄ (O ₃ SCF ₃) ₂]	263	5 KHz 6.6 KHz	7471 8956
CdS ₆	Cd[(SCHN(CH ₃) ₂) ₆](ClO ₄) ₂	403	3KHz 5KHz 7 KHz	8099 8095 20000

Cd(II)-thiourea Solution - LT	No. of Scans
A ₂	23473
B ₂	46123
C ₂	27128
D ₂	22000
E ₂	7909
F ₂	5218
G ₂	14000

Cd(II)-TU Solution -RT	No. of Scans
D ₂	19098
E ₂	4755
F ₂	19362
G ₂	1577

Cd(II)-NAC Solution (pH = 11.0)	No. of Scans
B ₁	31233
C ₁	28600
D ₁	36293
E ₁	23354
F ₁	32000
G ₁	31885

Cd(II)-NAC Solution (pH = 7.5)	No. of Scans
D ₂	36164
E ₂	24000
F ₂	35312
G ₂	34197

References

- ¹G. Chapman, S. Dunlop, *Environ. Res.* (1981) **26** 81 - 86
- ²H. Y. Li, E. L. Amma, *Inorg. Chimica Acta* (1990) **177** 5 - 7
- ³J. D. Otvos, I. M. Armitage, *Proc. Natl. Acad. Sci.* (1980) **77**(12) 7094 - 7098
- ⁴D. L. Rogers, S. S. Mason, *Inorg. Chem.* (1993) **32** 5216 - 5222
- ⁵E. A. H. Griffith, E. L. Amma, *Inorg. Chimica Acta* (1988) **148** 203 - 208
- ⁶(a) D. F. Flick, H. F. Kraybill, J. J. Dimitroff, *Environ. Res.* (1971) **4** 71, (b) Albert Roy, et al. *Environ. Physiol. Biochem.* (1973) **3** 65
- ⁷(a) <http://en.wikipedia.org/wiki/Cadmium>, (b) K. Nogawa, E. Kobayashi, Y. Okubo, Y. Suwazono, *Biomaterials* (2004) **17**(5) 581 - 587
- ⁸W. F. Furey, A. H. Robbins, L. L. Clancy, D. R. Winge, B. C. Wang, C. D. Stout, *Science* (1986) **231**(4739) 704 - 710
- ⁹M. Belcastro, T. Marino, N. Russo, M. Toscano, *J. of Inorg. Biochem.* (2009) **103** 50 - 57
- ¹⁰M. Zafarullah, W. Q. Li, J. Sylvester, M. Ahmad, *Cellular and Molecular Life Sciences* (2003) **60**(1) 6-20
- ¹¹N. De Vries, S. De Flora, *J. Cell. Biochem.* (1993) **17** 270 - 277
- ¹²V. V. S. Murty, M. Seshasayee, B. V. R. Murthy, *Indian J. of Physics, A* (1981) **55A**(4) 310 - 315
- ¹³F. Charbonnier, R. Faure, H. Loiseleur, *Revue de Chimie Minerale* (1979) **16**(6) 555 - 564
- ¹⁴I. Puigdomenech, 2002. Chemical Equilibrium Software MEDUSA and Data Base HYDRA, Royal Institute of Technology: Stockholm, <http://www.kemi.kth.se/utbildning/gk/kemiskjmv>
- ¹⁵M. R. Holdiness, *Clinical pharmacokinetics* (1991) **20**(2) 123 - 134
- ¹⁶I. Ziment, *Biomedicine and pharmacotherapy Biomedecine and pharmacotherapie* (1988) **42**(8) 513 - 519
- ¹⁷H. Sato, M. Tamba, T. Ishii, S. Bannai, *J. of Biol. Chem.* (1999) **274**(17) 11455 - 11458
- ¹⁸S. K. Tandon, *J. Appl. Toxicol.* (2002) **22** 67 - 71
- ¹⁹M. M. Shoukry, *Proc. Indian Acad. Sci. (Chem. Sci.)* (1990) **102** 19 - 24
- ²⁰A. L. Sheffner, *Annals of the New York Academy of Sciences* (1963) **106** 298 - 310
- ²¹B. Noszal, D. Visky, M. Kraszni, *J. Med. Chem.* (2000) **43** 2176 - 2182
- ²²S. H. L. Thomas, *Pharmacol. Ther.* (1993) **60** 91 - 120
- ²³B. H. Rumack, *The American J. of Medicine* (1983) **75**(5A) 104 - 112
- ²⁴M. Chol, N. Nevo, S. Cherqui, C. Antignac, P. Rustin, *Biochemical and Biophysical Research Commun.* (2004) **324** 231 - 235
- ²⁵R. D. Issels, A. Nagele, K. G. Eckert, W. Wilmanns, *Biochemical Pharmacology* (1988) **37**(5) 881 - 888
- ²⁶O. I. Aruoma, B. Halliwell, B. M. B. Hoey, *Free Radical Biology and Medicine* (1989) **6**(6) 593 - 597
- ²⁷X. Q. Shan, T. Y. Aw, D. P. Jones, *Pharmacol. Ther.* (1990) **47** 61 - 71

-
- ²⁸W. Wu, G. Goldstein, C. Adams, R. H. Matthews, N. Ercal, *Biomed. Chromatogr.* (2006) **20** 415 - 422
- ²⁹S. De Flora, A. Izzotti, F. D'Agostini, R. M. Balansky, *Carcinogenesis* (2001) **22**(7) 999 - 1013
- ³⁰W. H. Habig, M. J. Pabst, W. B. Jakoby, *J. Biol. Chem.* (1974) **249** 7130 - 7139
- ³¹E. Hoffer, Y. Baum, A. Tabak, U. Taitelman, *Toxicol. Lett.* (1996) **84**(1) 7-12
- ³²B. M. De Rooij, J. N. M. Commandeur, N. P. E. Vermeulen, *Biomarkers* (1998) **3**(4/5) 239 - 303
- ³³*Cambridge Structural Database (CSD)*, CSD version 5.30 (November 2008)
- ³⁴D. Papagiannopoulou, I. C. Pirmettis, M. Pelecanou, C. Tsoukalas, C. P. Raptopoulou, A. Terzis, E. Chiotellis, M. Papadopoulos, *Inorg. Chimica Acta* (2002) **346** 270 - 274
- ³⁵(a) J. J. Schwab, E. C. Wilkinson, S. R. Wilson, P. A. Shapley, *J. Am. Chem. Soc.* (1991) **113** 6124 - 6129; (b) R. Atencio, M. A. Esteruelas, F. J. Lahoz, L. A. Oro, N. Ruiz, *Inorg. Chem.* (1995) **34** 1004 - 1006
- ³⁶(a) M. I. Garcia-Seijo, A. Habtemariam, P. S. Murdoch, R. O. Gould, M. E. Garcia-Fernandez, *Inorg. Chimica Acta* (2002) **335** 52 - 60; (b) K. A. Mitchell, C. M. Jensen, *Inorg. Chem.* (1995) **34** 4441 - 4446; (c) K. A. Mitchell, K. C. Streveler, C. M. Jensen, *Inorg. Chem.* (1993) **32** 2608 - 2609
- ³⁷E. Suarez-Moreira, L. Hannibal, C. A. Smith, R. A. Chavez, D. W. Jacobsen, N. E. Brasch, *Dalton Transactions* (2006) **44** 5269 - 5277
- ³⁸G. Yi, L. Chen, M. A. Khan, G. B. Richter-Addo, *Inorg. Chem.* (1997) **36** 3876 - 3885
- ³⁹W. Eikens, C. Kienitz, P. G. Jones, C. Thoene, *J. Chem. Soc. Dalton Transactions* (1994) **1** 83 - 90
- ⁴⁰Y. Chen, N. Belzile, J. Gunn, *Limnology and Oceanography* (2001) **46** 1814 - 1818
- ⁴¹K. Seppanen, M. Kantola, R. Laatikainen, K. Nyysönen, V. P. Valkonen, V. Kaarlopp, J. T. Salonen, *J. Trace Elem. Med. Biol.* (2000) **14** 84 - 87
- ⁴²D. J. Williams, B. J. McKinney, B. Baker, K. P. Gwaltney, D. VanDerveer, *J. Chem. Crystallogr.* (2007) **37** 691 - 694
- ⁴³A. A. Isab, M. I. M. Wazeer, *J. of Coordination Chem.* (2005) **58**(6) 529 - 537
- ⁴⁴M. Epifani, C. Giannini, L. Manna, *Materials Letters* (2004) **58** 2429 - 2432
- ⁴⁵H. Tapiero, D. M. Townsend, K. D. Tew, *Biomedicine and Pharmacotherapy* (2003) **57** 134 - 144
- ⁴⁶R. D. Crosland, *Pharmacology and Toxicology* (1995) **77** 231 - 237
- ⁴⁷H. Takahashi, A. Nishina, R. Fukumoto, H. Kimura, M. Koketsu, H. Ishihara, *Life Sci.* (2005) **76**(19) 2185 - 2192
- ⁴⁸M. I. M. Wazeer, A. A. Isab, S. Ahmad, *Canadian J. of Analytical Sciences and Spectroscopy* (2006) **51**(1) 43 - 48
- ⁴⁹S. Ahmad, A. A. Isab, A. P. Arnold, *J. Coord. Chem.* (2003) **56** (6) 539 - 544
- ⁵⁰A. A. Isab, A. A. Al-Arfaj, M. N. Akhtar, *J. Coord. Chem.* (1994) **33** 287 - 294
- ⁵¹I. M. Cheremisina, É. V. Khlystunova, V. L. Varand, *Izvestiya Akademii Nauk SSSR, Seriya Khimicheskaya* (1972) **12** 2672 - 2675
- ⁵²É. V. Khlystunova, I. M. Cheremisina, V. L. Varand, V. M. Shu'lman, *Izvestiya Akademii Nauk SSSR, Seriya Khimicheskaya* (1971) **7** 1551-1552

-
- ⁵³A. Levent, E. Keskin, Y. Yardım, Z. Şentürk, *Rev. Anal. Chem.* (2011) **30** 45–51
- ⁵⁴IARC Working Group, *Evaluation of Carcinogenic Risks to Humans*, Lyon, France (2001) **79** 703-725
- ⁵⁵K. Kargosha, M. Khanmohammadi, M. Ghadiri, *Analyst* (2001) 126 1432–1435
- ⁵⁶V. N. Semenov, A. V. Naumov, *Russian J. of General Chem.* (2001) **71**(4) 533-537
- ⁵⁷W. Henderson, B. K. Nicholson, M. B. Dinger, *Inorg. Chimica Acta* (2003) **355** 428 - 431
- ⁵⁸S.M. RaviKumar, N.Melikechi, S.Selvakumar, P.Sagayaraj, *Physica B* (2008) **403** 4160–4163
- ⁵⁹R. Petrova, O. Angelova, J. Macicek, *Acta Crystallogr., Sect. C: Cryst. Struct. Commun.* (1997) **53** 565 - 568
- ⁶⁰R. Petrova, S. Bakardjieva, T. Todorov, *Zeitschrift fuer Kristallographie* (2000). **215** 118 - 121
- ⁶¹A. Korczynski, *Rocz. Chem* (1967) **41** 1197 - 1203
- ⁶²Y. Zhang, L. Jianmin, M. Nishiura, H. Hou, W. Deng, T. Imamoto, *J. Chem. Soc., Dalton Transactions* (2000) 293 - 297
- ⁶³J. W. Forstrom, J. J. Zakowski, A. L. Tappel, *Biochem.* (1978) **17**(13) 2639 - 2644
- ⁶⁴J. E. Cone, R. Martin del Rio, J. N. Davis, T.C. Stadtman, *Proc. Natl. Acad. Sci.* (1976) **73**(8) 2659 - 2663
- ⁶⁵X. Chen, G. Yang, J. Chen, X. Chen, Z. Wen, K. Ge, *Biol. Trace Elem. Res.* (1980) **2**(2) 91 - 107
- ⁶⁶http://autoimmunedisease.suite101.com/article.cfm/selenium_deficiency
- ⁶⁷P. Knekt, J. Marniemi, L. Teppo, M. Heliovaara, A. Aromaa, *American J. of Epidemiology* (1998) **148**(10) 975 - 982
- ⁶⁸H. E. Ganther, *Carcinogenesis* (1999) **20**(9) 1657 - 1666
- ⁶⁹<http://en.wikipedia.org/wiki/Selenium>
- ⁷⁰N. Chareonpong-Kawamoto, K. Yasumoto, *Bioscience, Biotechnology, and Biochemistry* (1995) **59** 302 - 306
- ⁷¹G. Feroci, R. Badiello, A. Fini, *J. of Trace Elements in Medicine and Biology* (2005) **18** 227 - 234
- ⁷²I. Andreadou, B. van de Water, J. N. M. Commandeur, F. J. Nagelkerke, N. P. E. Vermeulen, *Toxicology and Applied Pharmacology* (1996) **141** 278 - 287
- ⁷³T. Arai, T. Ikemoto, A. Hokura, Y. Terada, T. Kunito, S. Tanabe, I. Nakai, *Environ. Sci. Technol.* (2004) **38**(24) 6468 - 6474
- ⁷⁴H. Maeda, K. Katayama, H. Matsuno, T. Uno, *Angew. Chem. Int. Ed.* (2006) **45** 1810 - 1813
- ⁷⁵R. Longtin, *J. of the National Cancer Institute* (2004) **96**(7) 504 - 505
- ⁷⁶A. Boeck, K. Forchhammer, J. Heider, W. Leinfelder, G. Sawers, B. Veprek, F. Zinoni, *Molecular Microbiology* (1991) **5**(3) 515 - 520
- ⁷⁷B. Sohling, T. Parther, K. P. Rucknagel, M. Wagner, J. R. Andreesen, *Biol. Chem.* (2001) **382** 979 - 986
- ⁷⁸W. Thomas, *Tetrahedron* (1999) **55**(1) 1 - 28

-
- ⁷⁹Y. Chen, X. Zhou, J. Tong, Y. Truong, N. Belzile, *Analytica Chimica Acta* (2005) **545** 149 - 157
- ⁸⁰E.J. Lofgren, *UC Radiation Lab Document UCRL-3369 "Experiences with the BEVATRON* (1956)
- ⁸¹http://commons.wikimedia.org/wiki/File:Sch%C3%A9ma_de_principe_du_synchrotron.jpg
- ⁸²H. Winick, *Synchrotron Radiation Sources - A Primer* **1st ed.** World Scientific Publishing Co. Pte. Ltd. (1994)
- ⁸³http://www.spring8.or.jp/en/facilities/bl/light_source_optics/sources/insertion_device/w-hats_insertion_device
- ⁸⁴<http://www.esrf.eu/about/synchrotron-science/synchrotron>
- ⁸⁵<http://www.kajmunk.nl/grenoble/>
- ⁸⁶B. K. Teo, *EXAFS: Basic Principles and Data Analysis*, Springer-Verlag: Berlin, (1986) **Vol. 9**
- ⁸⁷http://chemwiki.ucdavis.edu/Physical_Chemistry/Spectroscopy/X-ray_Spectroscopy/EXAFS%3A_Application
- ⁸⁸R. A. Scott, *Methods in Enzymology* (1985) **117** 414 - 459
- ⁸⁹EXAFS structure analysis, Retrieved (September 14, 2010) from <http://smb.slac.stanford.edu/~ellis/Thesis/Chapter2.pdf>
- ⁹⁰G. N. George, I. J. Pickering, *EXAFSPAK: A Suite of Computer Programs for Analysis of X-ray Absorption Spectra*, SSRL: Stanford, CA (2000)
- ⁹¹T. Ressler, *J. Synchrotron Rad.* (1998) **5** 118 - 122
- ⁹²<http://radiology.rsna.org/content/215/1/286/F2.expansion?ck=nck>
- ⁹³A. L. Ankudinov, J. J. Rehr, *Physical Review B: Condensed Matter* (1997) **56(4)** R1712 - R1715
- ⁹⁴J. Mason, *Multinuclear NMR*, **1st ed.**, Plenum Press, (1987)
- ⁹⁵N. E. Jacobsen, *NMR Spectroscopy Explained: Simplified Theory, Applications and Examples for Organic Chem. and Structural Biology*, **1st ed.** John Wiley and Sons, (2007)
- ⁹⁶H. Friebolin, *Basic One- and Two-Dimensional NMR Spectroscopy*, **4th ed.**, Wiley-VCH: Weinheim, (2005)
- ⁹⁷A. D. Cardin, P. D. Ellis, J. D. Odom, J. W. Howard, *J. Am. Chem. Soc.* (1975) **97(7)** 1672 - 1679
- ⁹⁸R. J. Kostelnik, A. A. Bothner, *J. of Magnetic Resonance* (1974) **14(2)** 141 - 151
- ⁹⁹(a) D.C. Craig, I.G. Dance, P.A.W. Dean, J.M. Hook, H.A. Jenkins, C.W. Kirby, M.L. Scudder, U. Rajalingam, *Canadian J. Chem.* (2005) **83** 174 - 184; (b) A.V. Ivanov, A.V. Gerasimenko, A.A. Konzelko, M.A. Ivanov, O.N. Antzutkin, W. Forsling, *Inorg. Chimica Acta* (2006) **359** 3855 - 3864
- ¹⁰⁰M. F. Summers, *Coordination Chem. Reviews* (1988) **86** 43 - 134
- ¹⁰¹J. Sola, P. Gonzalez-Duarte, J. Sanz, I. Casals, T. Alsina, I. Sobrados, A. Alvarez-Larena, J. F. Phiella, X. Solans, *J. Am. Chem. Soc.* (1993) **115** 10018-10028
- ¹⁰²O. F. Z. Khan, P. O'Brien, *Polyhedron* (1991) **10(3)** 325-332

-
- ¹⁰³R. A. Allred, L. H. McAlexander, A. M. Arif, L. M. Berreau, *Inorg. Chem.* (2002) **41(25)** 6790-6801
- ¹⁰⁴M. D. Nyman, M. J. Hampden-Smith, E. N. Duesler, *Inorg. Chem.* (1997) **36** 2218-2224
- ¹⁰⁵R. A. Bulman, J. K. Nicholson, D. P. Higham, P. J. Sadler, *J. Am. Chem. Soc.* (1984) **106** 1118-1119
- ¹⁰⁶R. A. Allred, S. A. Huefner, K. Rudzka, A. M. Arif, L. M. Berreau, *Dalton Transactions* (2007) 351-357
- ¹⁰⁷B. R. Bobsein, R. J. Myers, *J. Biol. Chem.* (1981) **256** 5313-5316
- ¹⁰⁸A. Nolle, *Zeitschrift fuer Naturforschung, Teil A* (1978) **33A(6)** 666 - 671
- ¹⁰⁹P. D. Murphy, W. C. Stevens, T. T. P. Cheung, S. Lacelle, B. C. Gerstein, D. M. Kurtz, *J. Am. Chem. Soc.* (1981) **103(15)** 4400 - 4405
- ¹¹⁰U. Rajalingam, P. A. W. Dean, H. A. Jenkins, M. Jennings, J. M. Hook, *Canadian J. Chem.* (2001) **79** 1330-1337
- ¹¹¹P. G. Mennitt, M. P. Shatlock, V. J. Bartuska, G. E. Maciel, *J. of Physical Chem.* (1981) **85(14)** 2087 - 2091
- ¹¹²G. K. Carson, P. A. W. Dean, M. J. Stillman, *Inorg. Chimica Acta* (1981) **56(3)** 59 - 71
- ¹¹³(a) D. W. Fitzgerald, J. E. Coleman, *Biochem.* (1991) **30** 5195-5201; (b) D. P. Giedroc, B. A. Johnson, I. M. Armitage, J. E. Coleman, *Biochem.* (1989) **28** 2410-2418; (c) W. J. Roberts, T. Pan, J. I. Elliott, J. E. Coleman, K. R. Williams, *Biochem.* (1989) **28** 10043-10047; (d) T. L. South, B. Kim, M. F. Summers, *J. Am. Chem. Soc.* (1989) **111** 395-396
- ¹¹⁴W. Sun, X. Shi, L. Zhang, J. Hu, J. Wei, *J. of Inorg. Biochem.* (1999) **76** 259-263
- ¹¹⁵B. R. Bobsein, R. J. Myers, *J. Am. Chem. Soc.* (1980) **102** 2454-2455
- ¹¹⁶N. G. Charles, E. A. Griffith, P. F. Rodesiler, E. L. Amma, *Inorg. Chem.* (1983) **22(19)** 2717 - 2723
- ¹¹⁷P. F. Rodesiler, N. G. Charles, E. A. Griffith, K. Lewinski, E. L. Amma, *Acta Cryst* (1986) **C42** 396-399
- ¹¹⁸R. W. Turner, P. F. Rodesiler, E. L. Amma, *Inorg. Chimica Acta* (1982) **66(1)** L13 - L15
- ¹¹⁹P. F. Rodesiler, E. A. H. Griffith, N. G. Charles, L. Lebiada, E. L. Amma, *Inorg. Chem.* (1985) **24** 4595-4600
- ¹²⁰P. D. Ellis, R. R. Inners, H. J. Jakobsen, *J. of Physical Chem.* (1982) **86(9)** 1506 - 1508
- ¹²¹P. W. Dean, *Canadian J. Chem.* (1981) **59** 3221 - 3225
- ¹²²G. K. Carson, P. A. W. Dean, *Inorg. Chimica Acta* (1982) **66(2)** 37 - 39
- ¹²³R. Subramanian, N. Govindaswamy, R. A. Santos, S. A. Koch, G. S. Harbison, *Inorg. Chem.* (1998) **37** 4929 - 4933
- ¹²⁴M. T. Ng, P. A. W. Dean, J. J. Vittal, *Dalton Transactions* (2004) **18** 2890 - 2894
- ¹²⁵J. D. Kennedy, W. McFarlane, *J. of the Chemical Society, Perkin Transactions 2: Physical Organic Chem.* (1977) **9** 1187 - 1191
- ¹²⁶C. J. Turner, R. F. M. White, *J. of Magnetic Resonance* (1977) **26(1)** 1 - 5
- ¹²⁷D. D. Dominguez, M. M. King, H. J. C. Yeh, *J. of Magnetic Resonance* (1978) **32(1)** 161 - 165

-
- ¹²⁸H. J. Jakobsen, P. D. Ellis, R. R. Inners, C. F. Jensen, *J. Am. Chem. Soc.* (1982) **104**(26) 7442 - 7452
- ¹²⁹E. H. Curzon, N. Herron, P. Moore, *J. of the Chemical Society, Dalton Transactions: Inorg. Chem.* (1980) **5** 721 - 725
- ¹³⁰M. Holz, R. B. Jordan, M. D. Zeidler *J. of Magnetic Resonance* (1976) **22**(1) 47 - 52
- ¹³¹J. D. Otvos, I. M. Armitage, *J. Am. Chem. Soc.* (1979) **101**(26) 7734 - 7736
- ¹³²<http://www.fda.gov/downloads/ScienceResearch/FieldScience/UCM092243.pdf>
- ¹³³C. Trujillo, O. Mó, M. Yáñez, *J. of Physical Chem. B* (2008) **112** 5479 - 5486
- ¹³⁴G. B. Aitken, J. L. Duncan, G. P. McQuillan, *J. of the Chemical Society, Dalton Transa.: Inorg. Chem.* (1972-1999) (1972) **19** 2103-2107
- ¹³⁵Z. E. Mel'chekova, *Zhurnal Prikladnoi Khimii* (1982) **55**(12) 2719 - 2723
- ¹³⁶D. Y. Godovsky, A. E. Varfolomeev, D. F. Zaretsky, R. L. Nayana Chandrakanthi, A. Kuendig, C. Weder, W. Caseri, *J. of Materials Chem.* (2001) **11**(10) 2465-2469
- ¹³⁷M. Oussaid, P. Becker, C. Carabatos-Nedelec, *J. Raman Spectrosc.* (2000) **31** 529-533
- ¹³⁸M. Parvez, F. Jalilehvand, Z. Amini, *Acta Cryst.* (2012) **E68** m949 – m950
- ¹³⁹C. Amman, P. Meier, A.E. Merbach, *J. Magn. Reson.* (1982) **46** 319-321
- ¹⁴⁰G. E. Maciel, M. Borz, *J. Chem. Soc., Chem. Commun.* (1973) **12** 394
- ¹⁴¹R. Petrova, O. Angelova, S. Bakardjieva, J. Macicek, *Acta Crystallogr., Sect. C: Cryst. Struct. Commun.* (1996) **52** 2432 - 2434
- ¹⁴²C. M. V. Stalhandske, C. I. Stalhandske, M. Sandstrom, I. Persson, *Inorg. Chem.* (1997) **36** 3167 - 3173
- ¹⁴³Z. A. Shaikh, Kh. Zaman, W. Tang, T. Vu, *Toxicology and Applied Pharmacology* (1999) **154** 256 - 263
- ¹⁴⁴H. Ottenwälder, P. Simon, *Arch. Toxicol.* (1987) **60** 401 - 402
- ¹⁴⁵Z. A. Shaikh, Kh. Zaman, W. Tang, T. Vu, *Toxicology Letters* (1999) 104 137 - 142
- ¹⁴⁶V. Mah, F. Jalilehvand, *J. Biol. Inorg. Chem.* (2010) **15** 441 - 458
- ¹⁴⁷F. Jalilehvand, B. O. Leung, V. Mah, *Inorg. Chem.* (2009) **48** 5758 - 5771
- ¹⁴⁸H. Kozłowski, J. Urbanska, I. Sovago, K. Varnagy, A. Kiss, J. Szychala, K. Cherifi, *Polyhedron* (1990) **9** 831 – 837
- ¹⁴⁹E. P. Serjeant, *Potentiometry and Potentiometric Titrations*. John Wiley and Sons (1984) **V69** Chapter 8
- ¹⁵⁰I. M. Armitage, Y. Boulanger, Ed. Laszlo, *NMR of Newly accessible Nuclei*. P. **V2**. Academic Press: Toronto (1983) 319 - 363.
- ¹⁵¹S. H. Tarulli, O. V. Quinzani, E. J. Baran, O. E. Piro, E. E. Castellano, *J. Mol. Struct.* (2003) **656** 161 - 168
- ¹⁵²G. Oz, D. L. Pountney, I. M. Armitage, *Biochem. Cell. Biol.* (1998) **76** 223 - 234
- ¹⁵³E. S. Gruff, S. A. Koch, *J. Am. Chem. Soc.* (1990) **112** 1245 - 1247
- ¹⁵⁴I. J. Pickering, R. C. Prince, G. N. George, W. E. Rauser, W. A. Wickramasinghe, A. A. Watson, C. T. Dameron, I. G. Dance, D. P. Fairlie, D. E. Salt, *Biochimica et Biophysica Acta* (1999) **1429** 351 - 364
- ¹⁵⁵F. Jalilehvand, V. Mah, B. O. Leung, J. Mink, G. M. Bernard, L. Hajba, *Inorg. Chem.* (2009) **48** 4219 - 4230

¹⁵⁶F. Jalilehvand, Z. Amini, K. Parmar, EY. Kang, *Dalton Trans.* (2011) **40** 12771 – 12778